Università degli Studi di Ferrara

DOTTORATO DI RICERCA IN
BIOCHIMICA, BIOLOGIA MOLECOLARE E
BIOTECNOLOGIE

CICLO XVII

COORDINATORE Prof. FRANCESCO BERNARDI

Ivabradine induces an atheroprotective gene expression profile in the endothelium of ApoE deficient mice before plaque formation

Settore Scientifico Disciplinare BIO-11

Dottorando
Dott. Aquila Giorgio

Tutore
Prof. Rizzo Paola

Anni 2012/2014

CONTENTS Pag.

INTRODUCTION

1. Overview on atherosclerosis

Atherosclerosis is one of the leading causes of death in the developed world and consists in a chain of chronic multistep inflammatory events that lead to formation of a hard structure called “plaque”. Atherosclerotic plaques could represent a risk factor in the development of thrombotic events that can cause heart attack and stroke [1].

The first description of atherosclerosis dates back to 1755, when the Swiss anatomist Albrecht von Haller proposed the term “atheroma”, from Greek “athere”, in describing any kind of gruel materials which composed the plaques that he had analyzed [Haller, Albrecht von. Observatio XXXXVII: materia ossium morbosorum. In: Opuscula pathologica. Lausanne: Bousquet; 1755. p. 124–8.]. Thus, he used the term “atheroma” to describe mellow plaques and he studied them in various stages, from the softer and yellowish plaques to the harsher and calcified ones.

The German-French surgeon Johann F. Lobstein coined the term “arteriosclerosis” in 1833 to describe the stiffening (hence “scleros” i.e. hardening) of the arterial wall due to atherosclerosis. He noticed that only some area of arterial tree was affected by this particular disease, in particular the aortic arch and its branches [Lobstein JGCFM. Traités d’anatomie pathologique. Paris: Chez F.G. Levrault; 1833. p. 550–3].

In 1904, the German pathologist Felix Jacob Marchand, by combining the terms “atheroma” of von Haller and “arteriosclerosis” of Lobstein, minted the term “atherosclerosis” which represents a subtype of “arteriosclerosis” that involves primarily the intima and innermost part of the media of medium-sized and large arteries [Marchand JF. Über arteriosklerose (athero-sklerose). Verh Kongresses Innere Medizin. 1904;21:23–59].

The first pathological theory regarding the atherosclerosis was described in the mid-19th century by Karl von Rokitansky, who thought that atherosclerosis began with deposition of fibrin and other blood elements in the intima layer, which resulting degeneration, along with cholesterol crystals and fatty globules depositions, led to atheroma formation. In the same years, Rudolf Virchow proposed another theory, whereby the inflammation in the intima of arterial wall would be the major mechanism of plaque development and that the fibrous thickening evolves as a consequence of a reactive fibrosis induced by proliferating connective tissue cells [2].

The number of proposed theories on the pathogenesis, after these first descriptions, has gradually grown. Another theory proposed in the first decades of 1900 was the “lipid

hypothesis" which suggested that some diet constituents were involved in plaque formation, pointing out the importance of cholesterol as the major atherosclerotic risk factor. This theory led to "response-to-retention hypothesis" proposed by Williams and Tabas, which suggested that the augmentation of plasmatic LDL(s) was responsible of their retention in the inner arterial wall, where they are more susceptible to oxidation, triggering the inflammatory processes responsible for the development of atherosclerotic lesions [3]. In the last decades of 20th century, molecular biology studies furnished a new pathological theory, called "hypothesis of lesion reaction" which was proposed for the first time by Ross and Glomsett in 1976 [4]. They proposed that the atherosclerotic lesions were the result of focal injury to arterial endothelium, followed by adherence, aggregation and release of platelets. Since then, numerous studies have followed to define the causes and the molecular details of endothelial dysfunction.

To date, all of these main theories (inflammatory-, lipid- and lesion reaction-hypothesis i.e.) are closely linked to each other and not mutually exclusive in explaining the pathogenetic events which lead to atherosclerotic plaques formation.

2. The structure the arterial blood vessels

Arteries of medium and large caliber, responsible for blood transport from the heart to all body compartments, consist of three layers [5] (Figure 1). From vessel lumen to the outside we found:

- *Tunica intima*: the thinnest layer which consists a monolayer of endothelial cells (ECs), the endothelium, above the basal lamina, a thin layer of loose connective tissue, and a sub-endothelial elastic lamina. The ECs play a pivotal role in integrity and function maintenance of vessel wall: they exert a barrier function, by producing a wide range of factors that regulate cellular adhesion, thromboresistance and vessel wall inflammation [6]. Moreover they control blood pressure by releasing vasoconstrictors or vasodilators and the trafficking of different kinds of agents which could participate in preliminar phases of atherosclerotic plaque formation. Internal elastic lamina, which is fenestrated to ensure nutritive substances from blood to reach the tunica media, and collagen fibers (and fibroblasts) of the basal lamina participate to vessel elasticity.

- *Tunica media*: the thickest layer made of a connective stroma of collagen fibers which sustain concentric elastic fibers and smooth muscle cells (SMCs), which in turn

synthesize elastic fibers and collagen. SMCs, which contain contractile actin fibers, tend to be longitudinally aligned and are strictly associated with collagen fibers. The elastic fibers, interposed between the SMC, are relatively extensible and responsible of blood pressure maintenance, by allowing contraction (during diastole) and distension (during systole) of the artery wall during a cardiac cycle.

- *Tunica adventitia*: the outermost layer made of a fibrous connective tissue, which mostly contains SMCs, fibroblasts and, in larger vessels, nervous plexuses and lymphatic vessels. It is necessary for protecting the other layers below and allows them to be fixed to the surrounding tissues. In the largest arteries, such as aorta, this tunica is perfused by a system of small blood vessels, called *vasa vasorum*, that provide nutriments to the adventitia itself.

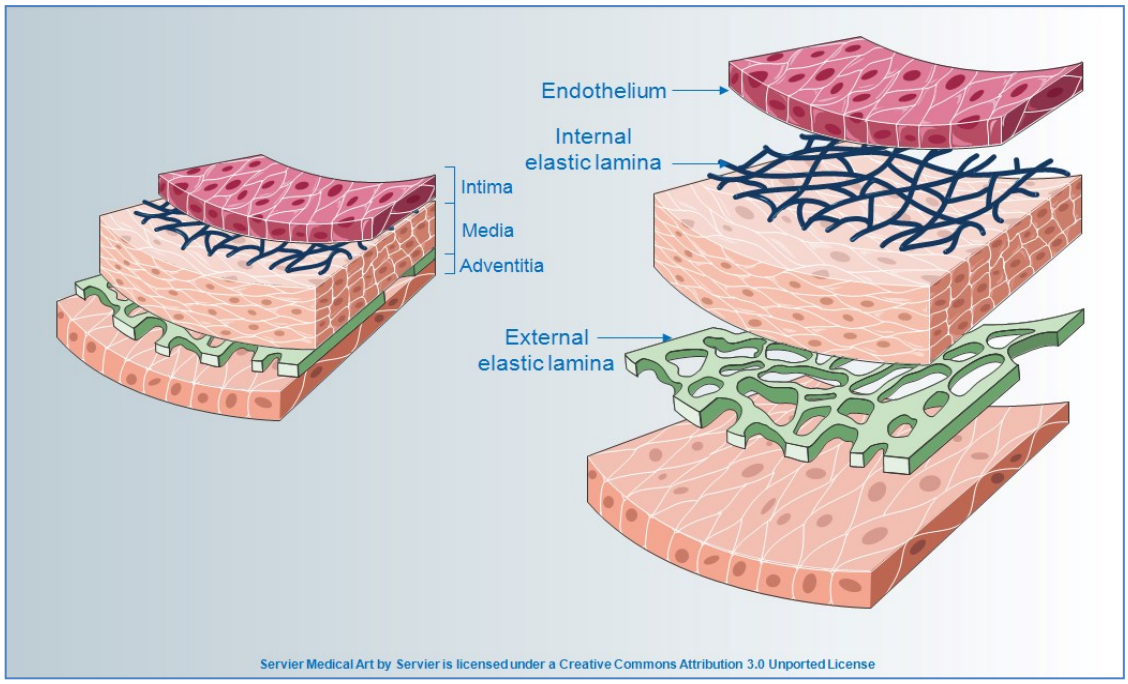

Figure 1: Structure of an artery (Image from Servier Medical Art - http://www.servier.com/Powerpoint-image-bank)

3. Atherosclerotic plaque development

In the development of atherosclerotic lesions, we can distinguish several stages: the initial processes that generate lesions clinically silent; the stages of the progression leading to the formation of a stenosis not necessarily symptomatic; the complicating events, at last, that are the basis of the clinical chronic or acute manifestations.

It is noteworthy that clinical onset of atherosclerotic lesions could have large variability due to the prevalence of one of these three main processes, which will be discussed below: 1) the accumulation of lipids in the sub-endothelium of the arteries 2) the establishment of an inflammatory status by infiltration of lymphocytes and macrophages which, engulfing lipids accumulated, become foam cells 3) migration and proliferation of smooth muscle cells (SMCs) with production of extracellular matrix [7]. Consequently, some atherosclerotic lesions appear predominantly dense and fibrous, whilst others can contain large amounts of lipid and necrotic debris, while most of them are the result of combinations of both characteristics.

3.1 Initial steps of atherosclerosis

The earliest events of atherosclerosis take place in the endothelium, the intima layer of artery walls. Normally an healthy endothelium exerts its antiatherogenic duty through the regulation of vascular tone and homeostasis, smooth muscle cells proliferation, platelet aggregation and adhesion, leukocyte migration, thrombosis and thrombolytic events [8].

Particularly, endothelial cells synthesize a wide range of autocrine and paracrine substances: for example, nitric oxide (NO), prostacyclin and histamin are involved into vasodilation while angiotensin, endothelin and serotonin are vasoconstrictors. The antithrombotic activity of endothelium is exerted through the secretion of antiaggregatory molecules, such as NO and prostacyclin, anticoagulatory molecules, (heparin and heparan sulfate), and through activation of fibrinolysis, by secretion of tissue plasminogen activator (t-PA) and plasminogen activator inhibitor-1 (PAI-I) [9].

It is evident that numerous biological pathways cooperate in ensuring vascular homeostasis and even a partial loss of their functionality can lead to endothelial dysfunction. The risk factors that contribute to the initial dysfunctions of atherosclerosis can be divided into two categories: systemic and hemodynamic. Among systemic factors, we find unchangeable risks, such as age, gender, race, heredity and changeable risk factors, such as hypertension, high cholesterol, hyperhomocysteinemia, smoke, obesity and physical inactivity. The

hemodynamic factors which contribute to endothelial dysfunction will be further discussed.

These pathological states are associated to pro-inflammatory stimuli and to the increase in oxidative stress, in particular, through the production of reactive oxygen species (ROS) [10]. High ROS levels cause a decrease in NO availability, which leads to vasoconstriction, smooth muscle cells proliferation and migration, platelet aggregation and leukocyte adhesion, all events that underlie plaque formation. Moreover low NO levels may induce caveolin 1-dependent oxidation of LDL cholesterol, which in turn inhibits endothelial NO syntase (eNOS) activity, causing a further reduction of NO synthesis [8]. LDL modification not only involves ROS but also other enzymes, such as myeloperoxidase which generates, from hydrogen peroxide and chloride, high levels of hypochlorous acid, that causes a further oxidation of lipoproteins [11]. Oxidation of LDL is known to be, along with endothelial dysfunction, one of the pivotal mechanisms of atherosclerotic plaque formation. Particularly, changes in the endothelial cells permeability cause a subendothelial retention of atherogenic cholesterol-containing LDL (Figure 2A) and numerous evidences suggest a tight link between high levels of circulating LDL and their accumulation, by a passive diffusion through EC tight junctions, in the subendothelial matrix [12]. LDL retention, mediated by interaction between LDL apoliprotein b (Apo B100) and matrix proteoglycans, predispose them to oxidative modification [13]; Oxidized LDL (oxLDL) in turn stimulate endothelial cells to produce adhesion molecules, such as Vascular Cell Adhesion Molecule 1 (VCAM-1) and Intercellular Adhesion Molecule 1 (ICAM-1), chemotactic molecules, such as Monocyte Chemoattractant Protein-1 (MCP-1), and growth factors, such as Macrophage Colony-Stimulating Factor (M-CSF)[14,15]. This "activated" status of endothelial cells mediate transmigration of T lymphocytes and monocytes through luminal endothelium in the intima. Here, monocytes proliferate and differentiate into macrophages (Figure 2B). The latter adopt a pro-inflammatory phenotype and encode a wide range scavenger receptors (LOX-1 and CD36 needed for oxLDL uptake) which in turn are stimulated by macrophages-produced cytokines, such as tumor necrosis factor α (TNFα) and interleukin-1β (IL-1β) [16]. This pro-inflammatory condition induces macrophages to constantly adsorb oxLDLs until they become like "foam cells" and their accumulation in the intima layer lead to fatty streaks formation (Figure 2B).

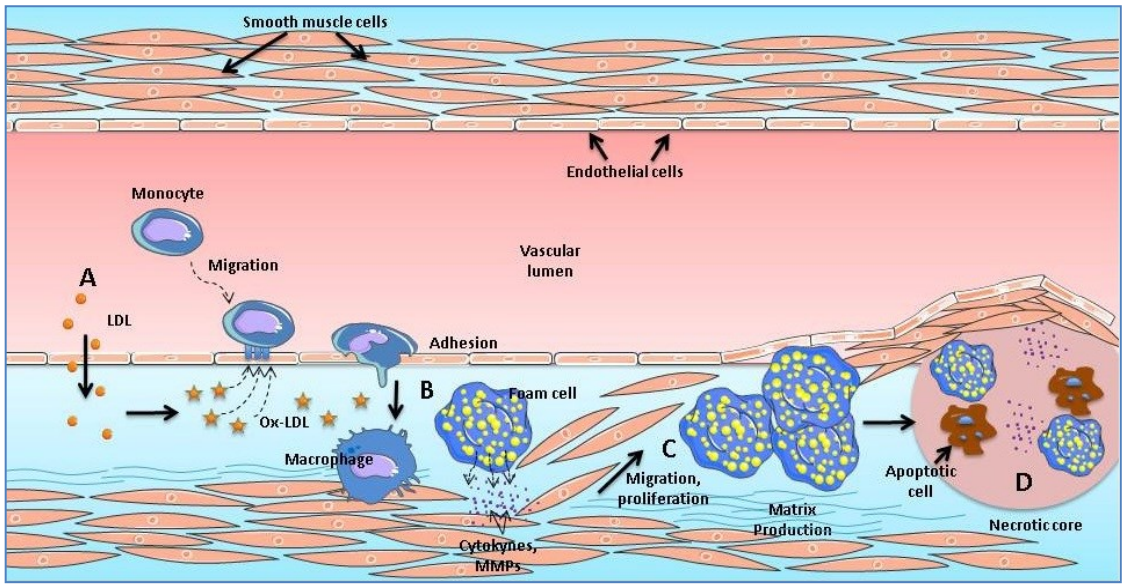

Figure 2: Atherosclerotic plaque formation. Alteration of endothelial cells permeability promotes lipids infiltration and accumulation (A). Monocytes from blood flow penetrate into the intima, differentiate in macrophages and internalize lipids, forming foam cells (B). In response to pro-inflammatory cytokines and MMPs secretion, VSMCs proliferate and migrate (C), secrete extracellular matrix which form the fibrous cap of atheroma (D) [17].

3.2 Progression of atherosclerotic lesion and advanced lesions

Recruitment of smooth muscle cells (SMCs) from tunica media is involved in plaque formation, too (Figure 2C). Numerous growth factors (EGF, PDGF, TGF, VEGF) and hormones, such as Angiotensin II, activate uncontrollably the SMCs and they switch from a quiescent phenotype to a migratory and synthetic one. These "active" SMCs secrete high levels of metalloproteinases (MMPs), which promote SMCs migration from the media into the intima via degradation of SMCs' membrane degradation [11]. Moreover, under the influence of cytokines and growth factors secreted by foam cells and T cells, SMCs synthesize extracellular matrix (ECM) proteins, resulting in pathogenic vascular remodeling and intimal stiffening [18,19].

These ECM molecules, including interstitial collagen and elastin, form a fibrous cap that covers the plaque and overlies macrophage-derived foam cells, some of which die by apoptosis and release lipids that accumulate in extracellular space. In the early stages of atherosclerosis the removal of apoptotic macrophages (efferocytosis), is efficient and stimulates production of anti-inflammatory cytokines, such as interleukin-10 (IL-10) and transforming growth factor-β (TGF-β). *Vice versa* in advanced lesions efferocytosis is compromised and necrotic macrophages, cellular debris and extracellular lipids form a lipid-rich pool called necrotic core (Figure 2D) [20]. The balance between fibrous cap and necrotic core influences the rupture of the plaques. It has been seen that caps of ruptured

plaques have high density of macrophages and a large lipid core topped by a thin fibrous cap [21]. Moreover, in lipid-rich plaque an important role is assumed by T lymphocytes, which elaborate high levels of interferon γ (IFN-γ). INF-γ inhibits SMCs proliferation and collagen synthesis, making plaques more prone to rupture. Conversely, stable plaques have a thick fibrous cap over a small fatty core and are rich in collagen. Thus, it is clear that two remodeling factors may operate during lesion formation: on one hand, SMCs stabilize the plaque by producing connective tissue preventing plaque rupture and, on the other hand, macrophages and T cells elaborate enzymes and cytokines respectively that weaken the plaque framework [22,23].

Plaque staibility may be influenced by calcification and neovascularization, processes which characterize advanced lesions.

Calcification, which reflects more stable lesions [24], consists in a gradual accumulation of mineral deposits, expecially hydroxyapatite, on death cells and extracellular lipids [25]. Moreover, in these plaques cell attachment proteins (osteopontin), proteins associated with calcium (osteonectin), and γ-carboxylated proteins that regulates mineralization (osteocalcin) were identified. Watson KE et al. demonstrated that TGF-β and 25-hydroxycholesterol stimulate bone morphogenetic protein-2, a powerful factor for osteoblastic differentiation, suggesting that calcification is a regulated process similar to bone formation [26].

Neovascularization consists in the growth of small vessels inside the plaque itself, mechanism highly influenced by inflammatory mediators and hypoxic signals. Monocytes and T-cells secrete factors such as fibroblast growth factor (FGF) and vascular endothelial growth factor (VEGF) that actively contribute to angiogenesis and, in turn, along with other cytokines (IL-6, MCP-1, TNF-alpha i.e.) and angiogenic factors (angiopoietin-2), stimulate inflammation and intraplaque hemorrhages, causing plaque instability and rupture [27,28].

3.3 Complications of atherosclerotic lesions

The evolution of the atherosclerotic lesions is extremely variable, so all the phenomena described for initial and late stages of atherosclerosis development may be more or less constant. Atherosclerosis' last event is plaque rupture: the exposure of tissue factor (TF) to blood flow leads to coagulation cascade activation with recruitment of platelets and inflammatory cells. The interaction between exposed atheroma tissue debris, platelet receptors and coagulation factors leads to the formation of a thrombus which may

compromise the arterial lumen, hindering blood flow *in situ* [29]. Some of these thrombi can detach from lesion site and, following the blood flow, can reach a branching site of a small vessels, blocking the blood flow.

Atherosclerosis does not have any clinical onset until an internal lamina is 40% clogged with plaque and symptoms depend on which arteries are affected.

The occluding stenosis are usually characteristic of the late stage of the plaque evolution. The effects of the reduction of blood inflow to the tissues, are more or less serious depending on whether the supply of oxygen is absent or reduced.

The most common complications of atherosclerosis are:

1. Coronary artery disease: it consists in an ischemic process involving the arteries that supply blood to the heart, resulting in i) *angina pectoris*, chest pain due to insufficient oxygenation of myocardium ii) myocardial infarction, an injury due to blood flow impairment in an area of the heart iii) heart failure, when heart is unable to pump blood to all body districts.
2. Carotid artery disease: carotid arteries supply blood to the brain and their narrowing can cause i) stroke, a sudden loss of brain function due to ischemia and symptoms may include speech and breath impairment, loss of vision and coordination, severe headache and paralysis ii) transient ischemic attack (TIA), due to a temporary blood supply deficit in a small area of brain causing a momentary loss of neurological skills.
3. Peripheral artery disease: it involves narrowing of major arteries that supply blood to the arms, legs and pelvis. Usually the main clinical events are pain and numbness but if artery occlusion is extreme, it leads to tissue death (gangrene).

Along with these complications, there are other minor atherosclerotic events that may involve kidneys (renal artery stenosis), sex organs (erectile dysfunction), eyes (eye stroke) and abdomen (mesenteric ischemia).

Lastly, another complication is the aortic aneurysm, due to the collapse of vessel wall resulting in an abnormal dilatation of aorta, especially in the abdominal region. Aneurysm rupture is the most dangerous event that could happen with consequent internal bleeding, eventually resulting in death [30].

4. Shear Stress: hemodynamic forces and molecular pathways

As previously described, the endothelium can be considered as a thin barrier between blood flow and vessel wall and, therefore, it is exposed to different hemodynamic forces. Particularly it is exposed to three different forces: i) *shear stress,* which is the tangential frictional force of the flowing blood on the endothelium, and his magnitude is expressed in units of force per unit area (Newtons per square metre or Pascals or dynes per square centimetre; 1 N/m^2 = 1 Pa = 10 dyn/cm^2), ii) cyclic strain, the transumural force acting on the vessel wall, due to the pulsatile nature of blood flow and iii) hydrostatic pressure, the force that blood exerts on the vessel walls (Figure 3) [31].

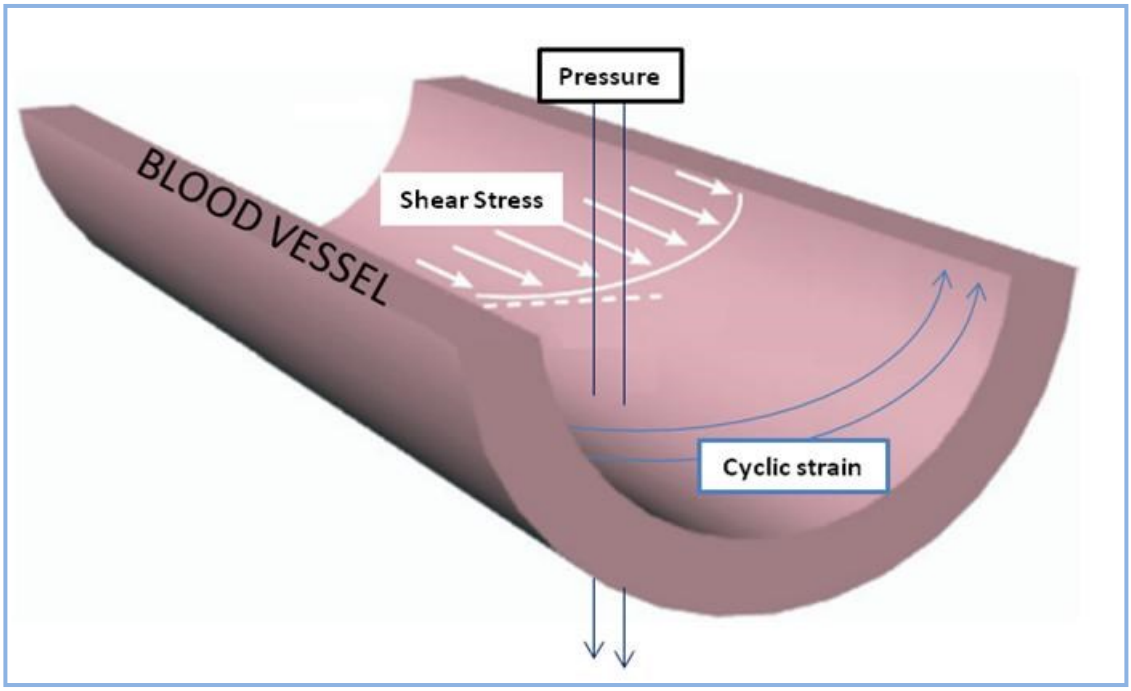

Figure 3: Hemodynamic forces. Scheme of principal forces acting inside the blood vessels (adapted from Chatzizisis et al. [32])

It has been well studied that endothelial cells are sensitive to those hemodynamic forces and, through mechanotrasduction, they convert a mechanic stress into a biological pathways, responsible for maintenance of vascular homeostasis. This process involves a wide range of mechanosensors (ion channels, receptors for tyrosine kinase, G protin-coupled receptors, junction proteins, integrins and membrane lipids i.e.) so that they under intensive study to understand the normal and pathological biochemical signals that they could generate [33].

Contextually to atherosclerosis, the geometric structure of the arterial tree has a pivotal role in regulating the hemodynamic forces which in turn modulate activation of

mechanosensors. In particular, *shear stress* has a critical role in determining where atherosclerotic plaques could form [34–36]. Endothelial SS (ESS) patterns are determined both by the pulsatile nature of blood flow in arteries and by the geometric structure of the vessels. Principally, in straight areas of vascular tree, the blood flow is laminar and the ESS is pulsatile and unidirectional (magnitude: 15-70 dyne/cm^2), whereas in geometrically irregular regions, such as curves and branches, the blood flow becomes disturbed and underlies Low and Oscillatory ESS (LO ESS). Low ESS, which occurs at the inner areas of curvatures, as well as upstream of stenoses, is unidirectional and with a fluctuating magnitude, resulting in a low time average (magnitude <10 to 12 dyne/cm^2) [32]. Oscillatory ESS, which occurs primarily at the lateral walls of bifurcations, in the vicinity of branch points and downstream of stenose, is bidirectional with a very low magnitude between systole and diastole (close to 0 dynes/cm^2) (Figure 4).

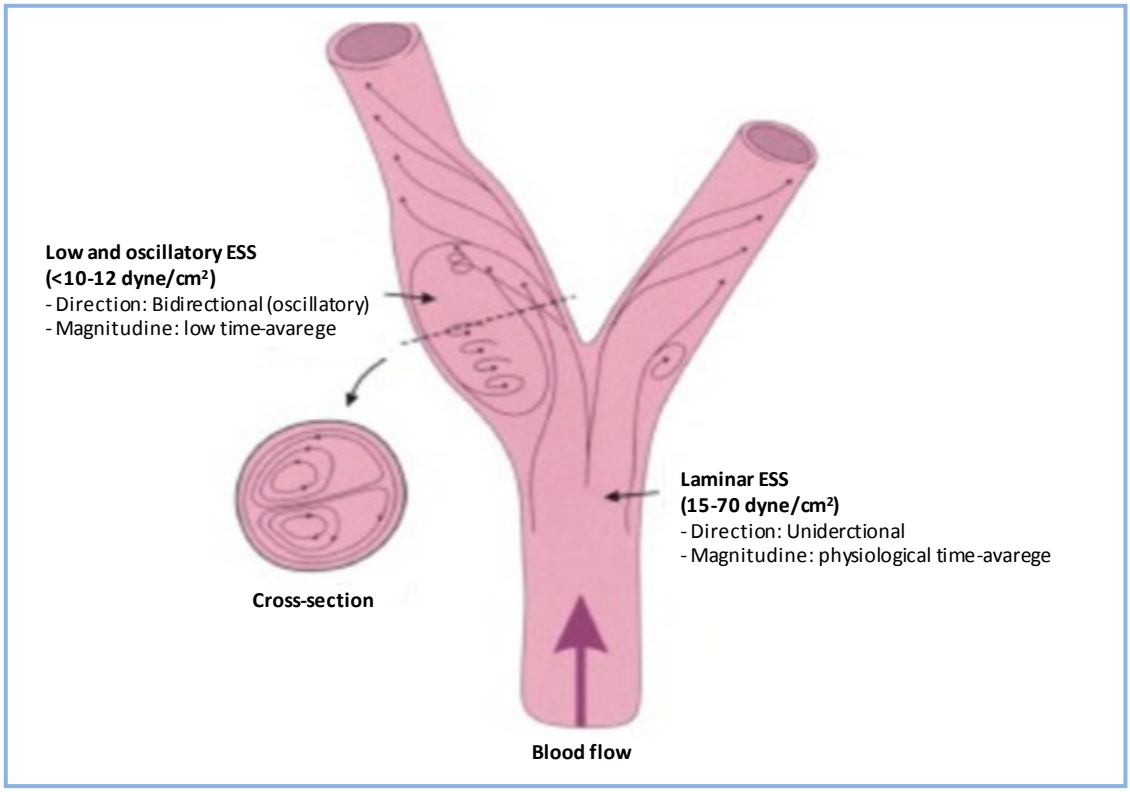

Figure 4: Definition and example of laminar (pulsatile) and low and oscillatory shear stress (Image from Chatzizisis et al. [32])

The link between ESS patterns and localization of atherosclerotic plaques was demonstrated for the first time in 1969 by Caro et al. [37] and, since then, numerous *ex vivo*/*in vivo* investigations and computational fluid dynamic simulations were carried on in the last years, showing that some areas of arterial tree subjected to LO ESS were more prone to plaques development [38–43]. These findings are supported by *in vitro* data

showing that endothelial cells cultured under low shear stress show high ROS levels, whereas high, laminar shear stress is protective, inhibiting apoptosis. [44,45].

Moreover, still today, numerous studies are conducted with the aim to define the shear stress patterns during systolic and diastolic phase of a cardiac cycle: in "linear" areas of the vasculature, where laminar shear stress occurs, during systole, the highest values of shear stress magnitude are reached, whereas during diastole the magnitude values are lower but still positive, indicating that in these districts blood flow is always arranged in ordered laminar patterns and his pulsatile nature causes only a variation of shear stress magnitude into a high-protective range. At the areas with a complex vascular geometry, such as the aortic arch, blood flow is organized in separated flow patterns and, as previously mentioned, LO ESS occur. Here, the shear stress exhibited remarkably lower and oscillatory values in systole as compared with that in diastole, favoring atherosclerosis onset and progression. Since the early studies correlating the position of the human carotid plaque and LO ESS [46], the relevance of these studies lies in the fact that elevated heart rate, increasing the relative time spent in systole, as compared to diastole, would increase the exposure of areas prone to plaque development to the most atherogenic shear stress patterns [47,48].

Numerous studies seem to indicate that LO ESS has a cardinal role in all the steps towards atherosclerotic plaques formation:

- LO ESS stimulates LDL retention within the subendothelial area, by enhancing endothelial cells turnover and altering tight junctions between cells, resulting in more LDL infiltration [33]. Moreover, low ESS enhances the espression of LDL receptor by activating sterol regulatory elements binding pronteins (SREBPs), a process mediated by integrins [49]
- Unidirectional ESS stimulate NO production, through eNOS gene expression and protein activation, leading endothelial cells to a more physiological condition. Conversely LO ESS inhibits NO production and stimulates other vasoconstrictors, such as endothelin-1 [50,51]. Moreover, NO bioavailability is decreased by high ROS levels (as a result of an increased NADPH oxidase gene expression), which augments oxidative stress and LDL oxidation [52]. This inflammatory status leads to the activation of adhesion molecules (VCAM-1, ICAM-1) chemotactic molecules (MCP-1) and cytokines (TNF-α, IL-1 and IFN-γ) which sustain atherosclerosis progression.
- LO ESS promotes SMCs migration from media to intima via ECMs degradation through upregulation of pro-inflammatory stimuli, which stimulate MMPs synthesis by macrophages.

- LO ESS-mediated IFN-γ inhibits ECMs synthesis by SMCs and contemporarily induces SMCs apoptosis, sustained by TNF-α, IL-1β, affecting plaque stability [53].
- Downregulation of eNOS e t-PA genes mediated by LO ESS increases plaque instability which, along with a simultaneous accumulation of platelets near the region of vascular wall subjected to low ESS, enhances thrombi formation [54].
- LO ESS promotes neovascularization by upregulating VEGF expression [55] and other angiogenic factors (angiopoietin-2 [56]). Along with increased inflammation, oxidative stress and MMPs synthesis, it enhances plaque instability.
- Bone morphogenic protein 2 and 4 (BMP2/4), which participate in plaque calcification, are upregulated in atherosclerotic lesions, and their inhibition reduces vascular calcification and atherosclerosis [57]. It has been seen that LO ESS stimulates BMP4 in ECs, inducing NADPH-mediated ROS production which, as previously described, enhances atherosclerotic lesion progression [58].

The evaluation of these pathway, along with the hemodynamic studies of the forces acting inside the artery vessels, could be a new diagnostic approach in identifying risk factors involved in development of atherosclerotic events [59].

5. Ivabradine: a pure heart rate-reducing molecule

Resting heart rate (HR) is regulated by spontaneous depolarization of sinoatrial node myocytes. These cells don't have a true resting potential, but they generate spontaneous action potential. The depolarization is sustained by voltage-sensitive membrane mixed Na^+-K^+ inward current, namely the current funny (I_f), which was first described in the late 1970s and has been widely characterized in the last decades [60,61].

Pacemaker activity makes funny channels an obvious target for new drugs aiming at regulation of heart rate. The research on these drugs has become of great interest in light of the fact that the link between elevated heart rate and cardiovascular events is well established in patients with cardiovascular disease [62,63].

The amplitude of I_f current determines the slope of the diastolic depolarization phase and thereby the HR. Ivabradine ({7,8-dimethoxy 3-propyl}1,3,4,5-tetrahydro-2*H*-3-benzazepin-2-one) (Figure 5) decreases HR by specific and selective binding of hyperpolarization-activated cyclic nucleotide-gated (HCN) channels, particularly HCN4 isoform, which generate the I_f current in the sinus node, slowing the diastolic depolarization slope without affecting blood pressure or cardiac contractility [64–66].

Ivabradine blocks I_f channels by interacting with them from the intracellular side, when they are in open state, indicating that it acts in current-dependent manner, since when the channels are closed it cannot reach its binding site [67].

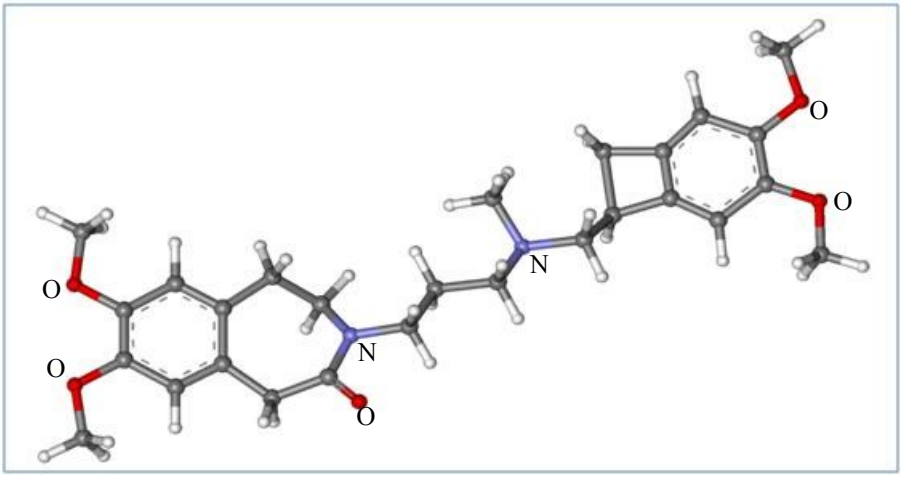

Figure 5: Ball-and-stick model of ivabradine molecule. N: Nitrogen; O: Oxygen. The structure is taken from ChemSpider.

Recent studies have demonstrated a protective effect of ivabradine on the vasculature (reviewed in [68]). In mouse models of mild (hApoB+/+ [69]), or severe (LDLr-/- hApoB+/+ [70]; ApoE-/- [71;,72;,73;,74]) dyslipidemia, ivabradine prevented endothelial dysfunction in several vascular beds (aorta, coronary, renal and cerebral arteries). Furthermore, ivabradine was able to reduce aortic plaque area in ApoE-/- [71;,73] and LDLr-/- hApoB+/+ [70] mice models of atherosclerosis fed a western diet.

The vascular effects of ivabradine were associated with a reduction of vascular oxidative stress (decrease of NADPH oxidase activity [71;,74] and eNOS uncoupling [74]), decrease of pro-inflammatory chemokine MCP-1 [71] and of AT1-R expression [74]. Ivabradine's vascular effects are not the consequence of a lipid-lowering activity, since the drug did not alter cholesterol and triglyceride levels [69;,71;,74]. Additionally, at therapeutic relevant concentrations, ivabradine *ex vivo* (i.e. directly incubated with isolated arteries) had no effects on normal vascular physiology [69]. Interestingly, the *in vivo* beneficial effects of ivabradine on endothelial dysfunction could not be reproduced *ex vivo* [69;,71]. Taken together, these results indicate that a direct effect of ivabradine on vessels is unlikely, and suggest that the reduction of heart rate could be the primary mechanism of action of the drug.

In cynomolgus monkeys with elevated heart rate, coronary artery atherosclerotic lesions were more than twice as extensive as their lower heart rate littermate [75]. In young post-

myocardial infarction patients, a significant correlation was found between heart rate and severity and progression or coronary atherosclerosis [76]. In accordance with these observations, the reduction in resting heart rate by metoprolol, a beta-blocker, slows endothelial cell replication (a marker of dysfunction/activation) in psychologically stressed cynomolgus monkeys [77], while the reduction in resting heart rate by surgical ablation of the sinoatrial node slows the atherosclerotic process in the cynomolgus monkeys fed a high fat diet [78;,79].

AIM OF THE STUDY

Data from the literature support the detrimental effect of elevated heart rate in the pathogenesis of atherosclerotic plaques which are prone to develop in the arterial regions characterized by disturbed flow.

Numerous studies demonstrated that ivabradine limits atherosclerotic plaques formation in animal models. The mechanism of this protection is still unknown. It has been hypothesized that as heart rate decreases, following ivabradine treatment, the diastolic phase increases, thereby decreasing the exposure time of aortic arch endothelium to systolic flow, which is characterized by a more atherogenic low and oscillatory shear stress (Figure 6).

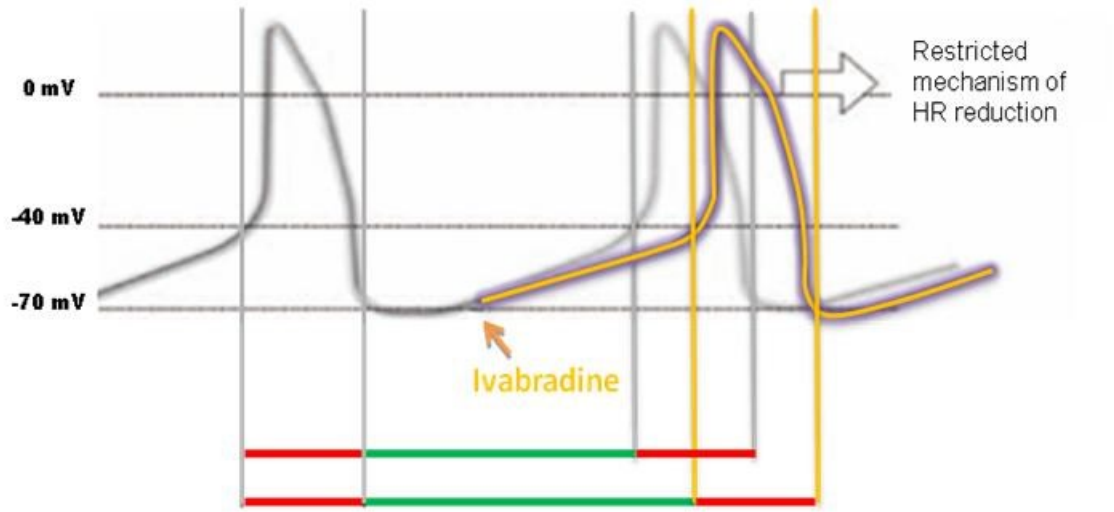

Figure 6: Schematic representation of systolic and diastolic phase during a cardiac cycle. Ivabradine treatment (orange arrow) does not alter the systole (red bars) but prolongs the diastole (green bar).

The aim of this study was to determine the molecular effect of a short-term treatment with ivabradine in the initial steps of atherosclerosis development in an *in vivo* model of severe dyslipidemia (ApoE deficient-mouse) fed a standard diet.

MATERIALS AND METHODS

1. Mice and ivabradine treatment

C57BL6/J and ApoE deficient mice were purchased from Charles River Laboratories (Wilmington, MA, US). In our animal facility, all animals were exposed to a semi-natural light cycle of 12:12 and were caged at room temperature (21-23 °C) with 55-60% of humidity. During the 6 days of acclimatation, all animals received water *at libitum*. At day 7 water was changed to ivabradine solution (15 or 30 mg/kg/day – Servier, France) for treating ApoE-/- mice. All animal studies were carried out according to the guidelines of the European (86/609/EEC) and the Italian (D.L.116/92) laws and after approval by the local ethical review panel of University Animal House and by the Italian Ministry of University and Research.

- **Endothelial enriched-RNA extraction studies**: preliminary experiments to determine the yield and the quality of RNA extraction from endothelium of mice aortic arches were conducted on ten 10-weeks old C57BL6J mice. Five 10-weeks old C57BL6/J mice were sacrificed to extract RNA from the whole aorta. Seven 10-weeks old C57BL6/J mice were sacrificed for qRT-PCR analysis of Notch components
- **Time course experiment**: sixteen 5-weeks old ApoE -/- mice were sacrificed when they reached the age of 6 (n=4), 7 (n=4) , 8 (n=4) and 10 (n=4) weeks.
- **Test ivabradine dose**: to establish the exact dose of ivabradine treatment, ten 5-weeks old ApoE-/- mice, after one week acclimatation, were treated for one week with 15 mg/kg/day (n=5) or with 30 mg/kg/day (n=5) of ivabradine.
- **Main experiment:** twenty two 5-weeks old ApoE -/- mice, after one week acclimation, were randomly assigned them to four treatment groups receiving 1) 30 mg/kg/day of ivabradine for two weeks (n=9), 2) 30 mg/kg/day of ivabradine for four weeks (n=9), 3) and 4) no treatment for two (n=2) and four weeks (n=2).
- **En-face studies**: for endothelial dysfunction studies thirteen 5-weeks old ApoE -/- mice were sacrificed when they reached the age of 10 (n=4), 18 (n=4) and 25 (n=5) weeks (no ivabradine treatment). Five 5-weeks old ApoE-/- mice, after one week acclimation, were treated for nineteen weeks with ivabradine (30 mg/kg/day) and then sacrificed when they reached the age of 25 weeks. For en-face analysis of Hes5 protein levels ten 5-weeks old ApoE-/- mice, after one week acclimation, were randomly assigned them to 2 treatment groups receiving 1) 30 mg/kg/day of ivabradine for four weeks (n=5) and 2) no treatment for 4 weeks. Eight 10 weeks old C57BL6/J mice were sacrificed for en-face analysis of Notch components.

2. Heart rate measurement

Animals were not anesthetized during this procedure to avoid interferences with ivabradine treatment. To avoid stress which could affect heart rate, at least 2 days before heart rate measurement, mice chest was shaved at third and fourth intercostal space, next to the sternum. Mice were handled carefully, taking them from the neck and placed with head up. Heart rate was monitored by Doppler echocardiography (Vivid ECG, GE Healthcare Worldwide) and using a pediatric probe (Vivid cardiovascular ultrasound 12S R-S, GE Healthcare Wordlwide), by counting the number of waveforms registered per minute. During each procedure, 20 measurements (30 seconds each) were obtained and averaged for each individual animal. In treated mice of main experiment, heart rate was measured before the beginning of treatment (baseline) and one week before sacrifice (9 and 21 days for the 2 weeks and 4 weeks treatment groups, respectively). Results were expressed as mean ± SEM. Differences between groups were analyzed by unpaired t-test and $p<0.05$ was considered significant.

3. Anesthesia

All procedures that implied the sacrifice of mice were carried out by inducing a pharmacological coma with an overdose of Zoletil (100 mg/kg; Parnell Laboratories, Alexandria, NSW, Australia) and Dexdomitor (25 mg/kg; Zoetis, Florham Park, NJ, US).

4. Cell culture

Human umbilical vein endothelial cells (HUVECs) pools (Life Technologies, CA, US), were plated in gelatin-coated tissue culture dishes and maintained in phenol red-free basal medium M200 (Life Technologies, CA, US) containing 5% FBS and growth factors (LSGS, Life Technologies, CA, US) at 37°C with 5% CO_2. Cells from passages 4 to 5 were actively proliferating (70–90% confluent) when subjected to cone and plate system studies for 24 hours.

5. *In vitro* flow experiments

To perform *in vitro* flow studies, a cone-and-plate flow apparatus was used. The cone is designed to fit into a 100-mm cell culture dish. The cone includes an upper lid that rests on the top of the dish to minimize the evaporation of the cell culture media. The lid also supports the free rotation of the cone on an axle secured by ball bearings and a setscrew, which controls the height of the cone from the cells plated in the cell culture dish. The cone is machined from a Teflon block to contain a 2.5-degree angle from its peak to its edge. Teflon does not typically bind proteins and additives from the media, and it does not interfere with cell viability. The cone can be smooth or grooved to mimic laminar or disturbed flows respectively. To rotate the cone, a magnetic stir bar is inserted into the cone that can be turned with a laboratory magnetic stirrer. The entire system (cone-and-plate and magnetic stirrer) is assembled in an incubator at 37 °C with 5% CO_2 (Figure 7).

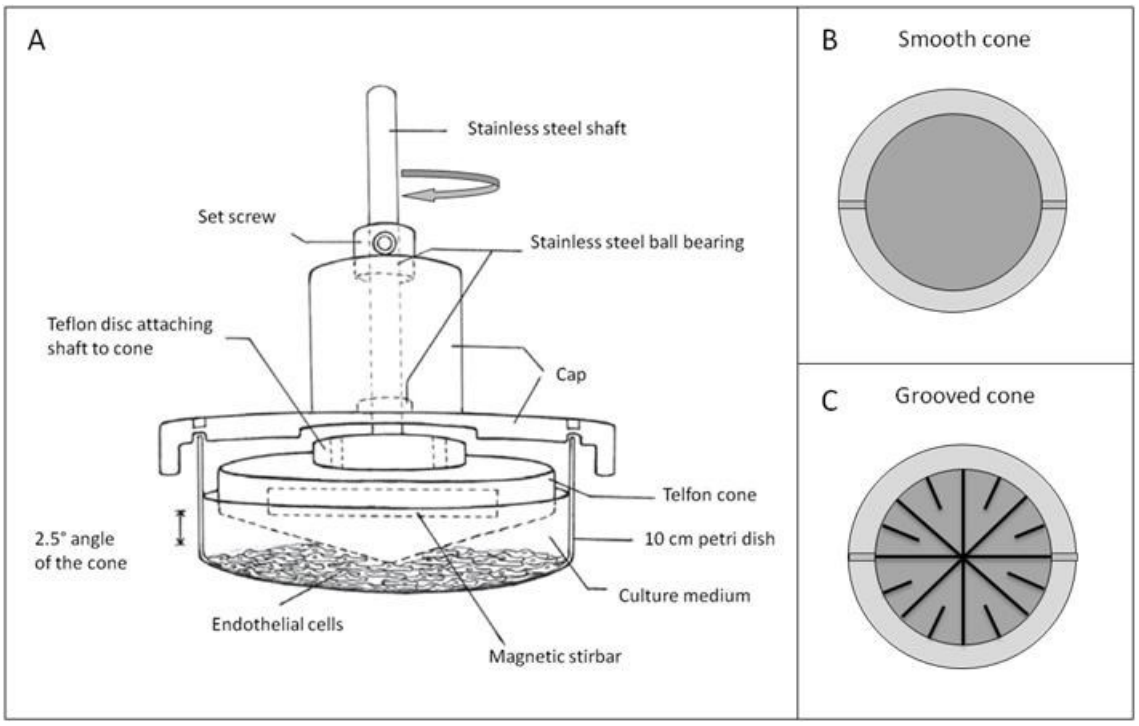

Figure 7: (A) Schematic representation of the cone and plate flow system. (B) Schematic representation of the contact surface area of a smooth cone. (C) Schematic representation of the contact surface area of a grooved cone. Image adapted from [80].

HUVECs cultured in 100-mm dishes were exposed to S-flow at 50 dyn/cm^2 (200 rpm) by using smooth cones or exposed to D-flow at 12.5 dyn/cm^2 (50 rpm) by using grooved cones for 24 hours. The shear stress imposed on the surface of cells was calculated by the formula $\omega\mu/\theta$ where ω is the rotation speed, μ is the fluid viscosity, and θ is the angle of

the cone. After 24 hours, at least five random images were taken for each 100-mm dish using a phase contrast microscope with a 4X objective to monitor the cells status.

6. Immunofluorescence on HUVEC cells

HUVECs grown on 100-mm dishes were rinsed in ice cold PBS 1X, fixed in 4% PFA for 15 min and rinsed twice in PBS 1X. HUVECs were permeabilized in PBS 1X + 0.2% Triton X-100 for 20 minutes and, after washing three times with PBS 1X, blocked in blocking buffer (10% NGS/PBS + 2.5% Tween-20) for 1 hour at room temperature. Cells were then incubated with the relative antibodies overnight at 4°C, previously prepared in the same blocking buffer. The primary antibodies used were Ve-Cadherin (1:250; BD Pharmingen), Notch1 (1:250; Millipore, MA, USA) and Notch4 (1:250; Millipore, MA, USA).

After washing cells three times in PBS 1X, secondary antibodies, previously prepared in blocking buffer, were added and incubated for 1.5 hours rocking at dark and at 4°C.

The secondary antibodies used were Alexa Flour 546 donkey Anti-Rabbit IgG (1:2000; Life Technologies, CA, US) and Alexa Flour 488 Goat Anti-Mouse IgG (1:500; Life Technologies, CA, US). After washing three times in PBS, ProLong Gold antifade (Life Technologies, CA, US) mounting medium was added and cells were covered with a coversplip. At least 5 images for a single staining were acquired on Zeiss LSM 510 confocal microscope with 40x magnification. Results were expressed as mean ± SEM. Differences between groups were analyzed by unpaired t-test and $p<0.05$ was considered significant.

7. RNA extraction from cells

Total RNA was extracted using a commercially available kit (Qiagen, CA, USA). RNA concentration and purity were determined by Agilent 2100 Bioanalyzer (Agilent Technologies, CA, US). Protocol for RNA extraction is summarized below:

1. Completely aspirate the cell-culture medium and disrupt the cells by adding 700µl of Buffer RLT to the cell-culture dish. Collect the lysate using a scraper. Pipet the lysate into a 2ml tube. Vortex or pipet to mix, and ensure that no cell clumps are visible before proceeding to step 2.

2. Pipet the lysate directly into a QIAshredder spin column placed in a 2ml collection tube, and centrifuge for 2 min at full speed.
3. Add 1 volume (700µl) of 70% ethanol to the homogenized lysate, and mix well by pipetting.
4. Transfer up to 700µl of the sample, including any precipitate that may have formed, to an RNeasy spin column placed in a 2 ml collection tube. Close the lid gently, and centrifuge for 15 s at 8000 x g (10,000 rpm). Discard the flow-through and reuse the collection tube in step 5.
5. Add 700 µl Buffer RW1 to the RNeasy spin column. Close the lid gently, and centrifuge for 15 s at 8000 x g (10,000 rpm) to wash the spin column membrane. Discard the flow-through and reuse the collection tube in step 6.
6. Add 500 µl Buffer RPE to the RNeasy spin column. Close the lid gently, and centrifuge for 15 s at 8000 x g (10,000 rpm) to wash the spin column membrane. Discard the flow-through and reuse the collection tube in step 7.
7. Add 500 µl Buffer RPE to the RNeasy spin column. Close the lid gently, and centrifuge for 2 min at 8000 x g (10,000 rpm) to wash the spin column membrane.
8. Place the RNeasy spin column in a new 2 ml collection tube (supplied), and discard the old collection tube with the flow-through. Close the lid gently, and centrifuge at full speed for 1 min.
9. Place the RNeasy spin column in a new 1.5 ml collection tube. Leave the tube open under chemical hood for 5 min to remove all traces of ethanol.
10. Add 30–50 µl RNase-free water directly to the spin column membrane. Close the lid gently, wait 3-5 min and centrifuge for 1 min at full speed to elute the RNA and the place the samples on ice.

8. Endothelial enriched-RNA extraction

After anesthesia, mice were placed in supine position and locked with needles. The peritoneum was opened and the thoracic cavity was completely cut, exposing heart and lungs. Then the left common iliac artery was cut to drain blood. To facilitate this procedure, a 26g needle was inserted into left ventricle and the heart was perfused, by gravity, with ice cold saline. When the effluent was completely clear, aorta was quickly and carefully isolated and placed into a Petri dish containing a RNAlater solution (RNA stabilization solution, Ambion). Under stereomicroscope (SMZ745T 6x-50x, Nikon, Chiyoda, Japan) the adventitial layer and fat portion of the aorta was cleaned off by

straining the aorta oppositely with angled forceps. Aortic arch was isolated cutting the aorta at the border of the thoracic portion. A microloader tip (Eppendorf - Germany) was adapted to an insulin syringe and filled with 300ul of Qiazol lysis solution (Qiagen, USA).

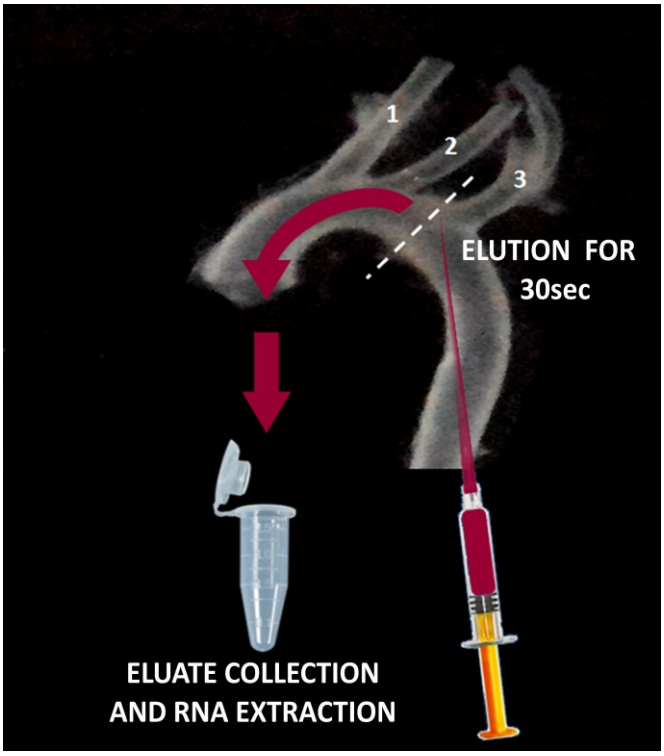

Figure 8: Scheme of technique utilized for flushing mice aorta. (1) Brachiocephalic trunk (2) Left common carotid artery (3) Left subclavian artery.

As shown in Figure 8, the microloader tip was carefully inserted in the aortic arch until it reached the left common artery, entering from the previously removed portion of thoracic aorta. Aortic arch was flushed with Qiazol lysis solution for 30 seconds and the eluate was collected into a RNase-free microfuge tube. As a control, RNA was isolated from other whole arch after mechanical disruption of the tissue using a Dounce homogenizer. In both cases, RNA was extracted using a commercially available kit (miRNeasy mini kit - Qiagen, CA, USA). RNA concentration and purity were determined by Agilent 2100 Bioanalyzer (Agilent Technologies). Protocol for RNA extraction is summarized below:

1. Add other 400ul of Qiazol lyisis buffer to the eluate
2. Add 140 µl chloroform to the tube containing the homogenate and cap it securely. Shake the tube vigorously for 15 s.
3. Place the tube containing the homogenate on the benchtop at room temperature for 2–3 min.

4. Centrifuge for 15 min at 12,000 x g at 4°C. After centrifugation, heat the centrifuge up to room temperature (15–25°C) if the same centrifuge will be used for the next centrifugation steps. After centrifugation, the sample separates into 3 phases: an upper, colorless ,aqueous phase containing RNA; a white interphase; and a lower, red, organic phase. The volume of the aqueous phase should be approximately 350µl.
5. Transfer the upper aqueous phase to a new collection tube (supplied). Add 1.5 volumes (usually 525 µl) of 100% ethanol and mix thoroughly by pipetting up and down several times. Do not centrifuge.
6. Pipet up to 700 µl of the sample, including any precipitate that may have formed, into an RNeasy Mini spin column in a 2 ml collection tube. Close the lid gently and centrifuge at ≥8000 x g (10,000 rpm) for 15 s at room temperature (15–25°C). Discard the flow-through.
7. Repeat step 6 using the remainder of the sample. Discard the flow-through.*
8. Pipet 500 µl Buffer RPE onto the RNeasy Mini spin column. Close the lid gently and centrifuge for 15 s at 8000 x g (10,000 rpm) to wash the column. Discard the flow-through.
9. Add another 500 µl Buffer RPE to the RNeasy Mini spin column. Close the lid gently and centrifuge for 2 min at 8000 x g (10,000 rpm) to dry the RNeasy Mini spin column membrane.
10. Transfer the RNeasy Mini spin column to a new 1.5 ml collection tube (supplied). Pipet 30–50 µl RNase-free water directly onto the RNeasy Mini spin column membrane. Close the lid gently and centrifuge for 1 min at 8000 x g (10,000 rpm) to elute the RNA.

9. Reverse Transcription and Real Time PCR

500 ng of total RNA (from cells) or 140ng of total RNA (pool from 2 aortas) were reverse transcribed in a volume of 25 ml using 250 units of SuperScript III reverse transcriptase and 50 ng of random hexamers. Here briefly report the protocol:

1. Mix and briefly centrifuge each component before use.
2. Combine the following components in a 0.2- or 0.5-ml RNAse free tube:

Random Primer (50ng/ul)	RNA (500ng)	dNTPs	DEPC- water	TOTAL
2,5 µl	4 µl	1,25 µl	8,5 µl	16,25 µl

3. Incubate at 65°C for 5 min, then place on ice for at least 1 min.

4. Prepare the following cDNA Synthesis Mix:

5x First Strand Buffer	0,1M DTT	Rnase OUT	SuperScript III RT	TOTAL
5 µl	1,25 µl	1,25 µl	1,25 µl	8,75 µl

5. Add 8.75 µl of cDNA Synthesis Mix to each RNA/primer mixture, mix gently, and collect by brief centrifugation. Incubate as follows.

- 10 min at 25°C
- 50 min at 55°C
- 15 min at 85°C → chill on ice.

2 µl of the cDNA mixture were used for realtime PCR experiments. Real-time PCR reactions were conducted on an Applied Biosystems 7500 Fast Real-Time PCR System using PerfeCta SYBR Green SuperMix with ROX kit (Quanta Biosciences, MD, US) according to the manufacturer's protocol in a final volume of 25 µl. Primers concentration was 500 nM. The following primers were used:

	Homo sapiens primers list	Mus musculus primers list
RPL13A forward	GGAGGTGCAGGTCCTGGTGCTT	AGCCCAGGGTGCTTTGCGG
RPL13A reverse	CGTACGACCACCACCTTCCGG	GCGCCATGGCTGCCTCCTATAC
Hey1 forward	CCGAGATCCTGCAGATGACCGT	
Hey1 reverse	AACGCGCAACTTCTGCCAGG	
Hey2 forward	AAAAGGCGTCGGGATCG	GAACAATTACCCTGGGCACG
Hey2 reverse	AGCTTTTTCTAACTTTGCAGATCC	TTCGATCCCGACGCCTTTTT
Hes1 forward	CGGACATTCTGGAAATGACA	
Hes1 reverse	CATTGATCTGGGTCATGCAG	
Hes5 forward		TAATCGCCTCCAGAGCTCCA
Hes5 reverse		GCTTCCGCAGTCGGTTTTTC
Notch 1 forward	GTCAACGCCGTAGATGACC	ACAGTGCAACCCCCTGTATG
Notch 1 reverse	TTGTTAGCCCCGTTCTTCAG	TCTAGGCCATCCCACTCACA
Notch2 forward	CAGGCACTCGGGGCCTACTCT	
Notch2 reverse	AGCCAGGCAAGCAGCGACAA	
Notch 4 forward	CAACTGCCTCTGTCCTGATG	TCCCTCTAACCTGCATCCCA
Notch 4 reverse	GCTCTGCCTCACACTCTG	TTTCTCACAGTGCCCGTTGT
Jagged-1 forward	GACTCATCAGCCGTGTCTCA	
Jagged-1 reverse	TGGGGAACACTCACACTCAA	
Jagged-2 forward	TGCAAAAACCTGATTGGCGG	
Jagged-2 reverse	TTCACCAGGTCCTTGCAGGT	
Olr 1forward		TGCAAACTTTTCAGGTCCTTGT
Olr1 reverse		AACTGGCCACCCAAAGATTG
NPPC forward	CCTGGGATGTTAGTGCGGC	ACACCACCGAAGGTCCCG
NPPC reverse	GCGTTGGAGGTGTTTCCAGA	TCGGTCTCCCTTGAGATTGG
SM 22 forward		GGGCGGCAGAGGGGTGACAT
SM 22 reverse		TGAGGCAGAGAAGGCTTGGTCGT
eNOS forward		TTCCCCGCCTAGTCCTCGCC
eNOS reverse		CCGGGGGTCCTGGCTGAGAG

Changes in gene expression were calculated by the $2^{-\Delta\Delta Ct}$ formula using RPL13A as reference gene. Results were expressed as mean ± SEM. Differences between groups were analyzed by unpaired t-test and $p<0.05$ was considered significant.

10. Microarray Analysis

Time course experiment: Sixteen ApoE -/- mice (5 weeks old) were received and let acclimate for one week in our animal facility before extracting RNA from the first group (6 weeks old). RNA from 6-, 7-, 8- and 10-weeks old ApoE -/- mice was isolated by flushing the aortic arch and was purified using the miRNeasy mini kit, as previously described. 70ng of RNA from 2 mice in each age group of age, analyzed in duplicate, were pooled to obtain a final amount of 140ng. RNA from 8 samples was hybridized on a slide containing 8 slots as described in the following table:

ApoE-/- mice (n=4/group)	**Microarray Chip**	
6 weeks old	**ApoE 1 + ApoE 2**	**ApoE 3 + ApoE 4**
7 weeks old	**ApoE 5 + ApoE 6**	**ApoE 7 + ApoE 8**
8 weeks old	**ApoE 9 + ApoE 10**	**ApoE 11 + ApoE 12**
10 weeks old	**ApoE 13 + ApoE 14**	**ApoE 15 + ApoE 16**

Main experiment: Eighteen 5 weeks old ApoE -/- mice were received and let acclimate for a week in our animal facility before beginning treatment (30 mg/kg/day in drinking water *ad libitum* – 2 o 4 weeks treatment). At the end of the treatment, a microarrays analysis was conducted to characterize changes in the gene expression profile in endothelial cell-enriched RNA purified from aortas of 8 and 10 weeks old ApoE-/- mice, following 2 weeks and 4 weeks ivabradine treatment respectively. RNA quality and yield was determined by Agilent 2100 Bioanalyzer (Agilent Technologies).

70ng of RNA from 2 mice in each treated group were pooled to obtain a final amount of 140 ng (each treated age group was analyzed in triplicate – n=6 per group). The remain RNAs (3 samples at 8 weeks and 3 samples at 10 weeks) were kept aside for qRT-PCR analysis. Moreover we analyzed gene expression in RNA from 8 weeks (n=2) and 10 weeks old (n=2) ApoE-/- mice, which did not received treatment, to obtained a triplicate analysis for untreated mice by including data from the time course experiment.

All the RNAs are described in the following table:

Microarray Chip	
ApoE 1 + ApoE 2 (8 weeks untreated)	**ApoE 3 + ApoE 4 (10 weeks untreated)**
ApoE 5 + ApoE 6 (8 weeks treated)	**ApoE 11 + ApoE 12 (10 weeks treated)**
ApoE 7 + ApoE 8 (8 weeks treated)	**ApoE 13 + ApoE 14 (10 weeks treated)**
ApoE 9 + ApoE 10 (8 weeks treated)	**ApoE 15 + ApoE 16 (10 weeks treated)**

For both experiments, all samples were hybridized on Agilent Whole Mouse Gene Expression Microarray (#G4122F, Agilent Technologies, Palo Alto, CA) and one-color gene expression was performed according to the manufacturer's procedure. Labeled cRNA was synthesized from total RNA using the Low RNA Input Linear Amplification Kit (Agilent Technologies) in the presence of cyanine 3-CTP (Perkin-Elmer Life Sciences, Boston, MA). Hybridizations were performed at 65°C for 17 hours in a rotating oven. Images at 5μm resolution were generated by Agilent scanner and the Feature Extraction 10.5 software (Agilent Technologies) was used to obtain the microarray raw data. Microarray results were analyzed by using the GeneSpring GX 11 software (Agilent Technologies). Data transformation was applied to set all the negative raw values at 1.0, followed by a quantile normalization. A filter on low gene expression was used to keep only the probes expressed in at least one sample (flagged as Marginal or Present). Differentially expressed genes were selected as having a $\geq$ 1.5-fold or $\geq$ 2-fold expression difference between the groups of interest and a p-value $\leq$ 0.05 or 0.01 at unpaired t test.
Hierarchical clustering was performed using Manhattan correlation as a measure of similarity. To identify underlying biological pathways the differentially expressed genes were then analyzed using MetaCore™ (GeneGo, Inc., St. Joseph, MI, USA) or DAVID Bioinformatics Resources 6.7 (National Institute of Allergy and Infectious Diseases NIAID, NIH), web-based computational platforms designed for systems biology.

11. En-face Analysis

Mice were euthanized and orta was perfused with saline solution and fixed for 10 minutes with 4% paraformaldehyde. Aorta was excised, cleaned of fat and fibrous material in a Petri dish containing ice cold saline solution.
Segments of thoracic aorta and aortic arch were isolated. From the aortic arches we identified and excised the areas corresponding to both lesser and major curvatures

(described in [81]). Staining procedure was performed in 2 ml tube filled with enough buffers to cover the tissue. Aorta segments were blocked with 1 ml of blocking buffer (PBS 1X + 0.1% Triton X-100 +2% BSA) rocking at room temperature for 1.5 hours.
Primary antibody incubations were performed overnight at 4°C. The primary antibodies used were Ve-Cadherin (1:100; BD Pharmingen), Hey2 (1:100; Millipore), Hes5 (1:100; Santa Cruz Biotechnology, Germany), Notch1 (1:100; Santa Cruz Biotechnology, Germany) and Notch4 (1:100; Santa Cruz Biotechnology, Germany). After washing the aortic segments three times in washing buffer (PBS 1X + 0.1% Triton X-100), secondary antibodies, previously prepared in blocking buffer, were added and incubated for 1.5 hours rocking at dark and at 4°C. The secondary antibodies used were Alexa Flour 546 Goat Anti-Rat IgG (1:500; Life Technologies, CA, US), Alexa Flour 633 Goat Anti-Rabbit IgG (1:500; Life Technologies, CA, US). After washing three times, aortic specimens were placed on a glass slide with the intima side up and, before covering samples with a coverslip, a drop of a liquid mountant was applied directly to fluorescently labeled tissue samples (ProLong Antifade Reagents – Life Technologies, CA, US). At least 5 images of the endothelial monolayer were obtained using a Zeiss LSM 510 confocal microscope with 40x magnification. Results were expressed as mean ± SEM. Differences between groups were analyzed by unpaired t-test and $p<0.05$ was considered significant.

12. Immunofluorescence on frozen section of aorta

Mice were euthanized and aorta was perfused with saline solution to flush blood inside the aorta itself. The portion of aorta corresponding to the aortic arch was isolated and snap-frozen in blocks of OCT gel. Longitudinal sections (10 µm thick) were placed on Superfrost Ultra Plus adhesion slides (Thermo Scientific- Waltham, MA, US) (3 sections per slide) and left dry for 2 hours at room temperature. Slides were fixed in ice-cold acetone for 15 min and left dry under chemical wood for 30 minutes. The surplus of OCT was discarded, using a scalpel, and a circle was drawn around every section, using a PAPpen (Ab2601 - Abcam - UK), to perform staining procedure. Slides were submerged in blocking buffer (PBS 1X + 0.1% Triton X-100 +2% BSA) for 1.5 hours.
Primary antibody incubations were performed overnight at 4°C. The primary antibodies (prepared in blocking buffer) used were Ve-Cadherin (1:100; BD Pharmingen) and Hes5 (1:100; Santa Cruz Biotechnology). After washing the aortic segments three times in PBS 1X, secondary antibodies, previously prepared in blocking buffer, were added and incubated for 1.5 hours rocking in the dark, at 4°C.

The secondary antibodies used were Alexa Flour 546 Goat Anti-Rat IgG (1:500; Life Technologies, CA, US) and Alexa Flour 633 Goat Anti-Rabbit IgG (1:500; Life Technologies, CA, US). After washing three times in PBS 1X, a drop of a liquid mountant (ProLong Antifade Reagents - Life Technologies, CA, US) was applied directly to fluorescently labeled tissue samples and covered with a coverslip. Images of the endothelial monolayer were obtained using a Zeiss LSM 510 confocal microscope with 40x magnification. At least 10 images were acquired for a single staining.

Image analysis was performed using ImageJ, an open source bioimaging software. Red signal, corresponding to VE-cadherin staining, was binarized and used as a mask image to select positive signal in correspondence of endothelium. Such a mask image was used to filter the raw signals for Hes5 (green channel) and to select the region of interest (ROI) where it co-localized with red signals. The average fluorescence intensities were calculated for each sample as described in [82]. The data obtained with this approach were compared with data obtained by manually conducted analyses. Specifically, a ROI corresponding to the endothelium (VE-cadherin staining), was manually selected within a box. The ROIs selected for each VE-cadherin staining were placed into the same images for HES5 staining (green channel) and the ratio pixel signal intensity levels for each ROI were recorded (described in [83]). Results were expressed as mean ± SEM. Differences between groups were analyzed by unpaired t-test and $p<0.05$ was considered significant.

RESULTS AND DISCUSSION

1. Validation of endothelial cells enriched-RNA extraction

In order to increase the specificity of microarrays we attempted to isolate RNA from endothelium only, using the method described by Krenek P et al., [84]. Aortic arch of five 10 weeks old C57BL6/J mice were flushed with different volumes of a phenol containing solution to achieve efficient lysis of endothelial cells only: more than 350 µlof Qiazol lysis buffer caused a disgregation of the whole arch, conversely smaller volume of lysis buffer resulted in insufficient RNA yield (data not shown). Noteworthy, to obtain an efficient RNA extraction and to avoid aorta dissolution, it was needed to constantly perfuse the aorta for not more than thirty seconds. As expected, this method gave a low yield of RNA (150-600ng from one arch, n=5 10 weeks old C57BL6/J) nevertheless every target gene was successfully amplified by qRT-PCR (Figure 9A). RNA was also isolated from the whole arch after mechanical disruption of the tissue using a Dounce homogenizer and the same lysis buffer used for flushing the aorta. This method gave good yield and good quality RNA (1.5 ug total RNA from one arch). Successful endothelial enriched-RNA extraction was confirmed by measuring mRNA levels of endothelial and smooth muscle specific genes (eNOS and SM22 respectively). As shown in Figure 9B, RNA extracted from endothelium only was enriched with eNOS and depleted of SM22 compared to RNA purified from whole aorta.

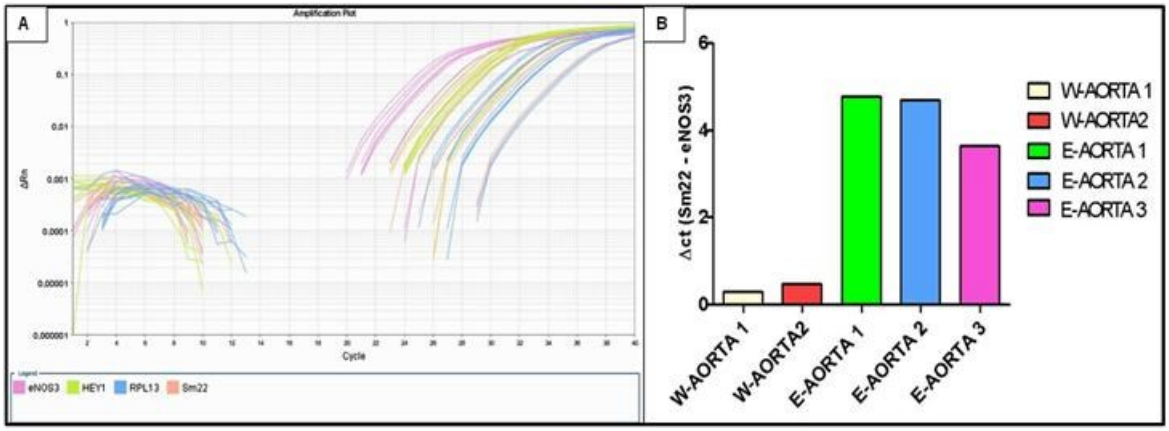

Figure 9: (A) Fluorescence amplification curves of tested genes; (B**)** Enrichment of endothelial specific markers in RNA extracted by the flushing technique: difference in eNOS and SM22 mRNA levels is shown by difference of relative Ct numbers (W-AORTA= RNA from whole aortic arch, E-AORTA:RNA from endothelium only).

2. PRELIMINARY EXPERIMENTS: Time course experiment and ivabradine treatment dose

The aim of these experiments was to establish i) the age to start the ivabradine treatment and the duration of treatment ii) the dose of ivabradine.

2.1 Time course experiment: microarray analysis in endothelial cell transcripts-enriched RNA purified from aortas of 6, 7, 8 and 10 weeks old ApoE-/- mice

To assess the age of the onset of changes in gene expression in the endothelium of ascending aorta and, thus, to determine the beginning and duration of ivabradine treatment, we compared the gene expression profile in 6, 7, 8 and 10 weeks old ApoE-/- mice. The time point of 6 weeks-old was chosen for ivabradine treatment start because it corresponds to the early stage of atherosclerosis development in chow-fed ApoE-/- mice (i.e. before start of monocyte adhesion) [85]. Whereas it has been reported that in ApoE-/- mice fed a normal diet, signs of atherosclerosis progression (monocyte adhesion, foam cell lesion) are present at 10 weeks of age [85], there are not many data available on changes in gene expression in the endothelium of aortic arch of younger mice fed the same diet. Therefore, we included in our analyses a group of mice to be sacrificed at 10 weeks of age as positive control for atherosclerosis progression and as validation of methodologies utilized for our study.

The overall quality of the expression chip was examined and all quality assessment variables were within the acceptance limits suggested by the manufacturer. In order to verify , in agreement with the literature, if we could detect under our experimental conditions changes in expression of atherosclerosis-associated genes at 10 weeks, we analyzed differences in gene expression between 6 weeks and 10 weeks (Figure 10 – left panel). The total number of genes significantly modulated between these two time points was 1080 (fold change cut-off: 2.0). Among these genes, 308 were down-regulated and 92 were up-regulated more than 4-fold. These same genes showed instead variable expression in 7 and 8 weeks old mice (Figure 10 – right panel). We detected changes in 137 uncharacterized expressed sequence tags (ESTs), 102 Riken cDNA sequences (sequences with open reading frames coding for unknown proteins) and 202 long intergenic non-coding RNAs (lincRNA)

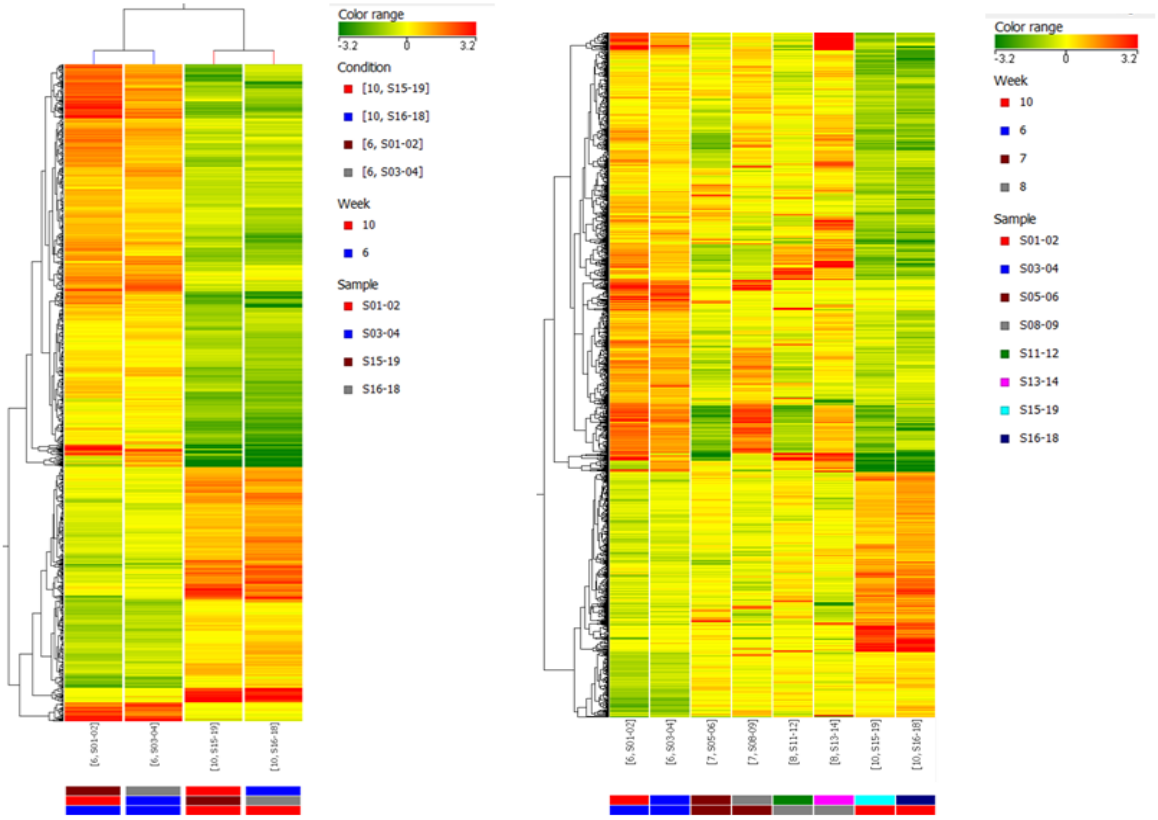

Figure 10: Left: Heatmap of gene expression hierarchical clustering comparing samples at 6 weeks versus 10 weeks. The represented genes were sorted out filtering values that were significantly differentially expressed between 6 and 10 weeks. Each column of data represents 1 of the 2 replicate experiments (pool of 2 aortas). **Right**: Heatmap of gene expression hierarchical clustering comparing samples at 6 weeks versus 10 weeks including expression levels of the same genes at 7 and 8 weeks.

The analysis of the affected pathways (MetaCore analysis) identified pathways involved in modulation of cell cycle, cell adhesion, immune response, atherosclerosis and apoptosis. We found downregulation of cyclin B1, cdk1, and survivin (an inhibitor of caspase 9) (Figure 11), which suggests apoptosis following G2/M cell cycle arrest [86,87]. Increased apoptosis was suggested also by up-regulation of Phap1, a stimulator of mitochondrial apoptotic pathway. We found significant differences in the expression of genes for chemokine receptors and their ligands (Ccl3, Ccr7, Ccr9, Ccrl1), for interleukins and their receptors (Il10ra, Il17rb, Il18bp, Il5ra, Il7r) and for the matrix metallopeptidase 9 (Mmp9).

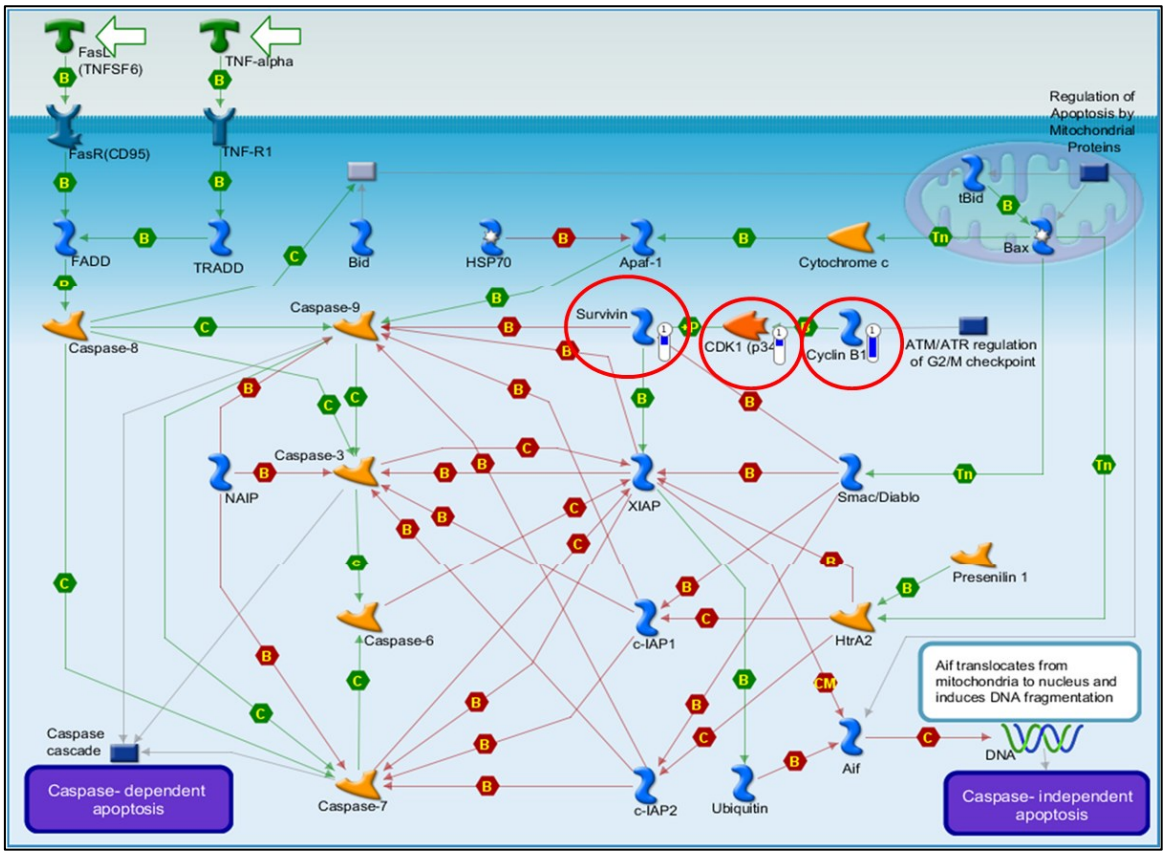

Figure 11: GeneGo pathway analysis. Down-regulation of cyclin B1, cdk1, and survivin (highlighted by red circles) is indicated by blue thermometer.

Since microarray data showing significant changes (above 2-fold) derived from low signal intensities maybe biased or masked by noise whereas a 1.4-fold change derived from strong signal intensities may reflect actual changes in mRNA concentration within a biological sample [88], we also checked genes giving a strong hybridization signal that showed changes progressing with time even if they not always reached statistical significance. Using this approach we identified additional chemokine receptors and their ligands (Ccl17, Ccl4, Cxcl17, Ccr6, Ccr9, Cxcr2, Cxcr5), interleukins and their receptors (Il1b, Il10ra, Il17rb, Il18bp, Il20rb, Il25) and cadherins 16 and 18. Of interest, since calcium signalling pathway is known to be involved in the inflammatory process of atheroscleros [89] and Clca1 has been shown to regulate endothelial cell permeability [90], we found a strong down-regulation of Clca3 (chloride channel calcium activated 3 gene, down-regulated 29-fold). Rag1 and Rag2 (recombination activating gene 1 and 2), involved in modulation of inflammation by controlling maturation of T and B cells [91] were downregulated 19.1- and 10.5-fold respectively and Mmp12 (matrix metalloproteases 12), associated to initiation of atherosclerosis [92], was up-regulated 3-fold.

We found upregulation of SerpinA3i (serine (or cysteine) peptidase inhibitor, clade A,member 3I) which belongs to family of protease inhibitors and is highly expressed in

ApoE-/- mice lesions compared with lesion-free vessels [93]. Moroever, Serpina3k (serine (or cysteine) peptidase inhibitor, clade A, member 3K), which protects retinal cells from oxidative stress-induced cell death [94], was downregulated 16-fold. We didn't detect changes in expression of ICAMs, VCAMs and MCP-1 at 10 weeks. Among the other modulated genes we identified: ATP-binding cassette, sub-family B (MDR/TAP), member 1A (Abcb1a), synaptogyrin 1 (syngr1) , complement component 1- q subcomponent- alpha polypeptide (C1qa), ring finger protein 149 (rnf149) , lipocalin 2 (Lcn2), interleukin 7 and 10 receptors (Il7r e Il10ra), RIKEN cDNA 5430435G22 gene (5430435G22Rik), Harvey rat sarcoma virus oncogene (Hras1), hepatocyte growth factor (Hgf), extra cellular proteinase inhibitor (Expi), ATP-binding cassette, sub-family C, member 3 (Abcc3). All these genes were previously identified by Tabibiazar and colleagues as associated to progression of atherosclerosis in ApoE-/- mice [95]. Interleukin 1 b (Il1b) was up-regulated (2.27-fold) as observed in endothelial cells Weibel-Palade bodies following an inflammatory stimulus [96]. This overlapping with published data is a validation of our methodology and analysis algorithm.

A statistical analysis of changes of gene expression at 7 weeks compared to 6 weeks (Figure 12, left) identified 603 genes (fold change cut-off: 2). Among these genes, 105 were up- or down-regulated more than 4-fold. We indentified changes in 34 uncharacterized ESTs, 50 Riken cDNA sequences and 169 lincRNA. Among the affected pathways we identified pathways related to immune response (including 2 pathways associated to oncostatin M involved in atherosclerosis progression [95]), atherosclerosis and cell adhesion. Of interest among these genes, we identified up-regulation of a chemokine receptor (Ccrl1) and ligands (Ccl11, Ccl12) and down-regulation of cadherin 1 (cdh1). Ccl2 (MCP-1) was up-regulated but not ICAM and VCAM. Svep1 (coding for a protein that includes complement binding motifs, von Willebrand factor (vWF-A) type A domain, Epidermal Growth Factor (EGF) and EGF-like calcium binding and pentraxin domains) involved in the regulation of expression of ICAM1 and E-selectin [97] was up-regulated 2.2-fold.

A statistical analysis of changes in gene expression at 8 weeks compared to 6 weeks (Figure 12, right) showed 538 genes affected (fold change cut-off: 2). 84 genes were up- or down-regulated more than 4-fold. We found changes in 118 lincRNA, 20 uncharacterized ESTs and 64 Riken cDNA sequences. Among the pathways identified there were some related to immune response, atherosclerosis, cell adhesion and apoptosis. Of interest

among the modulated genes we identified up-regulation (Ccl8, Ccrl1) and down-regulation (Ccr7) of chemokine receptors and ligands. We found upregulation of Ccl2 (MCP-1) but we didn't detect changes in ICAMs and VCAMs genes at 8 weeks.

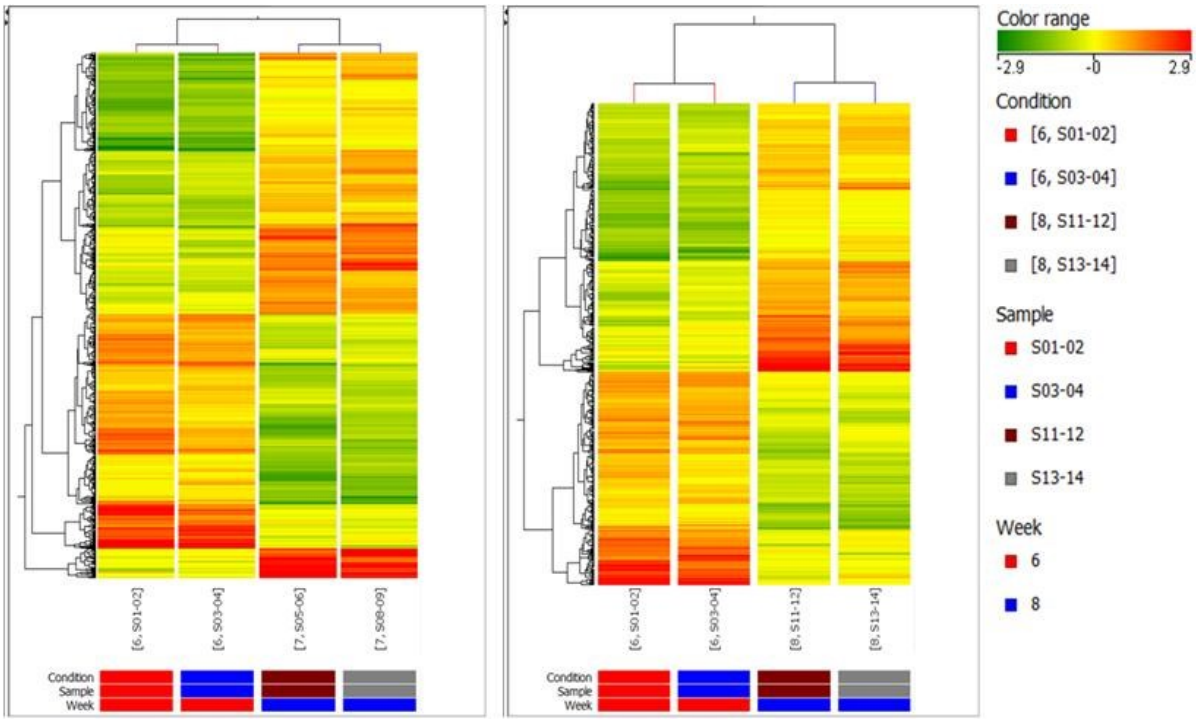

Figure 12: Heatmap of gene expression hierarchical clustering comparing samples at 6 versus 7 weeks (left panel) and 6 versus 8 weeks (right panel). The represented genes were sorted out filtering values that were significantly differentially expressed at 6 weeks versus 7 and 8 weeks.

As shown in Figure 13, many of the genes affected at 7 weeks followed a similar trend at 8 weeks (398 genes) (Figure 13, left) and maintained the same expression level at 10 weeks (Figure 13, right). 40 genes in this group were up- or down-regulated more than 4-fold. Among them there were chemokine receptors and ligands (Ccl8, Ccrl1, Ccr10, Ccr7). Of interest, a transcript containing sequences for von Willebrand factor A domain containing 3B (Vwa3b-003) was up-regulated at 7, 8 and 10 weeks. We also found up-regulation of platelet-activating factor receptor (Ptafr) , which has been shown to dissociate endothelial cells adherens junctions [98].

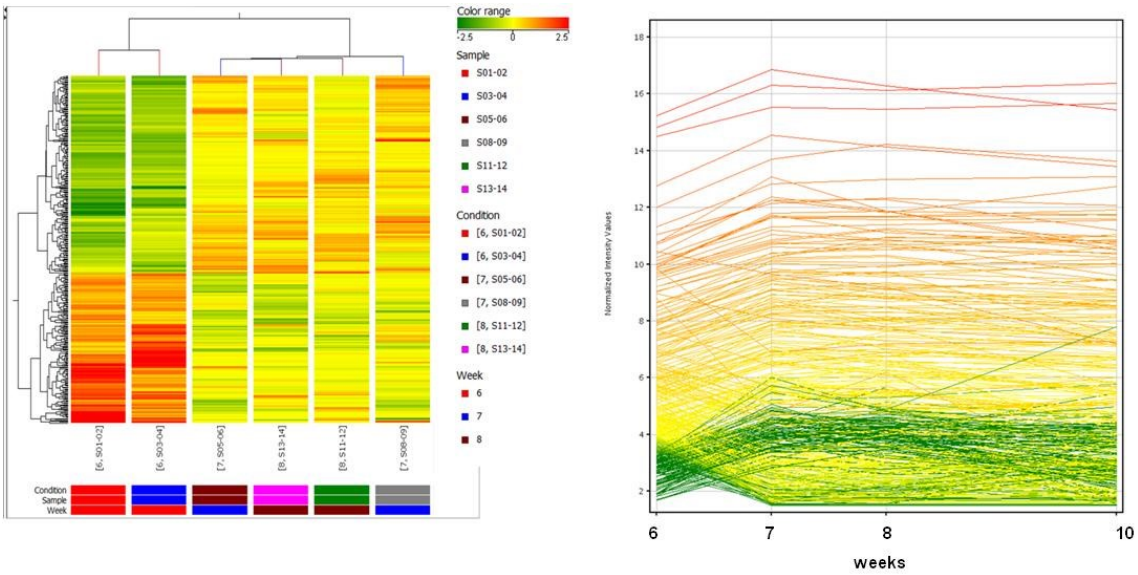

Figure 13: Left: Heatmap of gene expression hierarchical clustering comparing samples at 6 weeks versus 7 plus 8 weeks showing gene expression. The represented genes were sorted out filtering values that were significantly differentially expressed between 6 weeks versus 7 plus 8 weeks. **Right**: Graphic representation of genes significantly differentially expressed at 7 and 8 weeks and their expression level at 10 weeks.

In conclusion, we found changes in the expression of a significant number of genes and in particular genes related to inflammation as early as at 7 weeks of age. Some of the modulated genes followed the same trend at 8 and 10 weeks. The number of affected genes increased with time, therefore the highest variation in terms of gene number and degree of changes was seen at 10 weeks. Based on these results we conclude that either one or two weeks of ivabradine treatment beginning at 6 weeks of age could be chosen to study the effect of the drug on gene expression. Furthermore, based on the observation that at 10 weeks there is the highest number of affected genes, we reasoned that the inclusion of an additional 10 weeks time point (4 weeks of ivabradine treatment) could increase our chances to detect an effect of ivabradine on gene expression.

2.2 Heart rate reduction induced by ivabradine treatment

Preliminary experiments were conducted to determine the ivabradine treatment dose. 6 weeks old ApoE-/- mice (n=5) were treated with ivabradine for 6 days. The dose of 15 mg/kg/day was first chosen, since, as shown by Custodis and colleagues, 10 mg/kg/day of ivabradine treatment induce a reduction of 13% ± 2 and 20 mg/kg/day lead to a reduction of ~ 23% [99,100]. At the end of 6 days treatment HR was monitored and as indicated in Figure 14 we observed a mean HR of 639 BPM (beat per minutes) ± 8 after treatment compared to mean HR of 714 BPM ± 15 measured before treatment (baseline), with an

average percent reduction of heart rate (% HRR) of 10,5 % ± 2,6. The HR reduction obtained was slightly below to that found by Custodis et al with 10 mg/kg/day of ivabradine (~ 13%).

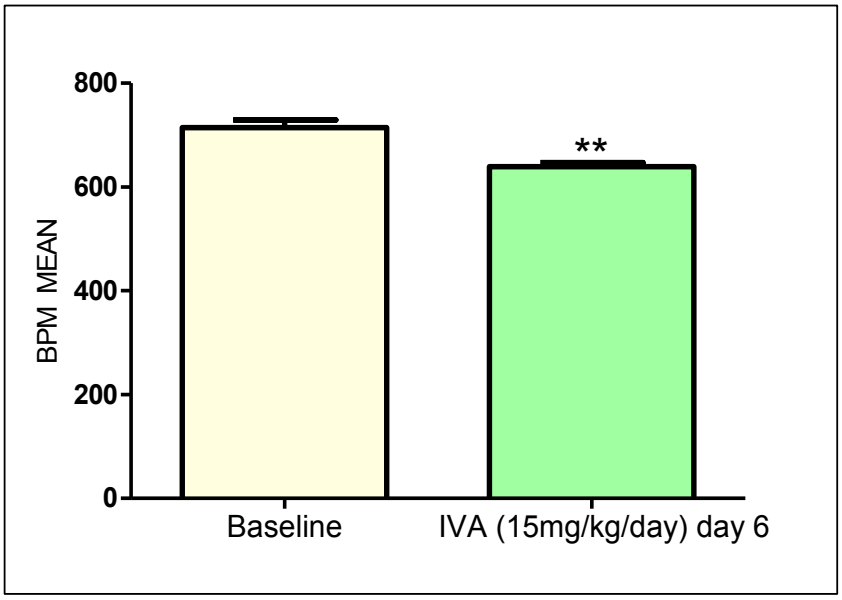

Figure 14: Mean HR (BPM) in ApoE -/- mice before and after ivabradine treatment. ** p value< 0,005

We used a higher dose of ivabradine (30 mg/Kg/day) to obtain a more sustained heart rate reduction.

As indicated in Table 1 and Figure 15, we observed an % HRR of 10,2 ± 5,6 at day 3. If we exclude one mouse (APO 5) in which there was no HR reduction (probably due to reduced water assumption) the % HRR was 12,2 ± 3,7. Treatment was continued for the following 3 days and led to a higher % HRR (17,8 ± 4,7).

	BASELINE (BPM)	HR (BPM) IVA DAY 3	HRR %	HR (BPM) IVA DAY 6	HRR %
APO 1	737,9	679	7,98%	644,4	12,67%
APO 2	768,9	679,8	11,59%	658,5	14,36%
APO 3	763,2	669,6	12,26%	635,3	16,76%
APO 4	771,8	641,5	16,90%	603,7	21,78%
APO 5	742,6	724,2	2,47%	580,5	23,66%
AVERAGE APO 1-5	756,9	678,82	10,24% ± 0,054	624,48	17,85% ± 0,047
AVAREGE APO 1-4	-	667,48	12,18% ± 0,037	-	-

Table 1: Heart rate measurement in Apo E -/- before and after ivabradine treatment. Measurement at day 3 and day 6.

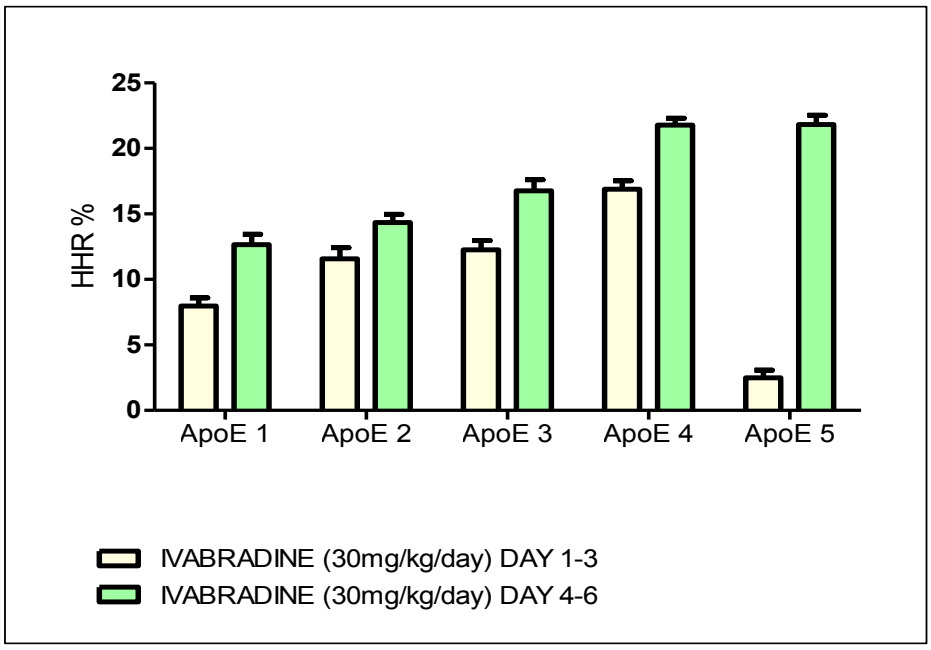

Figure 15: Percent heart rate reduction (% HRR) in Apo E -/- mice after ivabradine treatment (dose and time as indicated in the figure).

These results indicate that 6 days treatment with 15mg/Kg/day of ivabradine is adequate to induce an average reduction of heart rate of ~ 12% and that the highest dose of ivabradine (30 mg/Kg/day) is necessary if a more substantial heart rate reduction is desirable.

3. MAIN EXPERIMENT: Ivabradine treatment in ApoE -/- mice

Based on the data obtained by preliminary experiments, the higher dose was chosen for the "main experiment" (30mg/kg/day in drinking water)**.** Since both a longer exposure to ivabradine seemed to give a more reproducible effect on heart rate reduction, and many of the genes affected at 7 weeks followed a similar trend at 8 weeks (time course microarray), we chose to measure gene expression at 8 weeks, instead of 7 weeks (following two weeks treatment with ivabradine). We included an additional time point (4 weeks of ivabradine treatment) since, as previously reported in preliminary experiment, in 10 weeks old ApoE -/- mice we found the highest number of modulated genes. A 10 weeks time point can still be considered "early stage" in atherosclerosis progression since published data [95] have shown that gene expression profile in aortas of 10 weeks old ApoE -/- mice is more similar to the gene expression profile of younger and healthy mice than to the gene expression profile of 30 and 40 weeks old mice which show clear signs of advanced atherosclerosis.

3.1 Microarray analysis in endothelial cell transcripts-enriched RNA purified from aortas of 8 and 10 weeks old ApoE-/- mice following treatment with ivabradine

In treated mice, heart rate was measured before the beginning of treatment (baseline) and one week before sacrifice (day 9 and 21) (Figure 16). At day 0 (baseline) we observed a mean HR of 726 BPM ± 8. At day 9, we found a mean HR of 600 BPM ± 9, with a corresponding HRR % of 17,4 ± 1,7. At day 21, we found a mean HR of 560 BPM ± 12, with a corresponding HRR % of 22,9 ± 2,1.

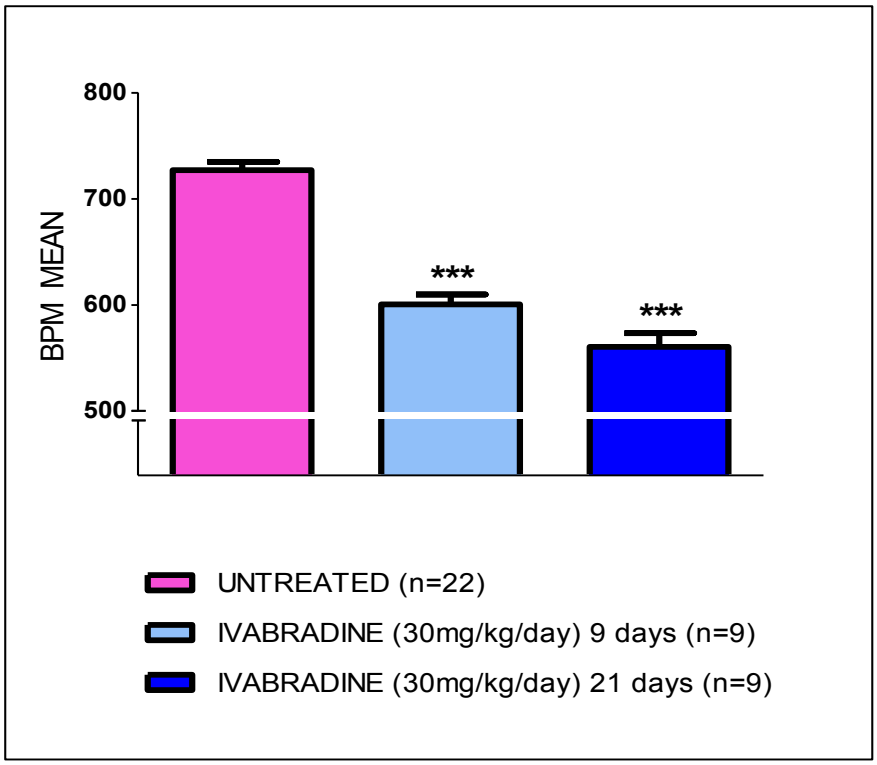

Figure 16: Mean HR (BPM) in ApoE -/- mice before and after ivabradine treatment. *** p value < 0,0001

At the end of the treatment, a microarrays analysis was conducted to characterize changes in the gene expression profile in endothelial cell-enriched RNA purified from aortas of 8 and 10 weeks old ApoE-/- mice, following 2 weeks and 4 weeks ivabradine treatment respectively (analysis performed in triplicate).

As described in "method", to obtain a triplicate analysis for untreated mice, in this microarray chip, it was analyzed RNAs from untreated 8 weeks- (n=2) and 10 weeks-old (n=2) ApoE-/- mice, which gene expression results were merged with data obtained from 8 weeks and 10 weeks old untreated mice from the time course experiment.

3.2 Identification of differentially expressed genes

List 1 – differentially gene expression in ApoE-/- at 8 weeks and 10 weeks after ivabradine treatment

We first analyzed separately the two groups of mice at different ages (8 and 10 weeks old) and compared changes in gene expression in untreated versus treated group (2 weeks or 4 weeks of ivabradine treatment).

Hierarchical clustering showed that the number of sequences significantly modulated (p-value cut-off: 0.01, fold change ≥ 2.0) after 2 weeks of treatment was 146 (80 upregulated and 66 downregulated) (Figure 17). Among the modulated sequences we found 17 uncharacterized ESTs, 14 Riken cDNA sequences and 52 lincRNAs. After 4 weeks of treatment, the number of sequences significantly modulated (p-value cut-off: 0.01, fold change ≥ 2.0) was 278 (127 upregulated and 151 downregulated) (Figure 17). Among them we found 17 uncharacterized ESTs, 12 Riken cDNA sequences and 78 lincRNAs.

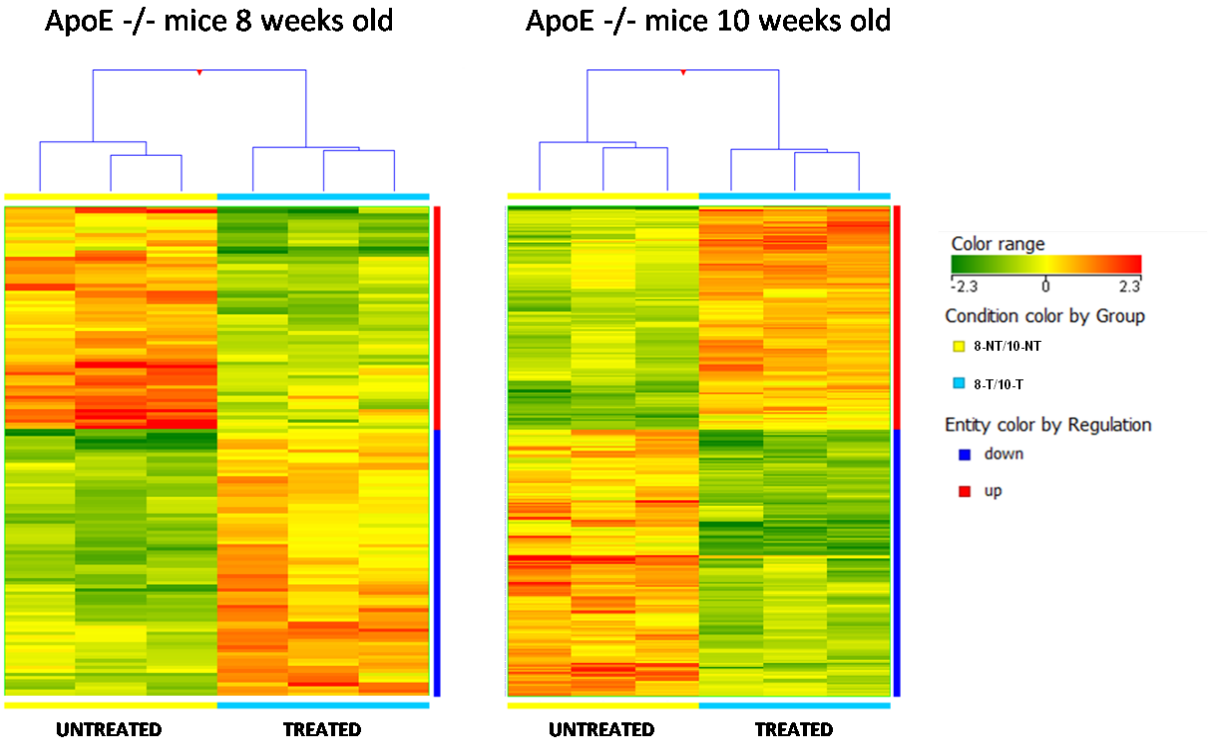

Figure 17: Heatmap of hierarchical clustering of gene expression in samples from 8 weeks old mice (untreated or ivabradine-treated) (left panel) and 10 weeks old mice (untreated or ivabradine-treated) (right panel). Each column represents expression data from 1 of 3 pools of aorta (each pool from 2 mice).

Eleven sequences were similarly modulated in both treatment groups (Table 2) Among the modulated sequences (8 upregulated and 3 downregulated) 4 sequences were long intergenic non-coding RNAs (lincRNA) and one sequence was a Riken cDNA. We found upregulation of paired box gene 2 (Pax2 – 2.16-fold), with anti-apoptotic function in renal collecting duct cells [101] and of zinc finger protein 407 gene (Zfp407 – 2-fold), key stimulator of Glucose Uptake and Glucose Transporter 4 (GLUT4), which impairment underlined hyperglycemia and increased risk of cardiovascular disease and neuropathy [102].

We found downregulation of T-cell leukemia, homeobox 2 gene (Tlx2 – 9.5-fold) which is induced by the BMP2 (bone morphogenetic protein)/SMAD pathway [103] which is activated by AngII in HUVECs and signals through NF-κB [104]. Among downregulated sequences, we found Lass3 (LAG1 homolog ceramide synthase 3 – 3.14-fold), involved in the synthesis of ceramide species, including C18:0- and C24:0-ceramides [105], that are elevated in subjects' plasma with type 2 diabete [106].

Gene name	FC(abs) (Moderated T-Test [10-T] Vs [10-NT])	p-value	Regulation	FC(abs) (Moderated T-Test [8-T] Vs [8-NT])	p-value	Regulation
lincRNA:chr19:54011403-54018978 forward strand	2,1	0,0060	up	3,2	0,0040	up
T-cell leukemia, homeobox 2 (Tlx2)	5,3	0,0047	down	9,5	0,0098	down
paired box gene 2 (Pax2)	2,8	0,0018	up	2,2	0,0059	up
zinc finger protein 407 (Zfp407)	2,6	0,0045	up	2,0	0,0005	up
603396379F1 NIH_MGC_94 cDNA clone IMAGE:5400378 5', mRNA sequence [BI872080]	2,2	0,0090	up	3,9	0,0055	up
lincRNA:chr7:69117827-69127242 reverse strand	3,4	0,0003	up	3,4	0,0051	up
lincRNA:chr9:56912321-56912932 reverse strand	3,7	0,0020	up	3,3	0,0026	up
LAG1 homolog, ceramide synthase 3 (Lass3)	2,1	0,0084	down	3,1	0,0016	down
lincRNA:chr5:121765763-121768660 forward strand	2,2	0,0020	up	2,3	0,0084	up
PDZ domain containing 1 (Pdzk1)	6,1	0,0059	down	4,5	0,0057	down
glutamate receptor, ionotropic, kainate 4 (Grik4)	2,3	0,0075	up	2,8	0,0062	up

Table 2: Overlapping genes modulated by ivabradine treatment at 8 weeks and 10 weeks.

LIST 2 – Comparison of gene expression profile between Treated and Untreated ApoE-/- mice

Three components PCA was carried out to determine whether the observed variability in gene expression could be attributed to ivabradine treatment or rather to mice age (mice were 8 and 10 weeks old at the end of the treatments). The results of this analysis are shown in Figure 18. In the graphic representation of the PCA are visible two clearly separated groups corresponding to treated and untreated individuals (blue vs red). The different ages in each group (triangles vs diamonds and circles vs squares) are randomly distributed in the 3D space. These results indicate that most of the variability in gene expression between the groups is ivabrabine- and not age- related and they provide the rational for generating a list which includes genes differentially expressed between treated and untreated groups.

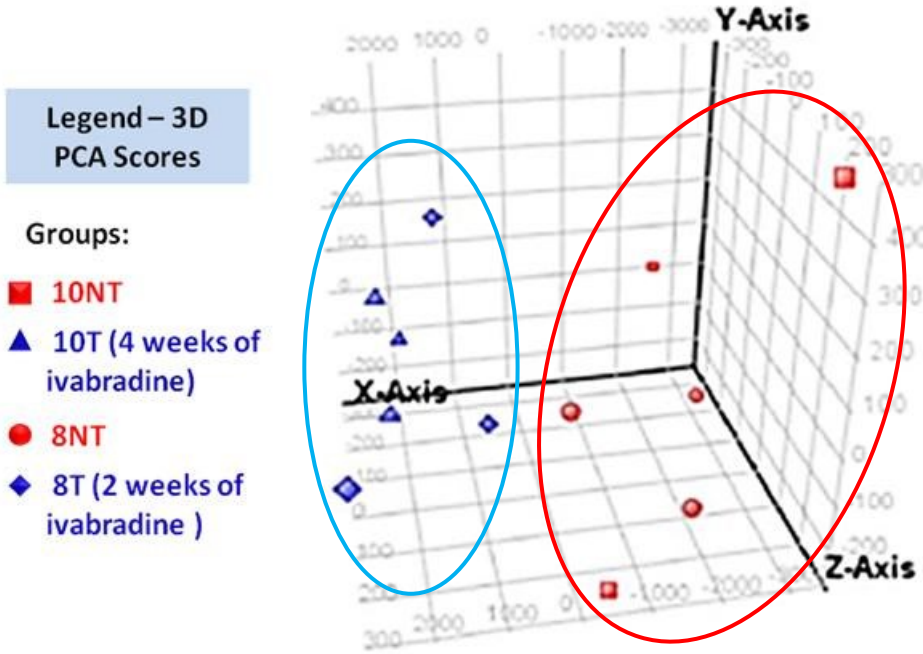

Figure 18: Unsupervised principal components analysis (36K expressed genes). In blue circle all the treated groups. In red circle all the untreated groups

Based on this result, we compared the gene expression data relative to untreated (8 and 10 weeks old) and treated mice (8 and 10 weeks old after 2 and 4 weeks treatment respectively).The heatmap indicating the clustering of treated and untreated groups is shown in Figure 19. The total number of sequences significantly modulated (p-value cut-off: 0.01, fold change ≥ 1.5) was 930 (630 upregulated and 300 dowregulated). Among the modulated sequences we found 73 uncharacterized ESTs, 61 Riken cDNA sequences and 314 lincRNAs.

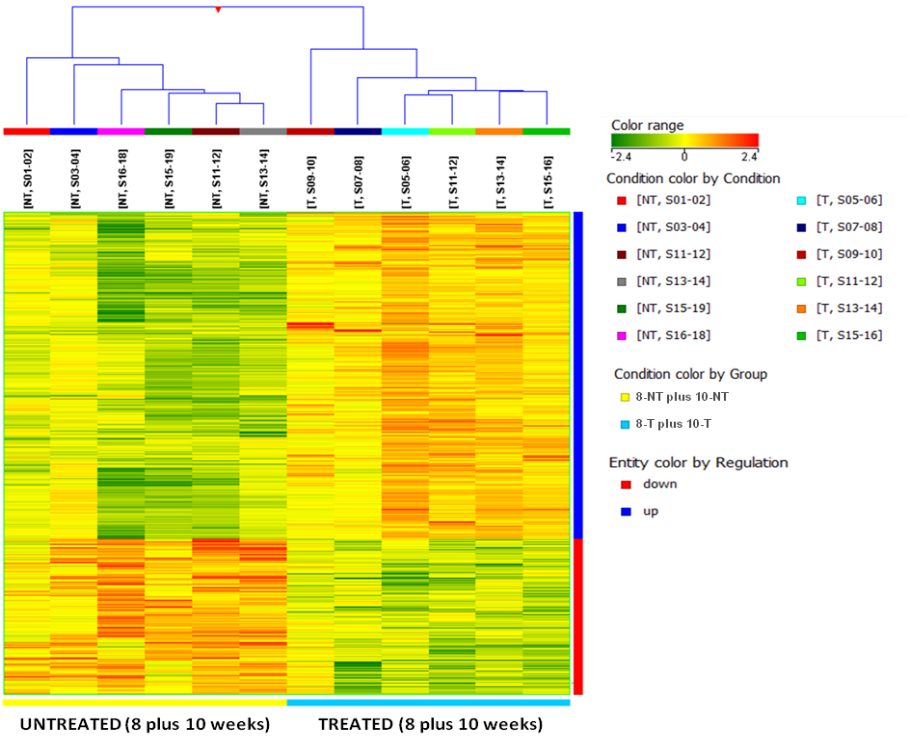

Figure 19: Heatmap of hierarchical clustering of gene expression in samples from untreated and ivabradine-treated (each group contains 8 and 10 weeks old mice). Each column represents expression data from 1 of 3 pools of aorta (each pool from 2 mice).

In order to ensure that the observed differences between the two groups were not due to the different levels of VSMCs RNA among the groups, clustering analyses were performed for selected VSMC-specific genes (Acta2,Taglin,Cnn1). Treated and untreated groups were randomly distributed when the specific VSMC transcripts were taken in consideration (Figure 20).

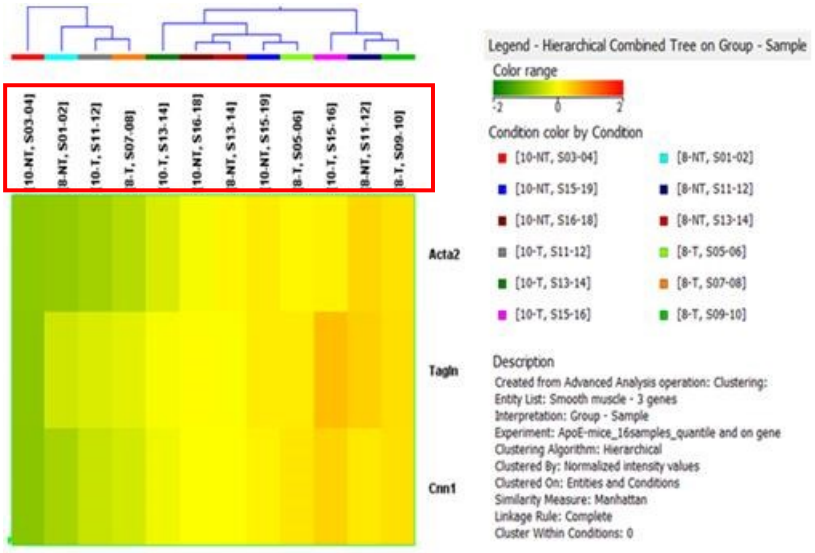

Figure 20: Heatmap showing hierarchical clustering of expression of Acta2, Tagln and Cnn1 in samples from 8 and 10 weeks old mice treated or not with ivabradine. The random distribution of treated and untreated groups is highlighted in red box. (T: treated; NT: untreated)

Additionally, correlation analyses showed that whereas the expression levels of transcripts (Rasgrf2 and PRKCA) modulated by ivabradine treatment showed high levels of correlation, with a separate distribution of untreated and treated groups (Figure 21)

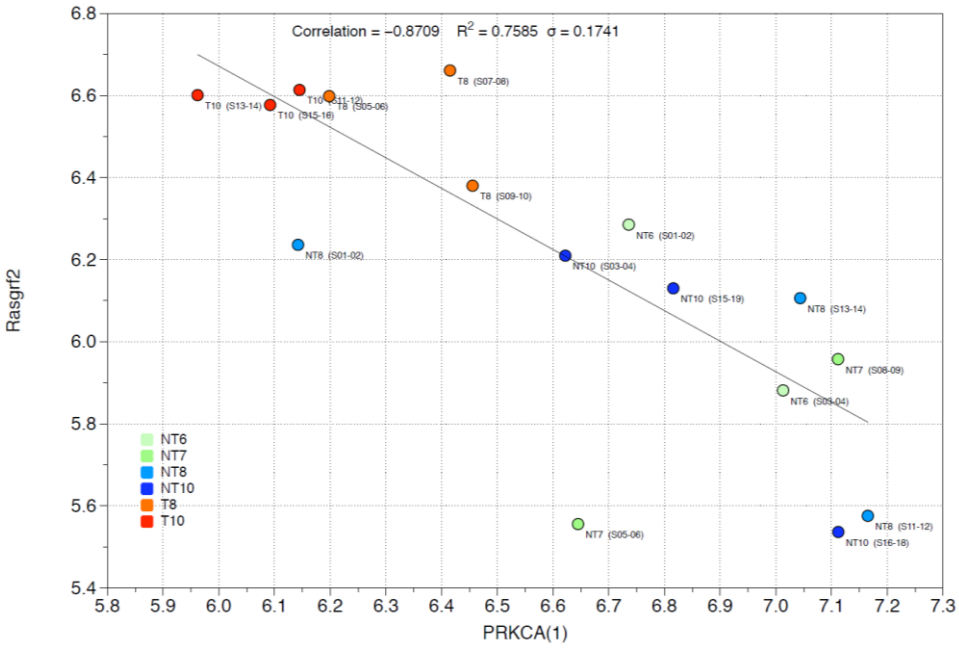

Figure 21: Correlation analysis between expression levels of ivabradine modulated genes (Rasgrf2 and PRKCA)

and, similarly, VSMC specific transcripts were highly correlated with random distribution of treated and untreated groups (Figure 22),

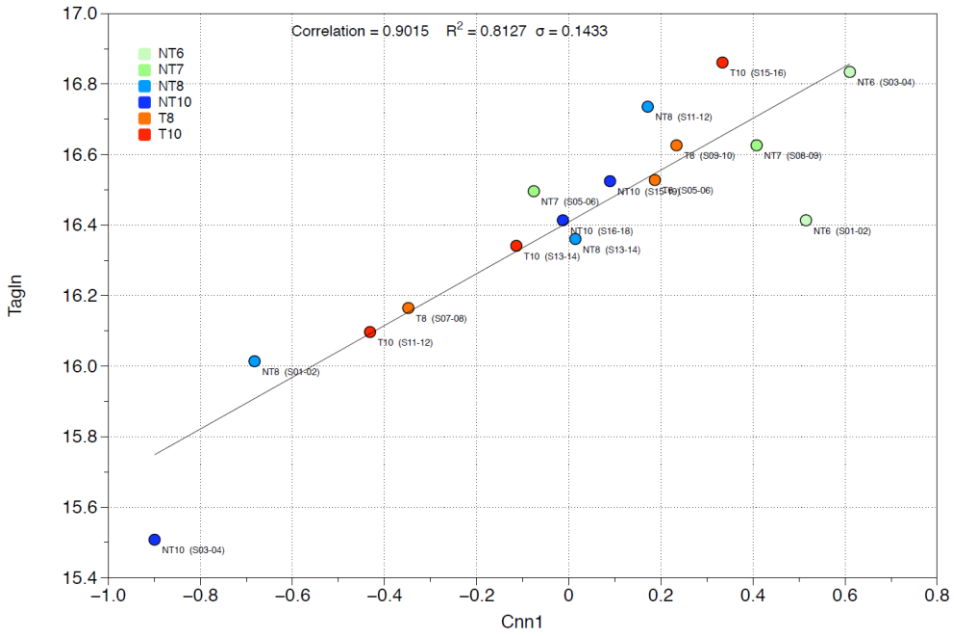

Figure 22: Correlation analysis between expression levels of VSMCs transcripts (Tagln and Cnn1)

there was no correlation between the expression levels of transcripts and VSMc specific transcripts (Figure 23).

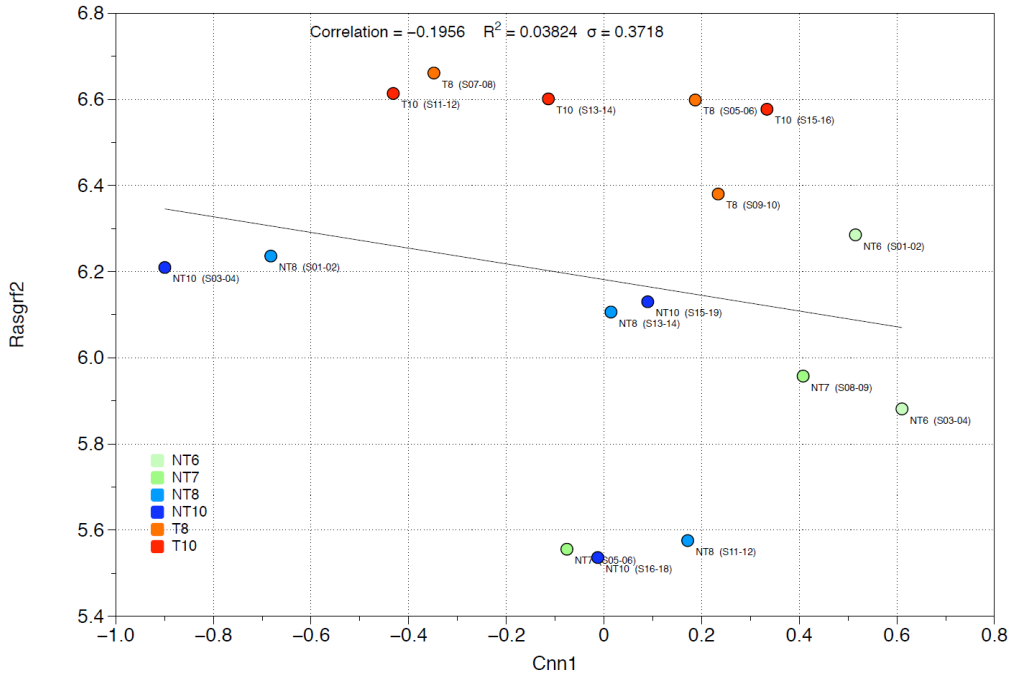

Figure 23: Correlation analysis between expression levels of ivabradine modulated gene (Rags) and a vascular smooth muscle cell transcript (Cnn1)

3.3 Analyses of individual genes

To identify potentially interesting genes on which to focus our analyses, we performed an automated literature search on PubMed for association between genes in List 2 and the terms “atherosclerosis” or “inflammation” or “shear stress” in published papers. These analyses brought to the identification of several genes involved in the first steps of atherosclerosis onset and progression, such as genes related to:

- **Endothelial cells integrity and permeability:**

  - ***Nppc (Natriuretic peptide type C - dowregulated 5.7-fold)***: atrial natriuretic peptide (ANP), B-type natriuretic peptide (BNP), and C-type natriuretic peptide (CNP) are all involved in the maintenance of electrolyte-fluid balance and vascular tone [107]. Many studies have shown that CNP is produced endogenously by the endothelium in response to blood vessels injury and it is thought to be involved in its repair. CNP is secreted by endothelium under the action of pro-inflammatory cytokines [108]. CNP expression is upregulated in human coronary atherosclerotic lesions of

asymptomatic patients [109], in serum of elderly patients carrying CAD [110] and patients with rheumatoid arthritis [111]. It is increased in urine of acute decompensated heart failure patients[112]. Clinical and functional improvement after physical training in heart failure patients is associated with a decrease in CNP concentration, which has been speculated might reflect an improvement in endothelial function [113]. Nppc is regulated by shear stress in HUVECs [114,115]. (Nppc expression level at 6, 7, 8 and 10 weeks is shown in Figure 24)

- ***Gjb3 (connexin 3 - dowregulated 4.40-fold)***: this gene belongs to a family of proteins that are component of gap junctions of endothelial cells and VSMc: gap junctions are implicated in the transmission of signals for the coordination in vasoconstriction and vasodilatation [116]. Alterations in the expression of this family of genes regulated by shear stress, hyperlipidaemia and TNF-α, is strongly implicated in atherosclerosis [115,116]. Other members of this family (Gja5 and Gjc2) are also modulated by ivabradines and are NF-κB target. (Gjb3 expression level at 6, 7, 8 and 10 weeks is shown in Figure 24)

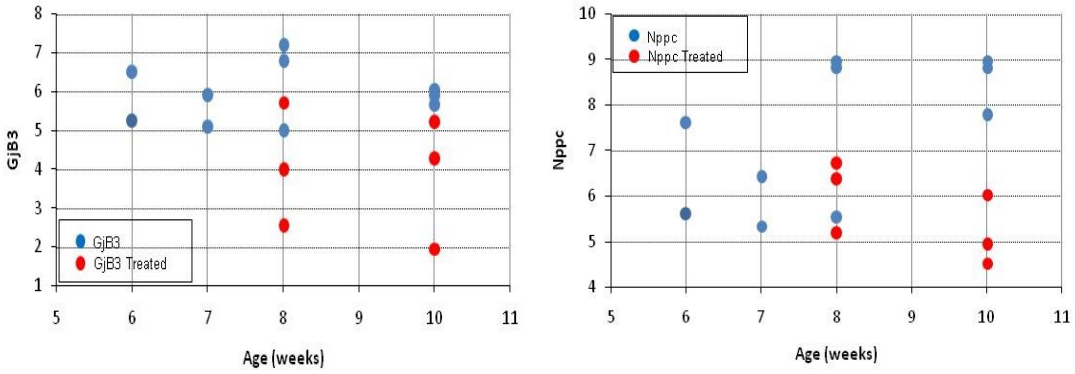

Figure 24: Diagrams showing expression levels of Gjb3 and Nppc (blue dots: untreated mice at 6, 7, 8 and 10 weeks ; red dots treated mice at 8 and 10 weeks).

- ***Prkca (Protein kinase alpha - downregulated 1.5-fold)***: activation of this gene may increase endothelial cell permeability by disassembling of VE-cadherin junctions [117].

- ***Ldlr1 (low density lipoprotein receptor 1 - downregulated 2.1-fold)***: Ldlr1 induces uptake of LDL in endothelial cells [49] and therefore its reduction would decrease endothelial cells permeability to LDL.

- ***Terc1 (telomerase RNA complex - upregulated 1.86-folds)***: telomerase length is associated to reduced senescence which leads to increased endothelium integrity [118].

- **Apoptosis**:

  - ***Dad1 (defender against cell death - upregulated 1.5-fold)***: Dad1 expression in transfected cells inhibits apoptosis *in vitro,* and his deletion induces apoptosis-associated embryonic death in mice [119].

  - ***Park 2 (parkin 2 - upregulated 1.5-fold)***: Park2 encodes for a component of a multiprotien E3 ubiquitin ligase complex. Loss of function in this gene inactivate the E3 ubiquitin ligase parkin, resulting in catecholaminergic neurodegeneration and a familial form of Parkinson disease. Its antiapoptotic duty is exerted by modulating the proaptotic function of Bax [120].

  - ***Pax2 (paired box gene 2 - upregulated 2.4-fold)***: murine collecting duct cell line, which expresses high endogenous levels of Pax2, undergoes apoptosis when transfected with anti-sense Pax2. In contrast, HEK293 cells expressing exogenous Pax2 are protected against apoptotic death induced by caspase-2 [101].

  - ***Olr1 (oxidized low density lipoprotein (lectin-like) receptor 1, LOX-1 - downregulated 3.2-fold)***: LOX-1 is not expressed in healthy endothelial cells but it is induced by elevated levels of LDL, inflammatory cytokines (TNF-α) and shear stress [121]. This receptor mediates the uptake of oxidized LDL, one of the first steps leading to endothelial dysfunctions and therefore high levels of Olr1 are strongly associated to atherosclerosis onset and progression [122]. Ox-LDL binding to LOX-1 decreases the expression of antiapoptotic proteins and then activates apoptotic signaling pathway caspase-9 and caspase-3 and finally results in apoptosis [121]. (Olr1 expression level at 6, 7, 8 and 10 weeks is shown in Figure 25)

  - ***Serpinb5 (maspin) (serine (or cysteine) peptidase inhibitor, clade B, member 5 - downregulated 5.02 fold)***. Maspin is a potent inhibitor of angiogenesis by regulating endothelial cell adhesion and migration [123]. Targeted expression of maspin in tumor vasculatures induces endothelial cell apoptosis [124]. Other

members of this family are also regulated by ivabradine. Additionally, other members of the family are regulated by shear stress in HUVEC [115]. (Serpinb5 expression level at 6, 7, 8 and 10 weeks is shown in Figure 25)

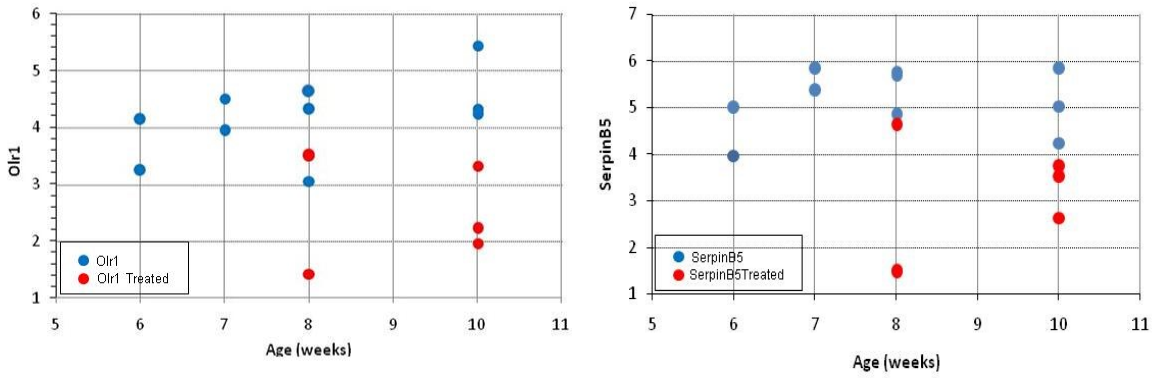

Figure 25: Diagrams showing expression levels of Olr1 and Serpinb5 (blue dots: untreated mice at 6, 7, 8 and 10 weeks ; red dots treated mice at 8 and 10 weeks).

- ***Pon2 (paraonoxase - upregulated 1.55-fold)***: it is involved in the reduction of oxidative stress and apoptosis in endothelial cells [125,126] and adenoviral-mediated human Pon2 expression in ApoE -/- protects against atherosclerosis [127].

- **Inflammation: pro-inflammatory genes**

  - ***ADAMTS7 (A Disintegrin And Metalloproteinase with Thrombospondin Motifs 7 - downregulated 2.7-fold)*** and ***ADAMTS8 (A Disintegrin And Metalloproteinase with Thrombospondin Motifs 8 - downregulated 4.7-fold)***: ADAMTS genes are shear stress regulated and induced by inflammatory cytokines. ADAMTS are involved in degradation of glycoproteins components of glycocalix, important regulator of endothelium integrity [128]. Recently, it has been demonstrated ADAMTS7 pivotal role in early inflammatory kidney damage associated with aging [129]. ADAMTS7 is induced by TNF–α and supports migration of smooth muscle cells, which promotes collagen deposition into the plaques [130].

  - ***Calca (calcitonin/calcitonin-related polypeptide, alpha – CGRP -downregulated 3,5-fold)***; ***Calcb (calcitonin-related polypeptide, beta or CGRP2 - downregulated 3.6-fold)***. Calca and Calcb are mediators of inflammation; Calca is involved in the accumulation of inflammatory cells in areas of inflammation [131]. It has been

shown that it is induced by TNF-α in the trigeminal ganglion neurons [132]. Additionally, Calca has pro-angiogenic action [133]. Calcb plays a pathogenic role in human joint inflammation and high levels of Calcb are measured in patients with osteoarthritis, gout and rheumatoid arthritis [134].

- ***Tnfsf18 (tumor necrosis factor (ligand) superfamily, member 18 - downregulated 2.25-fold)*** encodes for Glucocorticoid-Induced TNF-Related Ligand (GITRL) which, interacting with Glucocorticoid-induced tumour necrosis factor receptor family related protein (GITR), mediates atherogenesis via the induction of pro-atherogenic cytokines/chemokines, and destabilizes the atherosclerotic plaques through the induction of matrix metalloproteinase 9 (MMP-9) [135].

- ***Il1r2 (interleukin 1 receptor, type II - downregulated 2.5-fold)***, which pro-inflammatory activity is exert through IL-1 activity regulation [136,137].

- ***Ptgs2 (prostaglandin-endoperoxide synthase 2 - COX2 - downregulated 1.9-fold)***, which is expressed in atherosclerotic lesions in ApoE-/- mice and its inhibition prevents atherosclerosis [138,139]. It's modulated by shear stress [140].

- ***Has1 (hyaluronan synthesis 1 - downregulated 2.2-fold)*** is a key molecule of the extracellular matrix. High levels are associated to atherosclerosis and restenosis. The cyclooxygenase (COX) products, prostacyclin and prostaglandin E(2), induce hyaluran synthesis *in vitro* by transcriptional up-regulation of Has2 and Has1 [141].

- ***Tslp (thymic stromal lymphopoietin, downregulated 1.9-fold)***. Induced by ox-LDL in HUVECs [142]. Target of Ang II via AT1 receptor/NF kappaB pathway [143].

- ***Cd55 (CD55 antigen (DAF) - downregulated 1.7-fold)*** which role in atherosclerosis is well established in ApoE (-/-)/CD55(-/-) mice [144].

- ***Clip4 (CAP-GLY domain containing linker protein family, member 4 - RSNL2 - dowregulated 2.7-fold)***. Reduced expression of this gene has been found in peripheral blood monocytes after treatment with anti inflammatory annexin A1-derived peptide Ac1-25 [145]. Other members of Clip family are regulated by shear stress [146].

- **Inflammation: Anti-inflammatory genes**

  - ***Esr1*** *and* ***Esr2 (estrogen receptor 1 and 2 upregulated 1.9 and 1.5-fold respectively***) are known to protect against inflammation.

  - ***Ffar3 (free fatty acid receptor 3 - GPR43 - upregulated 1.6-fold)*** which assumes an anti-inflammatory role through his SCFAs (short-chain fatty acids)-mediated activation [147].

  - ***Rgs4 (regulator of G-protein signaling 4 – upregulated 1,82-fold)***: it is involved in PPARdelta-mediated antiinflammatory mechanism, which inhibits angiotensin II-accelerated atherosclerosis [148]. It's regulated by shear stress [146] and other members of Rgs family are modulated by ivabradine treatment.

  - ***Igf1 (insulin-like growth factor 1 - upregulated 1.3-fold)***: it reduces vascular inflammation, oxidant stress and decreases atherosclerotic plaque progression [149].

3.4 Pathways classification and enrichment analysis

To identify underlying biological pathways, the differentially expressed genes were then analyzed using MetaCore™ (GeneGo, Inc., St. Joseph, MI, USA), a web-based computational platform designed for systems biology. Similar analyses were conducted using DAVID Bioinformatics Resources 6.7 (National Institute of Allergy and Infectious Diseases NIAID, NIH).

These analyses allowed the identifications of enriched pathways. A pathway is considered enriched if it is more strongly represented in the list of differentially expressed gene than would be predicted by chance alone based on the total number of genes in the pathway proportionate to the number of genes on the array [150]. Some of these pathways are discussed below.

Both MetaCore and DAVID (Table 3) analyses identified with high statistical significance the Notch pathway among the enriched pathways. The role of Notch pathway in the vascular system is well established [151] where it plays a pivotal function in preserving endothelium integrity by protecting endothelial cells from apoptosis, induced by conditions such as inflammation and ischemia [152–154]. Notch signalling activation by high pulsatile flow was associated with increased expression of antiapoptotic genes Bcl-2 and

Bcl-xL, and reduced apoptosis [155]. Ivabradine treatment induced upregulation of receptor Notch1, downregulation of ligand Jagged2, upregulation of transcriptional co-activator of Notch Maml3 (mastermind-like 3), Notch-activated transcription factor Rbp-jk (recombination signal binding protein for immunoglobulin kappa J region), and Notch transcriptional target Hes5 (a major transducer of Notch signals in brain vascular development [156]). Our literature search identified modulation of two additional targets of Notch in our gene list, Nanog (2.5-fold upregulated) and Tlx2 (T cell leukemia, homeobox 2 - 7-fold downregulated). In microglial cells, Nanog inhibits LPS-induced expression of pro-inflammatory cytokines by blocking NF-κB [157]. Tlx2 is inhibited by Notch1 activation in amphioxus epidermal sensory neurons [158].

Pathway Name	Gene Symbol	Gene Name	p-value	FC (Abs)	up/down
Notch signaling pathway	Notch1	Notch gene homolog 1 (Drosophila)	0,0037354	1,59442	up
	Hes5	hairy and enhancer of split 5 (Drosophila)	0,0077782	3,34006	up
	Jag2	jagged 2	0,0028323	2,21664	down
	Maml3	mastermind like 3 (Drosophila)	0,0091298	1,52147	up
	Rbp-jK	recombination signal binding protein for immunoglobulin kappa J region	0,0045399	1,5319	up

Table 3: David analysis of individual components of the Notch signalling pathway significantly modulated

MetaCore and DAVID analyses identified MAPK pathway as significantly modulated by ivabradine treatment (Table 4). MetaCore analysis indicates downregulation Prkca (protein kinase C, alpha), Grb2 (Growth factor receptor-bound protein 2), Araf (V-Raf Murine Sarcoma 3611 Viral Oncogene Homolog) and Mras (muscle and microspikes RAS), which suggests inhibition of phosphorylation cascade which activates ERK1/2 signaling. David analysis identified upregulation of Ppma1 (protein phosphatase 1A, magnesium dependent, alpha isoform) which encodes for a Ser/Thr protein phosphatase that inactivates ERK2 [159]. Inhibition of ERK1/2 signalling leads to inhibition of NF-κB activity and therefore reduced inflammation and endothelial dysfunctions [116,160]. Of interest, ERK1/2 in endothelial cells is activated by shear stress [161]. Among the gene belonging to MAPK signaling pathway, we found Cacna1i (calcium channel, voltage dependent, alpha 1I subunit – upregulated 1,55-fold) which reduced expression was evaluated in VSMCs affected by atherosclerosis[162] and Cacng7 (calcium channel, voltage dependent, gamma

subunit 7 – upregulated 2,62-fold) whose expression is reduced in atrial and ventricular myocytes ischemic cardiomyopathy (Table 4 –David analysis)[163].

Pathway Name	Gene Symbol	Gene Name	p-value	FC (Abs)	up/down
MAPK signaling pathway	Rasgrf2	RAS protein-specific guanine nucleotide-releasing factor 2	9,54E-04	1,52216	**up**
	Map3k14	Mitogen-activated protein kinase kinase kinase 14	0,001384	1,69729	**up**
	Cacna1i	calcium channel, voltage-dependent, alpha 1I subunit	0,0084313	1,55184	**up**
	Cacng7	calcium channel, voltage-dependent, gamma subunit 7	0,0050768	2,61994	**up**
	Dusp14	dual specificity phosphatase 14	0,0089758	1,64527	**down**
	Il1r2	interleukin 1 receptor, type II	0,0070304	2,49972	**down**
	Mapk8ip2	mitogen-activated protein kinase 8 interacting protein 2	0,0034333	2,46491	**up**
	Map3k8	mitogen-activated protein kinase kinase kinase 8	0,0030304	1,52362	**down**
	Mras	muscle and microspikes RAS	0,0064321	2,11209	**down**
	Prkca	protein kinase C, alpha	0,0046626	1,52153	**down**
	Ppm1a	protein phosphatase 1A, magnesium dependent, alpha isoform	1,09E-04	2,40045	**up**
	Rras2	related RAS viral (r-ras) oncogene homolog 2	0,0024018	1,59421	**down**

Table 4: David analysis of individual components of the MAPK signaling pathway significantly modulated

Lastly MetaCore and DAVID analyses identified enrichment of sterol metabolic processes in our gene List 2 (Table 5). Ldlr and Hmgcs1 (3-Hydroxy-3-Methylglutaryl-CoA Synthase) expression is regulated by SREBP1 (sterol regulatory element- binding proteins) a family of transcription factors activated by low levels of sterols and by shear stress; while laminar flow induces only a transitory activation of SREBP1, under disturbed flow the activation is prolonged [49]. Of interest, Ch25h (downregulated by the treatment) plays a role in inflammation in addition to the more established role in the regulation of cholesterol homeostasis [164]. These gene encodes for an enzyme which catalyze the formation of 25-hydroxycholesterol from cholesterol, which increases macrophage foam cell formation in Apoe -/- mice [165].

Pathway Name	Gene Symbol	Gene Name	p-value	FC (Abs)	up/down
Cholesterol metabolic process	Hnf1a	HNF1 homeobox A	0,0092684	2,07714	up
	Nsdhl	NAD(P) dependent steroid dehydrogenase-like	0,0053965	1,94195	down
	Ch25h	cholesterol 25-hydroxylase	0,0021805	1,81742	down
	Cyp46a1	cytochrome P450, family 46, subfamily a, polypeptide 1	0,0094426	1,87193	up
	Cyp51	cytochrome P450, family 51	0,0034192	2,26716	down
	Lepr	leptin receptor	0,0083405	1,95811	up
	Ldlr	low density lipoprotein receptor	0,0052362	2,13844	down
	Hmgcs1	similar to Hmgcs1 protein; 3-hydroxy-3-methylglutaryl-Coenzyme A synthase 1	4,45E-04	3,28802	down
	Sc4mol	sterol-C4-methyl oxidase-like	0,0072525	1,6151	down
	Esr1	estrogen receptor 1 (alpha)	0,0047946	1,97645	up
	Nr1h4	nuclear receptor subfamily 1, group H, member 4	0,001839	2,24837	down

Table 5: David analysis of individual components of the cholesterol metabolic process significantly modulated

3.5 Ivabradine antagonizes NF-κB activation of target genes and Angiotensin II activation

In Table 6 are shown 10 genes that are downregulated by ivabradine and are induced (the same gene or a closely structurally/functionally related one) by nuclear factor KappaB (NF-κB). In the contest of atherosclerosis, activation of NF-κB is mediated by numerous stimuli, including local factors (such as vascular injury and wall thickness-mediated hypoxia), oxidative stress (Ox-LDL, homocysteine), cytokines (TNFα, IL-1), angiotensin II (AngII) , integrin/matrix pathway and hemodynamic forces [166–169]. Furthermore, NF-κB modulates expression of many genes involved in the initiation and progression of atherosclerotic lesions, such as VCAM-1, ICAM-1, P- and E-selectin and MCP-1. Activated nuclear NF-κB was detected in macrophages and vascular smooth muscle cells in atherosclerotic regions in humans and animal models [168]. The role of NF-κB in endothelial cells was elucidated by experiments showing that endothelial cells in the atheroprone aortic arch show higher levels of different NF-κB components compared with atheroprotected regions [168]. Moreover, endothelium-restricted inhibition of NF-κB reduces plaque formation in ApoE -/- mice fed with a cholesterol-rich diet [170].

The table was obtained by comparing the genes in List 2 with known NF-κB targets listed in the Boston University database (http://www.bu.edu/nf-kb/gene-resources/target-genes).

Among these genes we found Wnt7a (MMTV integration site 7A - downregulated 5.18-fold): this gene is an activator of Wnt signalling. Wnt-stimulates angiogenesis and it is a very well known Notch signaling modulator [171]. In VSMc, Wnt7a is induced by TNF α and it has been implicated in aorta calcification in diabetic Ldlr -/- mice [172]. Another gene listed in Table 6 is Slc6a4s (solute carrier family 6 (neurotransmitter transporter, serotonin), member 4 - downregulated 3.41-fold): this gene is involved in the uptake of 5-hydroxytryptamine (5-HT, serotonin) a well characterized neurotransmitter in the central nervous system which also plays diverse roles in the circulation by regulating vascular tone and platelet function. An elevated plasma concentration of 5-HT is a common feature of cardiovascular disease often associated with enhanced platelet activation and thrombosis. It has been shown that down-regulation of the serotonin transporter on the platelet surface may counteract the pro-thrombotic influence of elevated levels of serotonin in plasma [173]. Other members of the same family are also modulated by ivabradine and other genes belonging to this family are regulated by shear stress and are NF-κB target [115].

Gene name (ivabradine modulated)	FC (abs)	Regulation	Function	Gene name (Nk-kb modulated)	NF-kB Regulation	References
CD55 antigen (CD55)	1,77	down	Cell surface complement regulatory protein	CD55	up	Izban MG et al. PLoS One. 2012;7(11):e49318
Prostaglandin-endoperoxide synthase 2 (Ptgs2 COX-2)	1,91	down	Inflammation	PTGIS prostaglandin synthase	up	Yokoyama C et al. Genomics. 1996 Sep 1;36(2):296-304
			Inflammation	PGES, prostaglandin E synthase	up	Zhou A et al. Oncogene. 2003 Apr 3;22(13):2054-64
Hyaluronan synthase1 (Has1)	2,23	down	Synthesizes hyaluronic acid	HAS1	up	Saavalainen K et al. J Biol Chem. 2007 Apr 13;282(15):11530-9
Interleukin 1 receptor, type II (Il1r2)	2,50	down	inflammation	IL-1RN	up	Smith MF Jr et al. J Immunol. 1994 Oct 15;153(8):3584-93
Oxidized low density lipoprotein (lectin-like) receptor 1 (Olr1) Lox1	3,20	down	receptor for oxidized low density lipoprotein	LOX-1	up	Nagase M et al. J Biol Chem. 1998 Dec 11;273(50):33702-7
Solute carrier family 6 (neurotransmitter transporter, serotonin), member 4 (Slc6a4)	3,42	down	(neurotransmitter transporter, serotonin)	SLC6A6 (neurotransmitter transporter, taurine)	up	Mochizuki T et al. FEBS Lett. 2005 Jun 6;579(14):3069-74
Gap junction protein, beta 3 (Gjb3)	4,40	down	Communications between endotheliial cells	GJB1	up	Yamamoto T et al. Exp Cell Res. 2004 Oct 1;299(2):427-41
				GJA1		Florian Alonso et al. Cardiovascular Research (2010) 87, 166–176
Serine (or cysteine) peptidase inhibitor, clade B, member 5 (Serpinb5)	5,03	down	Endothelial cells apoptosis inducer	SERPINE2	up	Suzuki S et al. FEBS Lett. 2006 May 29;580(13):3257-62
Wingless-related MMTV integration site 7A (Wnt7a)	5,18	down	Induction of angiogenesis	WNT10B	up	Katoh M. Int J Mol Med. 2007 Apr;19(4):699-703
T-cell leukemia, homeobox 2 (Tlx2)	7,09	down	homeobox protein	TLX2	up	Zhang M et al. Vasc Med. 2008 Aug;13(3):239-45

Table 6: List of NF-κB related genes modulated by ivabradine

Our analysis identified 9 genes that are modulated in opposite direction by Angiotensin II and ivabradine (Table 7). Ang II is activated by dyslipidemia and it is a potent inducer of atherosclerosis [174] by enhancing the release of growth factors (e.g. PDGF, TGF-β, IGF-I), chemokines (MCP-1) and cytokines (IL-6, IL-1). Ang II can also alter the extracellular matrix remodeling via activation of metalloproteinases (MMP-2, MMP-9) and induce a procoagulant state. Ang II can increase expression of adhesion molecules (E-selectin, VCAM-1, and ICAM-1), enhance the recruitment of local macrophages into the atherosclerotic plaque and, not least, it can augment endothelial dysfunction and inflammation promoting NADPH oxidase-mediated ROS production, which in turn reduces NO bioavailability and promotes oxidation of LDL [31,175]. Our results confirm and expand Custodis et al. observations in Apo E-deficient mice in which ivabradine improves vascular compliance also by antagonizing Ang II activation [100].

Gene name (ivabradine modulated)	FC (abs)	Regulation	Function	Angiotensin II regulation	Reference
low density lipoprotein receptor (Ldlr)	2,14	down	Binds LDL and transpots it into cells by endotcytosis	Up	Sendra J et al. Cardiovascular research 2008 (LDL receptor related protein in VSMc)
muscle and microspikes RAS (Mras)	2,11	down	Acts downstream of TNF alpha in causing apoptosis	Up	http://betacellgenebank.ulb.ac.be/page/GeneMore/display/?seq_id=D89863
oxidized low density lipoprotein (lectin-like) receptor 1 (Olr1)	3,20	down	Endothelial receptor that mediates uptake of oxLDL and promotes plaque's formation.	Up	Henning Morawietz et al. Circulation. 1998;98[suppl I]:I-521
prostaglandin-endoperoxide synthase 2 (Ptgs2)	1,91	down	Key enzyme in prostaglandin biosynthesis. Promotes inflammation and atherosclerosis	Up	Schlondorff D et al. Am J Physiol. 1987; 253: C113–C120
regulator of calcineurin 1 (Rcan1)	1,53	down	Regulator of calcineurin which madiates pathological vascular wall remodelling and VSMCs migration	Up	Esteban V et al. J Exp Med. 2011 Sep 26;208(10):2125-39
thymic stromal lymphopoietin (Tslp)	2,00	down	Protein belonging to the cytokine family and It's upregulated in atherosclerosis	Up	Hui Zhao et al.Cell Physiol Biochem. 2012 Nov 16;30(6):1383-1397
T-cell leukemia, homeobox 2 (Tlx2)	7,09	down	Induced by BMP2 which is activated by AngII	Up	Zhang M et al. Vasc. Med 2008
phosphodiesterase 3A, cGMP inhibited (Pde3a)	1,60	up	PDE3A has cardioprotective effects against AngII-induced cardiac injury	Negative regulator of AngII	Masayoshi Oikawa et al. Circulation. 2012; 126: A9719
regulator of G-protein signaling 4 (Rgs4)	1,83	up	RGS4 has been reported to be negative regulator of AngII signaling through the AT1 receptor	Negative regulator of AngII	Yasunori Takata et al. Proc Natl Acad Sci U S A. 2008 Mar 18;105(11):4277-82

Table 7: List of Angiotensin II related genes modulated by ivabradine

3.6 qRT-PCR validation of microarray analysis results

To validate the microarray results, qRT-PCR was carried out to measure the expression levels of some of the genes affected by the treatment. Among the genes identified, we focused on Nppc (one of the most sensitive shear-stress responsive gene, downregulated 5.7-fold), and Olr1/LOX-1 (for the pivotal role in atherosclerosis, downregulated 3.2-fold) The reduction of Nppc mRNA by ivabradine was confirmed in two groups of RNAs. In the remaining RNA utilized for the main microarray experiment (Figure 26) and in RNA not included in microarray analysis (Figure 27).

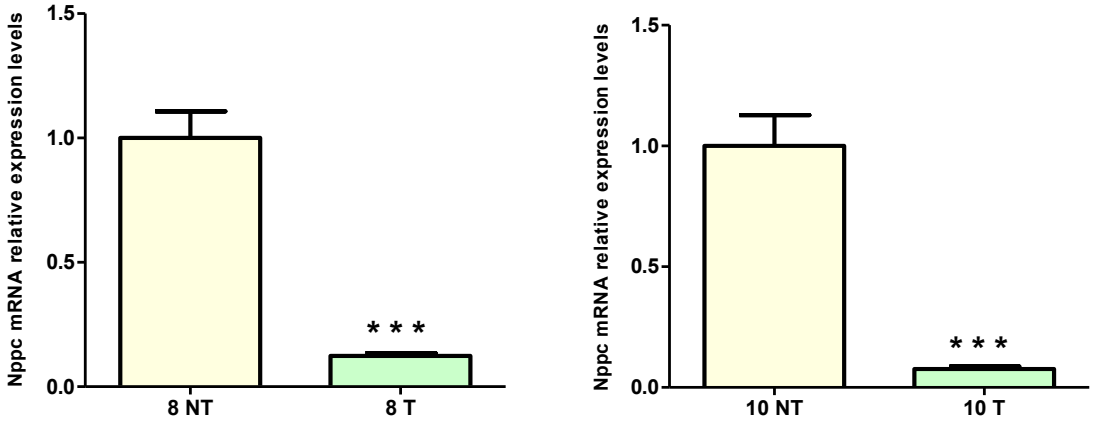

Figure 26: qRT-PCR analysis of Nppc expression before and after 2 (left panel) or 4 (right panel) weeks treatments with ivabradine (30mg/kg/day in drinking water). Each point is a mean value of 3 pool of RNA (each pool is a collection of two ApoE -/- mice aortic arch endothelial cells enriched-RNA, previously analyzed by microarray). Relative changes in mRNA expression levels were calculated according to the $2^{-\Delta\Delta Ct}$ method using RPL13 as reference gene (*** $p < 0.0001$). T: treated; NT: untreated.

In this first analysis (Figure 26), we found a highly significant reduction (87.6%) in Nppc mRNA, following two weeks of ivabradine treatment (8NT Vs T). This reduction was even greater (92,3%) after four weeks of ivabradine treatment (10NT Vs 10T). The ivabradine-mediated Nppc mRNA reduction was also confirmed in RNA from the second group (Figure 26). In order to demonstrate the effect of ivabradine on Olr1 gene expression, we could only rely on RNAs from the second group. As shown in Figure 27, Olr1 was downregulated after two weeks of treatment (68% of reduction compared to untreated group). This reduction was even more evident in 10 weeks old ApoE -/- mice aortic arch endothelial cells enriched-RNA, following four weeks of treatment (92%).

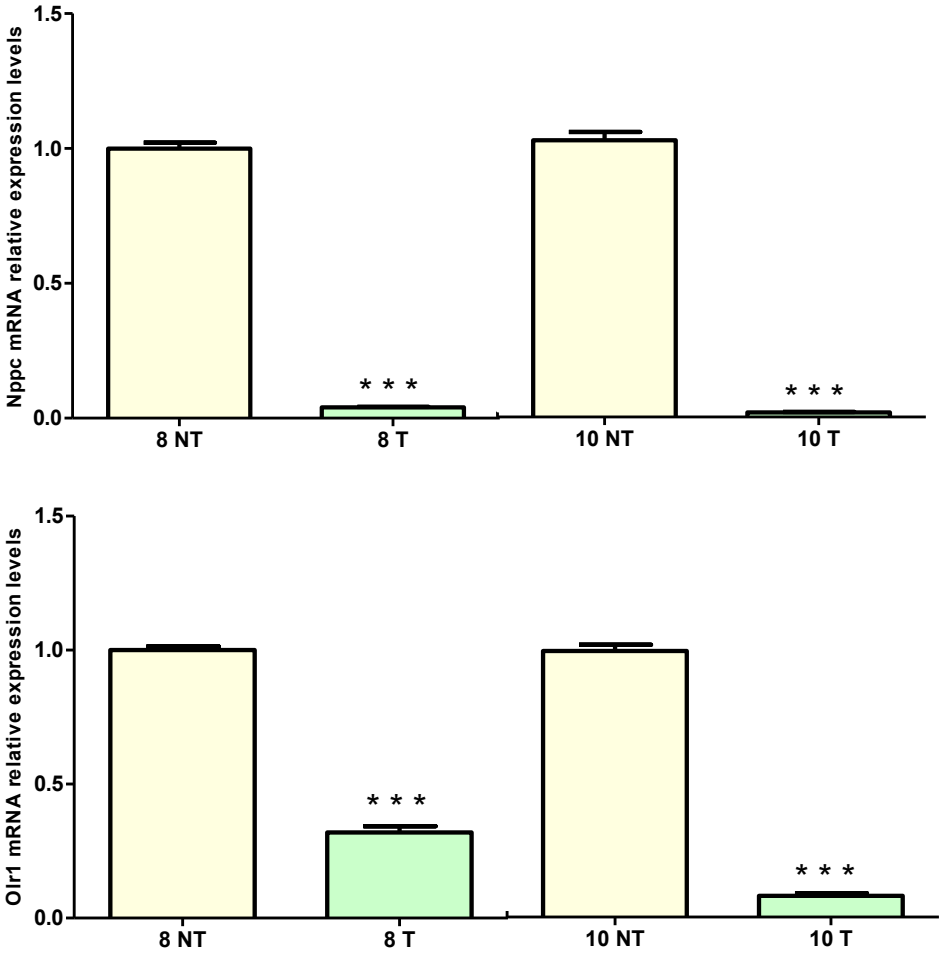

Figure 27: qRT-PCR analysis of Nppc (upper panel) and Olr1 (bottom panel) expression before and after 2 or 4 weeks treatments with ivabradine (30 mg/kg/day in drinking water). Each point is a pool of two ApoE -/- mice aortic arch endothelial cells enriched-RNA. Relative changes in mRNA expression levels were calculated according to the $2^{-\Delta\Delta Ct}$ method using RPL13 as reference gene. (*** $p < 0.0001$). T: treated; NT: untreated.

3.7 En face analysis of endothelium: endothelial dysfunction and Hes5

This analysis aimed to characterize the effect of ivabradine treatment in counteracting endothelial dysfunction in ApoE-/- mice.

We first tried to measure endothelial dysfunction in 10 weeks old ApoE-/- mice (n=4) by en face analysis of VE-Cadh, a cell-cell adhesion glycoprotein which controls the intracellular junctions integrity [176]. As shown in Figure 28, no lesions were visible in endothelium of untreated ApoE-/- mice. We tried to perform again the same measurement of endothelial integrity grade, in untreated 18 weeks old ApoE-/- mice (n=4). Even in this case no dysfunctions were detected (data not shown).

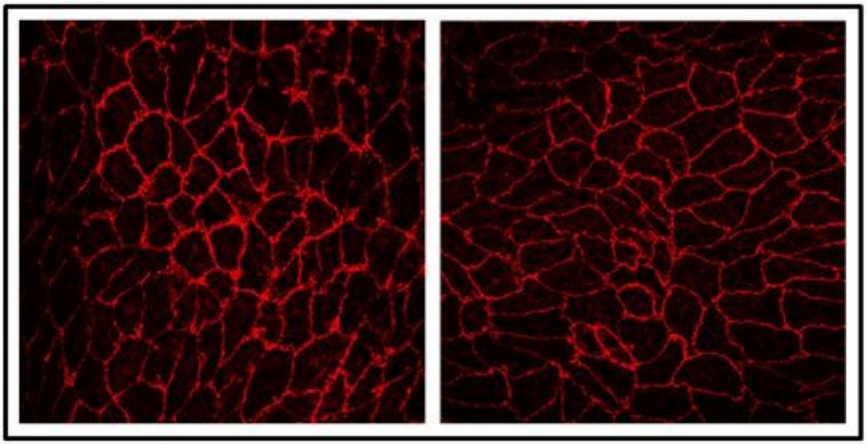

Figure 28: VE-cadherin staining in aortic arches arch lesser curvature of 10 weeks old ApoE -/- untreated mice. Images acquired with Zeiss Confocal microscope (magnification 40X) (n=4; images from 5 fields)

Based on these results, in order to increase our chances to detect differences in in VE-Cadh staining, between treated and untreated mice, 5 weeks old ApoE-/- mice (n=10) were treated or not with ivabradine (30 mg/kg/day) beginning from 6 weeks of age, and were sacrificed when they were 25 weeks old, age at which plaques have been shown in mice fed a chow-diet [85].

In lower arches of untreated mice we observed extensive areas of endothelium covered with atheromatous plaques. The endothelium outside the plaque was heavily damaged, as indicated by the high disorganization of VE-Cadh (images from different field are shown in Figure 29).

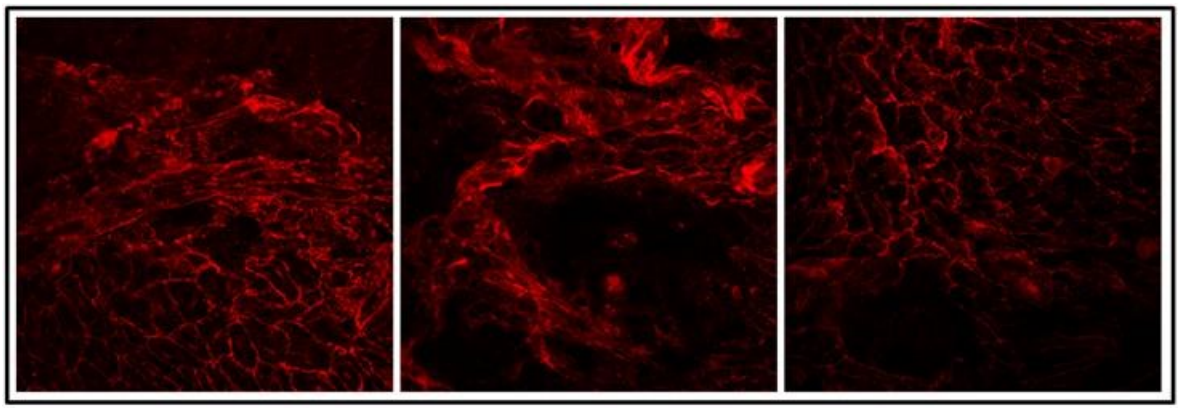

Figure 29: VE-cadherin staining in aortic arches lesser curvature of 25 weeks old ApoE -/- untreated mice. Images were acquired with Zeiss Confocal microscope (magnification 40X) (n=5; images from 5fields)

There were no atheromatous plaques in the lesser curvature of aortic arch in the treated group and the endothelium was mostly intact (images from different fields are shown in Figure 30). In order to obtain a quantitative measure of endothelium damage, we measured

(in four different fields for each section) by Image J the percent area with endothelial damage.

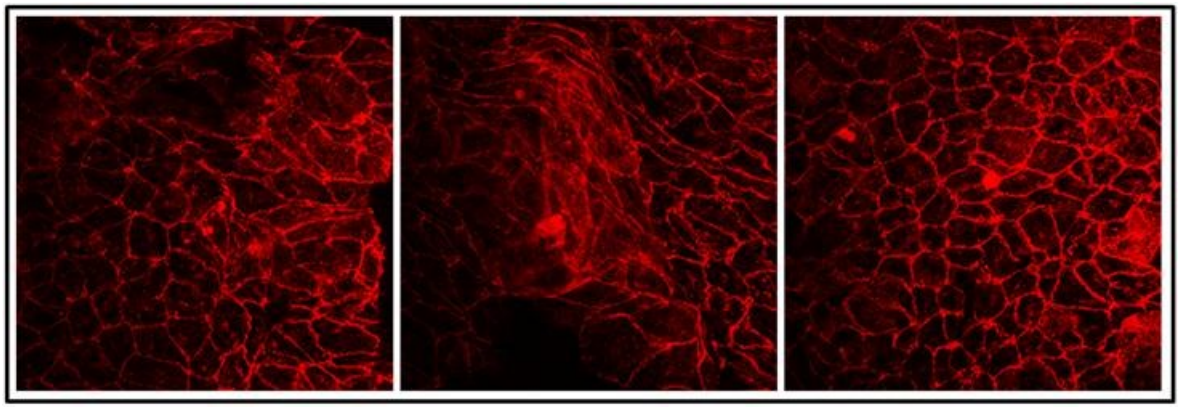

Figure 30: VE-cadherin staining in aortic arches lesser curvature of 25 weeks old ApoE -/- treated mice (30 mg/kg/day in drinking water). Images were acquired with Zeiss Confocal microscope (magnification 40X) (n=5; images from 5fields)

As shown in Figure 31 there was a significant difference in the percentage of damaged endothelium between the two groups of mice (untreated 91,74 ± 4,08 vs treated 28,98 ± 7,28).

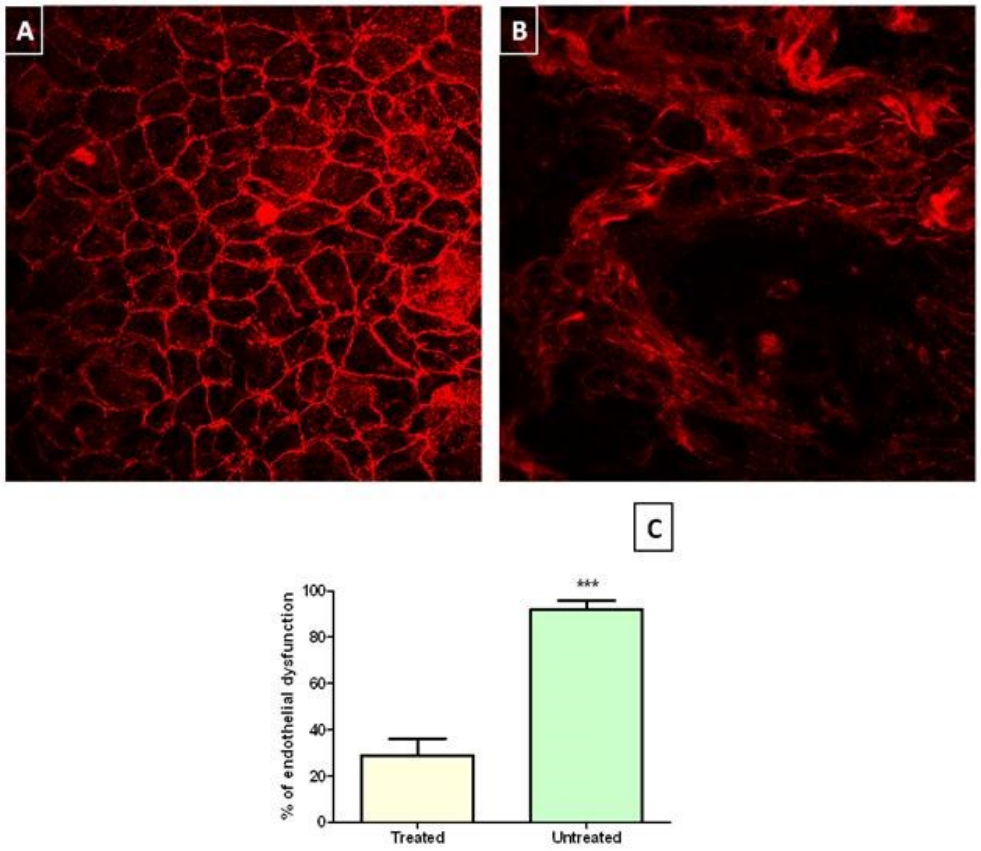

Figure 31: Representative staining for Ve-Cadherin in 25 weeks old ApoE -/- aortic arch lesser curvature, following 19 weeks of treatment with (A) ivabradine (30 mg/kg/day in drinking water) or (B) no treatment. (40X magnification). (C) Difference in area with endothelium damages between treated and untreated mice (*** $p < 0.0001$).

Consistently with our microarray data suggesting a protective effect of ivabradine on the endothelium of the aortic arch, 19 weeks of treatment with ivabradine slowed down endothelial dysfunctions in the lesser arch of the aortic arch. In the same age groups mentioned so far, we tried to validate the effect of ivabradine in modulating Hes5. In 10 weeks old ApoE-/- mice, following 4 weeks of ivabradine treatment (30 mg/kg/day), immunofluorescence analysis for Hes5 was conducted in longitudinal sections of frozen aortic arch fixed in ice cold acetone. Image analysis showed no differences in the expression levels of Hes5 (Figure 32) in the endothelial layer of the aortic arch of ivabradine-treated mice compared with untreated animals.

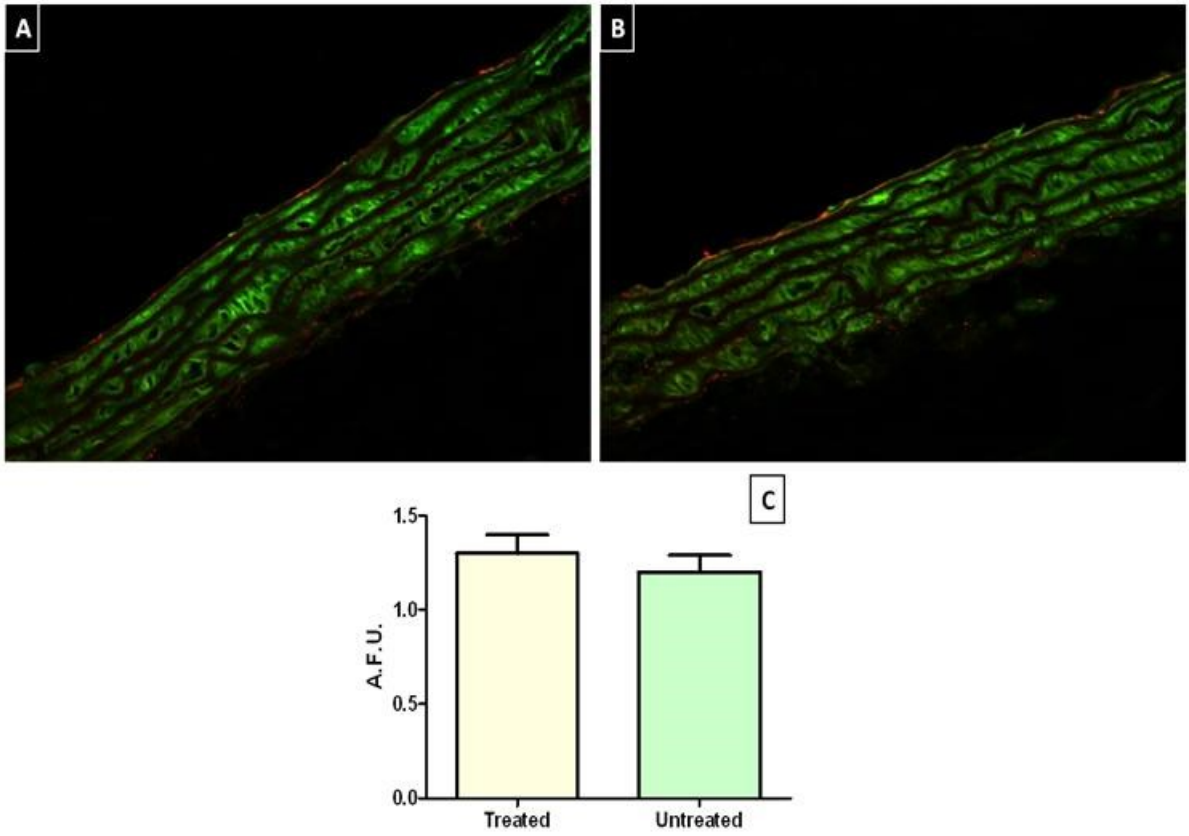

Figure 32: Hes5 (green) and VE-cadherin (red) staining in 10 weeks old ApoE-/- mice aortic arches following 4 weeks of treatment with (A) ivabradine (30 mg/kg/day in drinking water) or (B) no treatment. Images acquired with Zeiss Confocal microscope at 40X magnification. (C) Difference in Hes5 fluorescence values between treated (n=5) and untreated (n=5) mice. Results are expressed as mean ± SEM.

In the same 25 weeks old ApoE-/- mice, following 19 weeks of ivabradine treatment, used for endothelial dysfunction analysis in the inner curvature of aortic arch, we performed Hes5 staining in the upper side of aortic arch, which undergoes the same hemodynamic forces of the inner curvature of aorta. In the upper arch, as seen in the lower one, the endothelium was more extensively damaged in the untreated mice, making Hes5 detection

very complicated and his quantification impossible to achieve, due to the limited number of images taken in this samples. Nonetheless, as shown in Figure 33, Hes5 staining seemed to be more intense in upper arch of treated mice compared to untreated mice, data consistent with ivabradine-mediated Hes5 upregulation observed in microarray analysis.

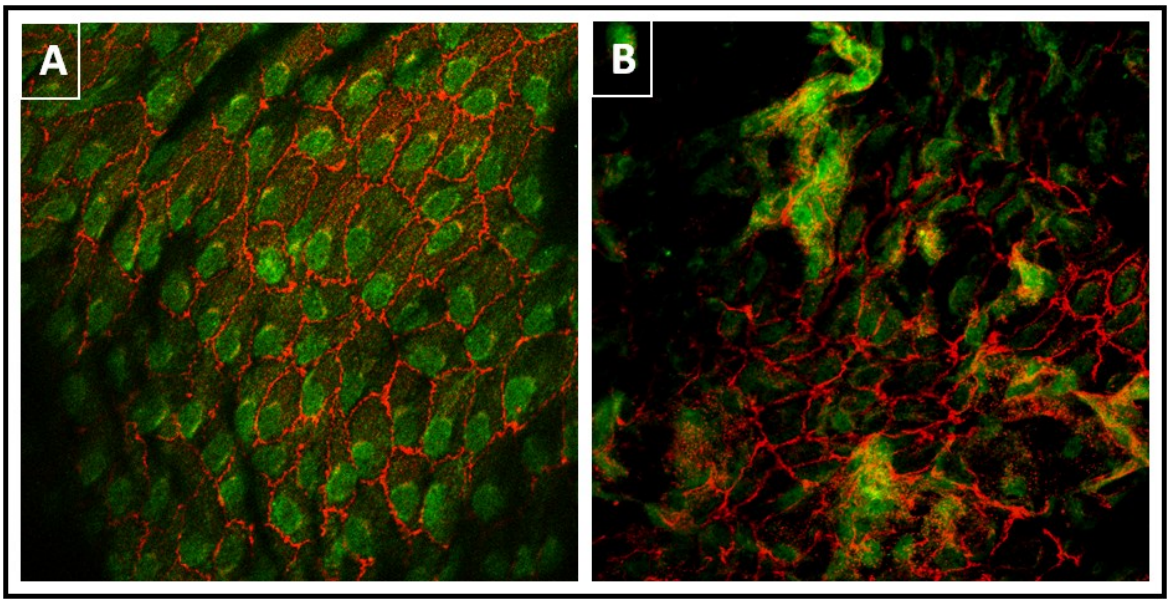

Figure 33: Representative staining for Hes5 (green) and VE-cadherin (red) in aortic arches upper curvature of 25 weeks old ApoE-/- mice aortic arches following 19 weeks of treatment with (A) ivabradine (30 mg/kg/day in drinking water – n=5) or (B) no treatment (n=5). Images acquired with Zeiss Confocal microscope at 40X magnification.

4. The role of shear stress in ivabradine-mediated protective gene expression profile. Does ivabradine alter the shear stress forces on the endothelium?

The results of our experiments show that, in dyslipidaemic mice fed a standard chow-diet, treatment with ivabradine induces an atheroprotective gene expression profile in the endothelium of the aortic arch characterized by changes in the expression of genes involved in the modulation of ox-LDL uptake, cell permeability, apoptosis, inflammation and, as previously mentioned, reduces the degree of damage to the endothelium of ApoE -/- mice aortic arch.

Many of the genes listed in Table 8, thoroughly discussed above, are shear stress sensitive, supporting the hypothesis that ivabradine may exert its protective role through the regulation of shear stress.

Gene Name (ivabradine modulated)	FC (Abs)	p-value	Regulation by ivabradine treatment	Shear Stress modulation Reference
hyaluronan synthase1 (Has1)	2,23	0,0063	down	(Mohamadzadeh et al. 97-108)
Natriuretic peptide type C (Nppc)	5,73	0,0018	down	(Zhang, Xiao, and Diamond 419-26)
Low density lipoprotein receptor (Ldlr)	2,14	0,0052	down	(Liu et al. 76-81)
Notch gene homolog 1 (Notch1)	1,59	0,0037	up	(Brooks, Lelkes, and Rubanyi 27-41)
Jagged 2 (Jag2)	2,22	0,0028	down	
T-cell leukemia, homeobox 2 (Tlx2)	7,09	0,0001	down	
CAP-GLY domain containing linker protein family, member 4 (Clip4)	2,73	0,0058	down	(Peters et al. 25-33)
regulator of G-protein signaling 4 (Rgs4)	1,83	0,0090	up	
Protein kinase C, alpha (Prkca)	1,52	0,0047	down	
prostaglandin-endoperoxide synthase 2 (Ptgs2)	1,91	0,0060	down	(Passerini et al. 2482-87)
Serine (or cysteine) peptidase inhibitor, clade B, member 5 (Serpinb5)	5,02	0,0013	down	(Dai et al. 14871-76)
Solute carrier family 6 (neurotransmitter transporter, serotonin), member 4 (Slc6a4)	3,42	0,0002	down	
dual specificity phosphatase 14 (Dusp14)	1,65	0,0090	down	(Andersson et al. 441-52)
interleukin 1 receptor, type II (Il1r2)	2,50	0,0070	down	
mitogen-activated protein kinase 8 interacting protein 2 (Mapk8ip2)	2,46	0,0034	up	
mitogen-activated protein kinase kinase kinase 8 (Map3k8)	1,52	0,0030	down	
related RAS viral (r-ras) oncogene homolog 2 (Rras2)	1,59	0,0024	down	
Wingless-related MMTV integration site 7A (Wnt7)	5,17	0,0079	down	(Avvisato et al. 2672-82)
Gap junction protein, beta 3 (Gjb3)	4,40	0,0066	down	
Oxidized low density lipoprotein (lectin-like) receptor 1 (Olr1, LOX1)	3,19	0,0036	down	(Li and Mehta 566-68)
sterol-C4-methyl oxidase-like (Sc4mol)	1,62	0,0073	down	
A disintegrin-like and metallopeptidase with thrombospondin type 1 motif, 8 (Adamts8)	4,67	0,0068	down	(Hohberg et al. 350-61)
leptin receptor (Lepr)	1,96	0,0083	up	
Paraxonase 2 (Pon2)	1,55	0,0021	up	(White et al. 2841-48)
Parkinson disease (autosomal recessive, juvenile) 2, parkin (Park2)	1,52	0,0052	up	
HNF1 homeobox A (Hnf1a)	2,08	0,0093	up	
similar to Hmgcs1 protein; 3-hydroxy-3-methylglutaryl-Coenzyme A synthase 1 (Hmgcs1)	3,29	0,0004	down	
RAS protein-specific guanine nucleotide-releasing factor 2 (Rasgrf2)	1,52	0,0010	up	
Mitogen-activated protein kinase kinase kinase 14 (Map3k14)	1,70	0,0014	up	
NAD(P) dependent steroid dehydrogenase-like (NSDHL)	1,94	0,0054	down	(Dolan et al. C1109-C1118)
muscle and microspikes RAS (Mras)	2,11	0,0064	down	
ATP-binding cassette, sub-family B (MDR TAP), memeber 1A (Abcb1a)	1,93	0,0028	down	(Vion et al. 1323-33)
Cholesterol 25-hydroxylase (Ch25h)	1,82	0,0022	down	(Keuschnigg et al. e74293)
A disintegrin-like and metallopeptidase with thrombospondin type 1motif, 7 (Adamts7)	2,75	0,0042	down	(Bond et al. 366-72)

Table 8: List of ivabradine-modulated genes shear stress sensitive

Among the pathways highlighted in the previous analysis, we found that ivabradine modulated Notch signalling. The Notch pathway has been shown to be upregulated and activated by laminar shear stress *in vitro* [177] but since there are scarce data on the *in vitro* effect of low and oscillatory shear stress on Notch signalling and on the regulation of Notch by shear stress *in vivo*, we attempted to better define the molecular details of Notch signaling modulation by shear stress.

4.1 Notch signalling modulation by *in vitro* shear stress system

The aim of this experiment was to mimic *in vitro*, by using an *ex vivo* culture system (cone-and-plate viscometer), the shear stress patterns found in different regions of mouse aorta, and to study their effect on Notch gene expression profile. Specifically, to simulate low and oscillatory shear stress, peculiarity of the aortic arch, we used a grooved cone and low shear stress force (D-flow-50 rpm-12 dynes/cm^2), whereas to imitate the laminar flow of thoracic aorta, we used a smooth cone and high shear stress force (S-flow-200 rpm-50 dynes/cm^2). After a 24-hours exposition to shear stress, images of HUVECs were taken to evaluate the effect of shear stress on cells shape, an endothelial morphological response to flow and the resultant of shear stress [178–180]. As shown in Figure 34, HUVECs exposed to S-flow were elongated with the major axis aligned in the direction of flow, whereas those exposed to D-flow were round in shape with a not well defined axis direction.

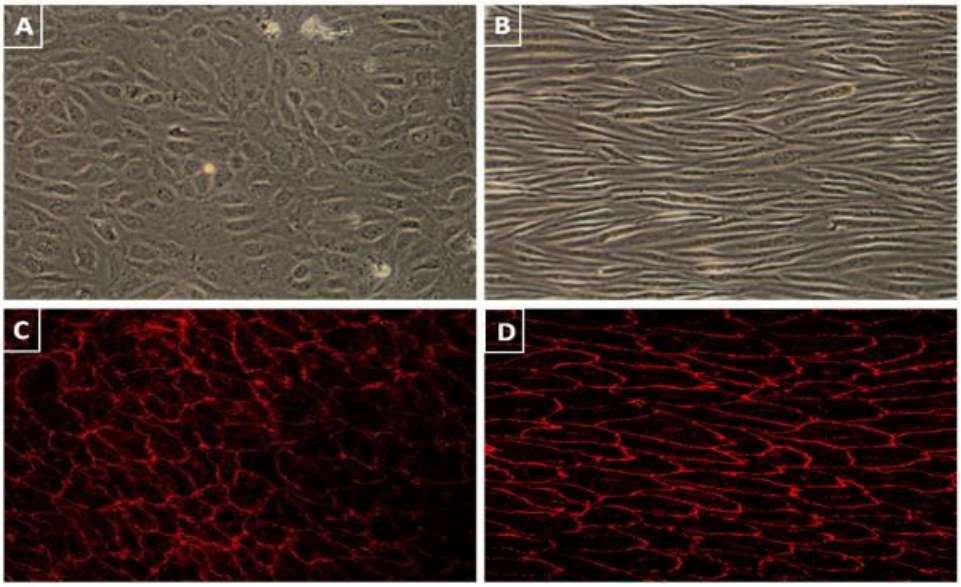

Figure 34: Representative images of HUVECs subjected to (A) D-flow or (B) S-flow (Images acquired at 4X objective), compared to images of endothelium (Ve-Cadherin in red) of whole mount preparation of mouse aortic arch (C) and thoracic aorta (D) (Images acquired with Zeiss Confocal microscope at 40X magnification).

RNA from HUVECs was extracted and qRT-PCR was carried out to measure the expression levels of Notch components. Data obtained showed a significant increase of Hey1 (3.9-fold), Hey2 (3.9-fold), Hes1 (2.74-fold), Notch1 (2.37-fold), Notch2 (2.59-fold) and Jagged-1 (6.31-fold) mRNAs levels in S-flow, compared to static control (Figure 35).

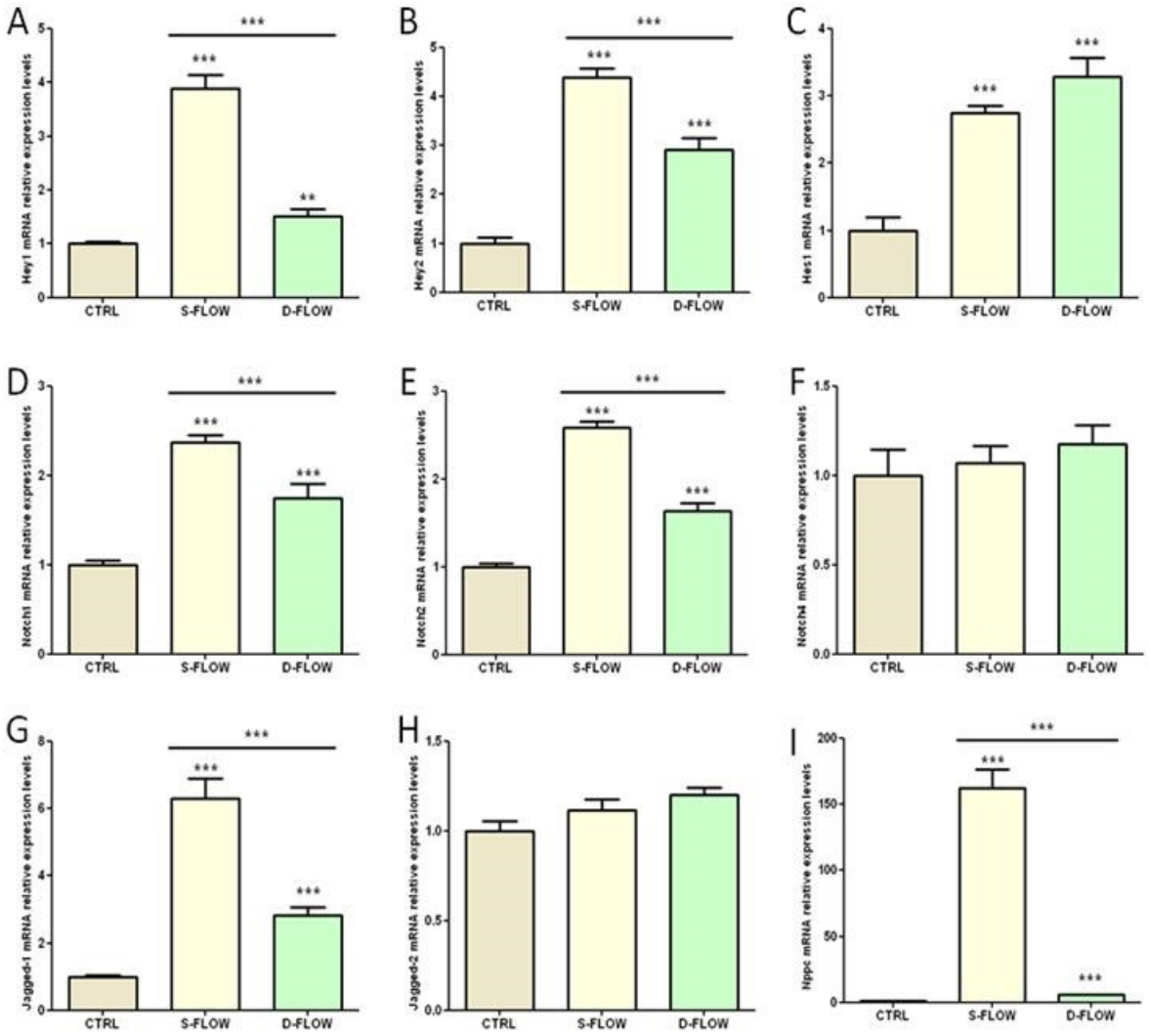

Figure 35: HUVECs were subjected to S-flow and D-flow for 24 hours. Total RNA was extracted and qRT-PCR analysis for (A) Hey1, (B) Hey2, (C) Hes1, (D) Notch1, (E) Notch2, (F) Notch4, (G) Jagged-1, (H) Jagged-2 and (I) Nppc genes expression was performed. mRNA expression levels were calculated according to the $2^{-\Delta\Delta Ct}$ method using RPL13 as reference gene. HUVECs under static flow were used as control. Results are expressed as mean ± SEM of three independent experiments, each performed in triplicate (*** $p < 0.0001$; ** $p < 0.001$).

An increase of the Hey1, Hey2, Hes1, Notch1, Notch4 and Jagged-1 mRNA levels was also found in D-flow condition when compared to static control. This data is not surprising since it has been shown that in HUVECs there are sets of genes regulated by laminar and disturbed flow stimulations in a similar pattern when compared to a static control [115]. Nonetheless, there is no denying that Notch components, except Hes1 in which difference

did not achieve significance, exhibited high mRNA levels in HUVECs in S-flow compared to D-flow condition. No differences in gene expression was found for Notch4 and Jagged-2 under different shear stress conditions. Along with Notch, Nppc was analyzed, which is a well-known laminar shear stress-induced gene [114,181]. As expected, Nppc was highly upregulated by S-flow (162-fold) and, albeit to a lesser extent, by D-flow stimulation (5-fold) (Figure 35).

HUVECs after 24h under static, D- and S- flow were fixed in 4% PFA and stained for Notch1 and Notch4. Microscopy analysis was carried out to measure protein levels.

As shown in Figure 36, in D-flow treated cells we found reduction of Notch1 and Notch4 compared to S-flow and Static control.

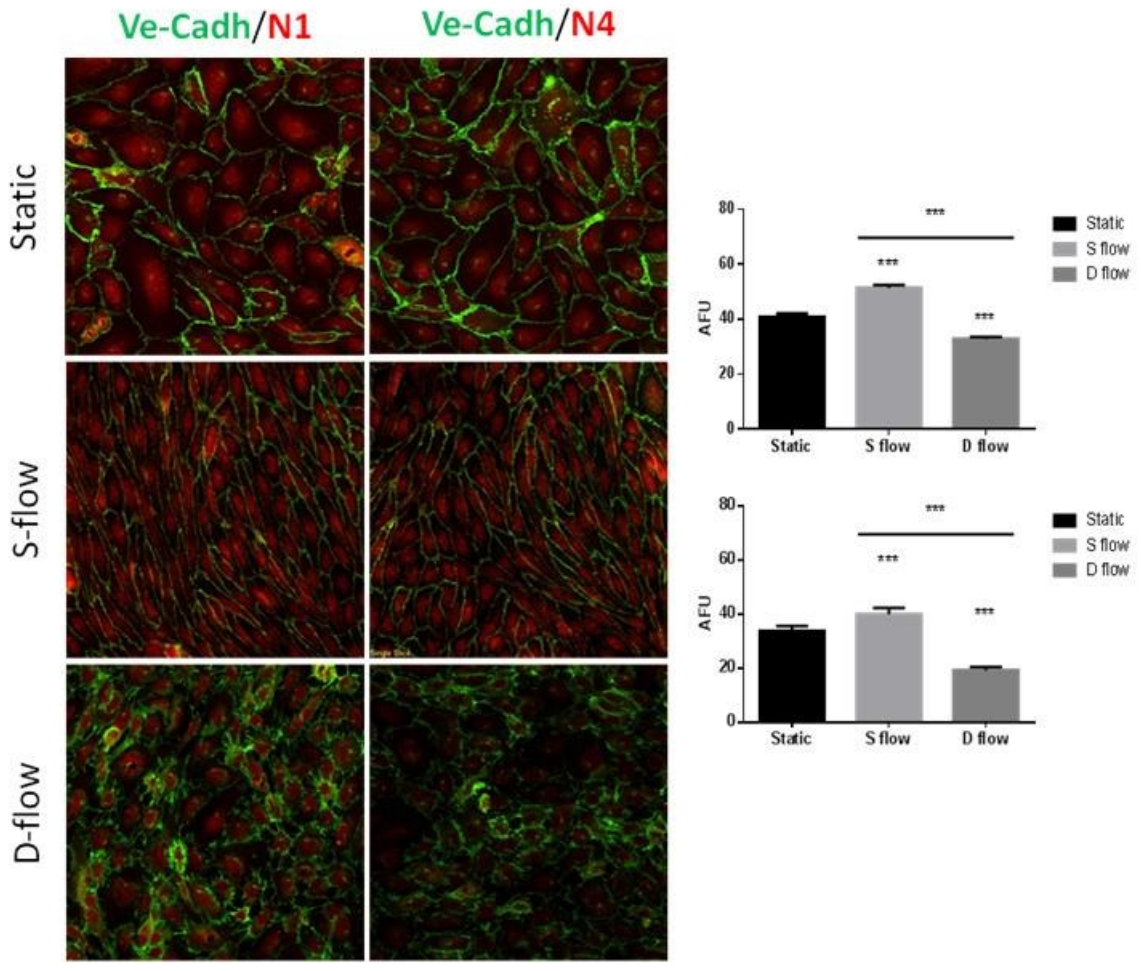

Figure 36: (A) Representative microscopy images of HUVECs (Static, S- and D-flow) stained for Notch1 and 4 (red) and VE-cadherin (green). Images acquired with Zeiss Confocal microscope at 40X magnification. (B) Difference in Notch1 and Notch 4 fluorescence values between HUVECs subjected to the three different flows (static, S- and D- flow). Results are expressed as mean ± SEM of three independent experiments. (*** $p < 0.0001$).

These data suggest a differential Notch regulation by different shear stress conditions, confirming that laminar shear stress induces Notch activation [182] compared to low and oscillatory shear stress.

4.2 Effect of shear stress on gene expression in endothelium of C57BL6/J mice aortic arch and thoracic aorta

Since we demonstrated that Notch is regulated by shear stress *in vitro*, we evaluated differential Notch expression profile between regions of mice aorta subjected either to laminar shear stress (thoracic aorta) or to low and oscillatory shear stress (aortic arch).
We first qualitatively evaluated protein levels of Notch receptors (Notch1 and Notch4) and Notch target genes Hey2 and Hes5 (upregulated by ivabradine treatment - 3,34-fold) in the endothelium of whole mount preparations of aortic arch and thoracic aorta of C57BL6/J mice. Protein levels of Notch4, Hes5 and Hey2 were lower in the aortic arch compared to the thoracic aorta. Notch1 protein levels were similar between the two portions of mice aorta (Figure 37).

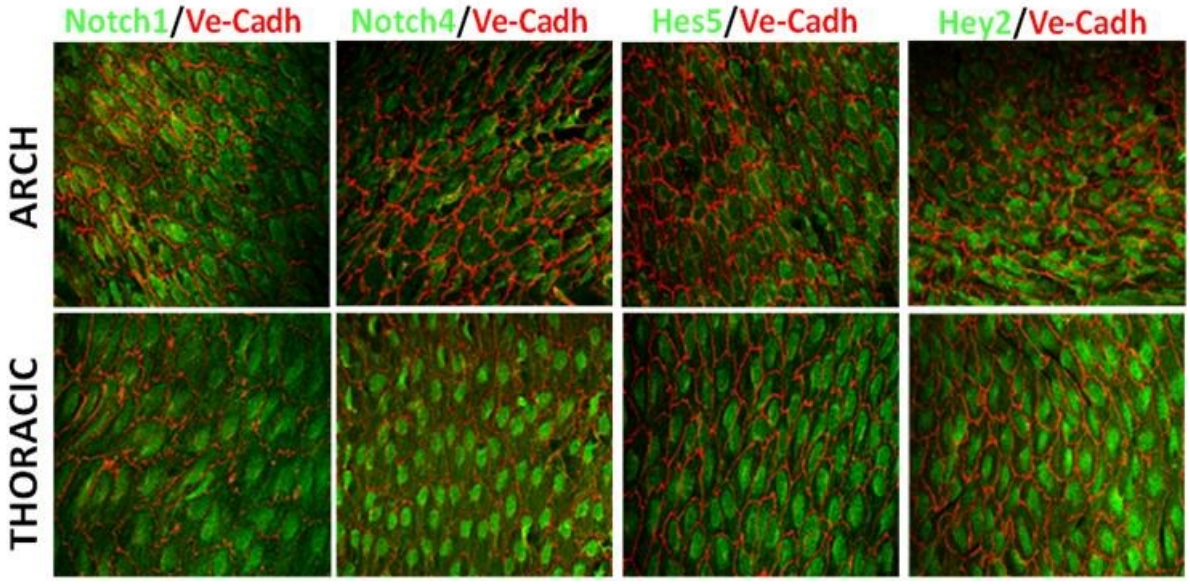

Figure 37: Rapresentative images showing staining of the endothelium of the aortic arch lesser curvature and of thoracic aorta from C57BL6/J mice for Notch 1, Notch 4, Hes5 and Hey2 (green). Endothelial cells membrane was identified by staining for VE-Cadherin (red). Images acquired with Zeiss Confocal microscope at 40X magnification

We also measured their mRNA levels in endothelium-enriched RNA isolated from those regions (n=7). Quantitative RT-PCR showed a significant reduction of Hey2 (0.70-fold) and Notch4 (0.78-fold) mRNAs in the aortic arch, indicating an activation of their gene

expression in the thoracic portion of aorta. The strongest activation was measured for Hes5 mRNA, which was upregulated 11-fold in thoracic aorta compared to aortic arch. There were no clear differences between aortic arch and thoracic aorta in Notch 1 mRNA levels, which resembles his protein levels evaluated by en-face analysis (Figure 38).

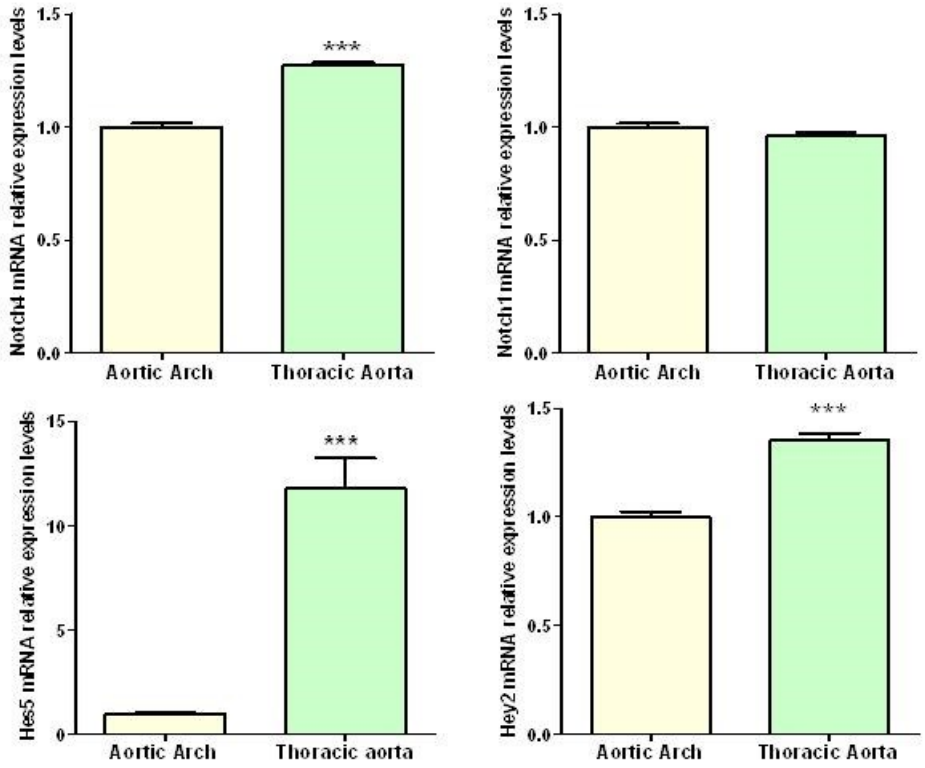

Figure 38: qRT-PCR histograms showing the differences in mRNA expression levels for Notch4, Notch1, Hes5 and Hey2 between aortic arch and thoracic segment. Relative changes in mRNA expression were calculated according to the $2^{-\Delta\Delta Ct}$ method using RPL13 as reference gene (3 experiments, ***P<0.001).

Along with Notch components, we measured the expression of Nppc and Olr1 genes: we found a significant reduction of expression of these two genes in endothelium-enriched RNA isolated from the thoracic aorta compared to aortic arch (Figure 39).

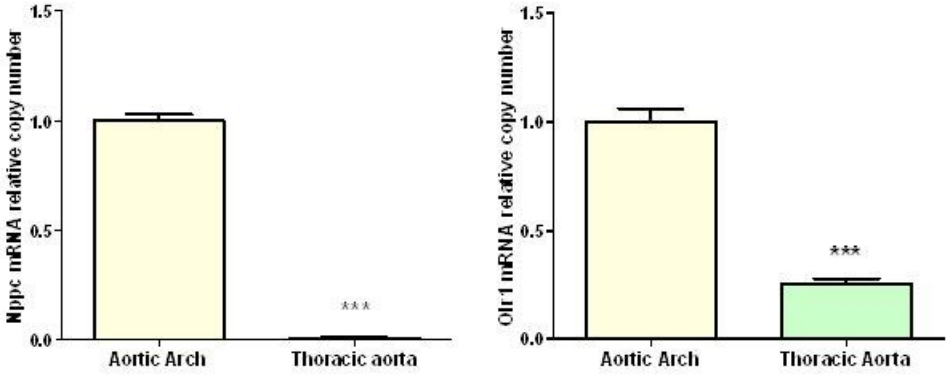

Figure 39: qRT-PCR histograms showing the differences in mRNA expression levels for Nppc and Olr1 between aortic arch and thoracic segment. Relative changes in mRNA expression were calculated according to the $2^{-\Delta\Delta Ct}$ method using RPL13 as reference gene (3 experiments, ***P<0.001).

Our Nppc data of qRT-PCR analysis above are in contrast with those obtained by *in vitro* flow experiments, in which we found a strong activation of Nppc by atheroprotective laminar shear stress. Passerini and collaborators had pointed out that there are some discrepancies between genes identified as modulated by shear stress in other *in vitro* studies, and the same genes which they found out as differentially expressed between lesion-prone areas and protected sites of adult porcine aorta [135]. Actually, these differences could be explained by the disparate systems used in *in vitro* experiments to simulate shear stress, the different type of cell origins and the sensitivities of techniques used. Mostly, it could be quite intricate to compare a long-adapted condition which occurs in the endothelium of blood vessels with a short-time simulation of shear stress patterns *in vitro*.

CONCLUSIONS

This study shows that in dyslipidemic mice fed a standard chow-diet, treatment with ivabradine induces a "protective" gene expression profile in the endothelium suggestive of a reduction of LDL uptake, endothelial cells permeability, oxidative stress and apoptosis. Moreover ivabradine could regulate the endothelium inflammatory status, by both upregulating anti-inflammatory genes and reducing expression of pro-inflammatory genes. It is also noteworthy that the genes we found modulated by ivabradine treatment are regulated in the opposite direction by Nf-κB. Nf-κB is "primed" for activation in atheroprone regions and this "priming" effect is determined by local shear stress which causes an increase in the expression of NF-κB components [168]. Ivabradine didn't alter the mRNA expression levels of NF-κB components, indicating that the drug may inhibit NF-κB action by affecting downstream pathways. Similarly, the analysis of ivabradine-modulated genes shows inhibition of AngII-mediated signalling. AngII signalling is activated under dyslipidemic conditions [183] and it has been shown that in ApoE -/- mice, ivabradine antagonizes AngII also by reducing the mRNA of the AT-1 receptor in the vascular wall [99]. We didn't found changes in the expression levels of AT-1 in treated mice, suggesting that, as with NF-κB, ivabradine may antagonize AngII-mediated signalling by affecting downstream pathways. Of interest, we found MAPK pathways as significantly modulated by ivabradine treatment, with changes suggestive of an inhibition of ERK1/2 signalling. Since both NF-κB and AngII require the activation of the ERK1/2 [116,160], the inhibition of MAPK-related pathways by ivabradine could determine the observed inhibition of NF-κB- and AngII-mediated signalling.

Many of the genes modulated by ivabradine treatment, some of which belong to MAPK, NF-κB, AngII pathway and cholesterol metabolic processes, are shear stress sensitive and this evidence suggests that modulation of shear stress could be part of ivabradine mechanism of protection exerted in aortic arch endothelium of our animal model of atherosclerosis. Our data are in agreement with a recent report showing that ivabradine could alter shear stress at the inner curvature of mice aorta by increasing shear stress magnitude and reducing oscillatory index, along with induction of protective eNOS expression and reduction of inflammatory VCAM-1 [184]. Among the pathways which are modulated by ivabradine and are shear stress sensitive we found Notch signalling. Our *in vitro* flow experiments showed a sustained upregulation of Notch signalling by atheroprotective laminar shear stress. Our *in vivo* analyses on mice aorta confirm the activation of Notch signalling components by the atheroprotective laminar shear stress and

provide the first *in vivo* evidence of differences in expression levels of Notch components between different regions of mouse aorta.

In agreement with these data, suggesting a protective effect of ivabradine on the endothelium of the aortic arch, 19 weeks of treatment with ivabradine significantly reduces endothelium damage and slows down plaque formation in the lesser curvature of aortic arch of ApoE-deficent mice, along with preliminary evidences of higher levels of Hes5 in the upper aortic arch of treated mice compared to untreated ones. Notch activation by ivabradine treatment was also highlighted by microarray data, indicating upregulation of Hes5 and several Notch signalling components. It remains to be established whether downregulation of Notch signalling in the aortic arch could be involved in atherosclerosis onset and/or progression. A possible role of Notch in the context of inflammation and apoptosis, which underlie the first step of atherosclerosis, could derive from his interaction with pathways known to be involved in this process. A link between shear stress and Notch–mediated EC apoptosis has been demonstrated *in vitro* in bovine retinal endothelial cells, where Notch signalling activation by high pulsatile flow was associated with increased expression of antiapoptotic genes Bcl-2 and Bcl-xL, and reduced apoptosis [180]. In the context of inflammation, NF-κB inhibition by activation of Notch signaling has been described. In macrophages, Toll like receptor (TLR4) activation by LPS upregulates Notch target Hes5 which in turns modifies the pattern of expressed cytokines from pro- to anti-inflammatory activity. In these cells, activation of Notch1 mediates ERK1/2 inactivation which inhibits NF-κB induction of inflammatory cytokines [184]. In endothelial cells TNF-α-induced Notch4 and Hes1 downregulation is associated with NF-κB-mediated I-CAM induction [153]. A recently published study has shown that Notch1 activation in endothelial cells downregulates miR155, an activator NF-κB [185]. Thus, activation of Notch could therefore underlie the observed Nf-κB inhibition following ivabradine treatment.

In conclusion this study provides strong evidence of ivabradine-mediated induction of a protective gene expression profile in the endothelium of aortic arch of ApoE-deficient mice. Among the identified pathways, Notch signalling modulation by ivabradine treatment may contribute this protection. Since numerous of these reported genes, including Notch, are shear stress modulated [115], our data are in agreement with the shared views that ivabradine, through heart rate reduction, modifies the shear stress on endothelium.

Reference List

1. Libby P, Ridker PM, Hansson GK (2011) Progress and challenges in translating the biology of atherosclerosis. Nature 473: 317-325. nature10146 [pii];10.1038/nature10146 [doi].

2. Mayerl C, Lukasser M, Sedivy R, Niederegger H, Seiler R, Wick G (2006) Atherosclerosis research from past to present--on the track of two pathologists with opposing views, Carl von Rokitansky and Rudolf Virchow. Virchows Arch 449: 96-103. 10.1007/s00428-006-0176-7 [doi].

3. Williams KJ, Tabas I (1995) The response-to-retention hypothesis of early atherogenesis. Arterioscler Thromb Vasc Biol 15: 551-561.

4. Ross R, Glomset JA (1976) The pathogenesis of atherosclerosis (first of two parts). N Engl J Med 295: 369-377. 10.1056/NEJM197608122950707 [doi].

5. Kenneth S.Saladin (2012) Anatomy Physiology.

6. Giannotti G, Landmesser U (2007) Endothelial dysfunction as an early sign of atherosclerosis. Herz 32: 568-572. 10.1007/s00059-007-3073-1 [doi].

7. Stary HC, Chandler AB, Glagov S, Guyton JR, Insull W, Jr., Rosenfeld ME, Schaffer SA, Schwartz CJ, Wagner WD, Wissler RW (1994) A definition of initial, fatty streak, and intermediate lesions of atherosclerosis. A report from the Committee on Vascular Lesions of the Council on Arteriosclerosis, American Heart Association. Circulation 89: 2462-2478.

8. Deanfield JE, Halcox JP, Rabelink TJ (2007) Endothelial function and dysfunction: testing and clinical relevance. Circulation 115: 1285-1295. 115/10/1285 [pii];10.1161/CIRCULATIONAHA.106.652859 [doi].

9. Namrata Chhabra (2009) Endothelial Dysfuction - A predictor of atherosclerosis. Internt Journal of Medical Update 4: 33-41.

10. Vogiatzi G, Tousoulis D, Stefanadis C (2009) The role of oxidative stress in atherosclerosis. Hellenic J Cardiol 50: 402-409.

11. Winterbourn CC, Kettle AJ (2000) Biomarkers of myeloperoxidase-derived hypochlorous acid. Free Radic Biol Med 29: 403-409. S0891-5849(00)00204-5 [pii].

12. Lusis AJ (2000) Atherosclerosis. Nature 407: 233-241. 10.1038/35025203 [doi].

13. Williams KJ, Tabas I (1995) The response-to-retention hypothesis of early atherogenesis. Arterioscler Thromb Vasc Biol 15: 551-561.

14. Cushing SD, Berliner JA, Valente AJ, Territo MC, Navab M, Parhami F, Gerrity R, Schwartz CJ, Fogelman AM (1990) Minimally modified low density lipoprotein induces monocyte chemotactic protein 1 in human endothelial cells and smooth muscle cells. Proc Natl Acad Sci U S A 87: 5134-5138.

15. McMurray HF, Parthasarathy S, Steinberg D (1993) Oxidatively modified low density lipoprotein is a chemoattractant for human T lymphocytes. J Clin Invest 92: 1004-1008. 10.1172/JCI116605 [doi].

16. Ley K, Miller YI, Hedrick CC (2011) Monocyte and macrophage dynamics during atherogenesis. Arterioscler Thromb Vasc Biol 31: 1506-1516. 31/7/1506 [pii];10.1161/ATVBAHA.110.221127 [doi].

17. Cinzia Fortini CCGAMBMRPaPR (2014) The Role of the Notch Pathway in Atherosclerosis. Indian journal of Cardio Biology & ClinicalSciences 1.

18. Louis SF, Zahradka P (2010) Vascular smooth muscle cell motility: From migration to invasion. Exp Clin Cardiol 15: e75-e85.

19. Risler N, Castro C, Cruzado M, Gonzalez S, Miatello R (2002) Early changes in proteoglycans production by resistance arteries smooth muscle cells of hypertensive rats. Am J Hypertens 15: 416-421. S089570610202263X [pii].

20. Tabas I (2010) Macrophage death and defective inflammation resolution in atherosclerosis. Nat Rev Immunol 10: 36-46. nri2675 [pii];10.1038/nri2675 [doi].

21. Lendon CL, Davies MJ, Born GV, Richardson PD (1991) Atherosclerotic plaque caps are locally weakened when macrophages density is increased. Atherosclerosis 87: 87-90.

22. Libby P (1995) Molecular bases of the acute coronary syndromes. Circulation 91: 2844-2850.

23. van der Wal AC, Becker AE (1999) Atherosclerotic plaque rupture--pathologic basis of plaque stability and instability. Cardiovasc Res 41: 334-344. S0008-6363(98)00276-4 [pii].

24. Rosa GM, Bauckneht M, Masoero G, Mach F, Quercioli A, Seitun S, Balbi M, Brunelli C, Parodi A, Nencioni A, Vuilleumier N, Montecucco F (2013) The vulnerable coronary plaque: update on imaging technologies. Thromb Haemost 110: 706-722. 13-02-0121 [pii];10.1160/TH13-02-0121 [doi].

25. Bostrom K, Watson KE, Stanford WP, Demer LL (1995) Atherosclerotic calcification: relation to developmental osteogenesis. Am J Cardiol 75: 88B-91B.

26. Watson KE, Bostrom K, Ravindranath R, Lam T, Norton B, Demer LL (1994) TGF-beta 1 and 25-hydroxycholesterol stimulate osteoblast-like vascular cells to calcify. J Clin Invest 93: 2106-2113. 10.1172/JCI117205 [doi].

27. Lucerna M, Zernecke A, de NR, de Jager SC, Bot I, van der Lans C, Kholova I, Liehn EA, van Berkel TJ, Yla-Herttuala S, Weber C, Biessen EA (2007) Vascular endothelial growth factor-A induces plaque expansion in ApoE knock-out mice by promoting de novo leukocyte recruitment. Blood 109: 122-129. blood-2006-07-031773 [pii];10.1182/blood-2006-07-031773 [doi].

28. Cheng C, Chrifi I, Pasterkamp G, Duckers HJ (2013) Biological mechanisms of microvessel formation in advanced atherosclerosis: the big five. Trends Cardiovasc Med 23: 153-164. S1050-1738(12)00425-2 [pii];10.1016/j.tcm.2012.10.004 [doi].

29. Badimon L, Vilahur G (2014) Thrombosis formation on atherosclerotic lesions and plaque rupture. J Intern Med 276: 618-632. 10.1111/joim.12296 [doi].

30. Ronak Delewi M, Hayang Yang M, John Kastelein MP (2013) Textbook of Cardiology.

31. Hsieh HJ, Liu CA, Huang B, Tseng AH, Wang DL (2014) Shear-induced endothelial mechanotransduction: the interplay between reactive oxygen species (ROS) and nitric oxide (NO) and the pathophysiological implications. J Biomed Sci 21: 3. 1423-0127-21-3 [pii];10.1186/1423-0127-21-3 [doi].

32. Chatzizisis YS, Coskun AU, Jonas M, Edelman ER, Feldman CL, Stone PH (2007) Role of endothelial shear stress in the natural history of coronary atherosclerosis and vascular remodeling: molecular, cellular, and vascular behavior. J Am Coll Cardiol 49: 2379-2393. S0735-1097(07)01220-X [pii];10.1016/j.jacc.2007.02.059 [doi].

33. Chien S (2008) Effects of disturbed flow on endothelial cells. Ann Biomed Eng 36: 554-562. 10.1007/s10439-007-9426-3 [doi].

34. Chatzizisis YS, Jonas M, Coskun AU, Beigel R, Stone BV, Maynard C, Gerrity RG, Daley W, Rogers C, Edelman ER, Feldman CL, Stone PH (2008) Prediction of the localization of high-risk coronary atherosclerotic plaques on the basis of low endothelial shear stress: an intravascular ultrasound and histopathology natural history study. Circulation 117: 993-1002. CIRCULATIONAHA.107.695254 [pii];10.1161/CIRCULATIONAHA.107.695254 [doi].

35. Stone PH, Coskun AU, Kinlay S, Popma JJ, Sonka M, Wahle A, Yeghiazarians Y, Maynard C, Kuntz RE, Feldman CL (2007) Regions of low endothelial shear stress are the sites where coronary plaque progresses and vascular remodelling occurs in humans: an in vivo serial study. Eur Heart J 28: 705-710. ehl575 [pii];10.1093/eurheartj/ehl575 [doi].

36. Wentzel JJ, Chatzizisis YS, Gijsen FJ, Giannoglou GD, Feldman CL, Stone PH (2012) Endothelial shear stress in the evolution of coronary atherosclerotic plaque and vascular remodelling: current understanding and remaining questions. Cardiovasc Res 96: 234-243. cvs217 [pii];10.1093/cvr/cvs217 [doi].

37. Caro CG, Fitz-Gerald JM, Schroter RC (1969) Arterial wall shear and distribution of early atheroma in man. Nature 223: 1159-1160.

38. Andreou I, Antoniadis AP, Shishido K, Papafaklis MI, Koskinas KC, Chatzizisis YS, Coskun AU, Edelman ER, Feldman CL, Stone PH (2014) How Do We Prevent the Vulnerable Atherosclerotic Plaque From Rupturing? Insights From In Vivo Assessments of Plaque, Vascular Remodeling, and Local Endothelial Shear Stress. J Cardiovasc Pharmacol Ther . 1074248414555005 [pii];10.1177/1074248414555005 [doi].

39. Suo J, Ferrara DE, Sorescu D, Guldberg RE, Taylor WR, Giddens DP (2007) Hemodynamic shear stresses in mouse aortas: implications for atherogenesis. Arterioscler Thromb Vasc Biol 27: 346-351. 01.ATV.0000253492.45717.46 [pii];10.1161/01.ATV.0000253492.45717.46 [doi].

40. Gambillara V, Chambaz C, Montorzi G, Roy S, Stergiopulos N, Silacci P (2006) Plaque-prone hemodynamics impair endothelial function in pig carotid arteries. Am J Physiol Heart Circ Physiol 290: H2320-H2328. 00486.2005 [pii];10.1152/ajpheart.00486.2005 [doi].

41. Endo S, Goldsmith HL, Karino T (2014) Flow patterns and preferred sites of atherosclerotic lesions in the human aorta - I. Aortic arch. Biorheology 51: 239-255. Y688387W20452014 [pii];10.3233/BIR-14005 [doi].

42. Asakura T, Karino T (1990) Flow patterns and spatial distribution of atherosclerotic lesions in human coronary arteries. Circ Res 66: 1045-1066.

43. Vergallo R, Papafaklis MI, Yonetsu T, Bourantas CV, Andreou I, Wang Z, Fujimoto JG, McNulty I, Lee H, Biasucci LM, Crea F, Feldman CL, Michalis LK, Stone PH, Jang IK (2014) Endothelial shear stress and coronary plaque characteristics in humans: combined frequency-domain optical coherence tomography and computational fluid dynamics study. Circ Cardiovasc Imaging 7: 905-911. CIRCIMAGING.114.001932 [pii];10.1161/CIRCIMAGING.114.001932 [doi].

44. Ding Z, Liu S, Wang X, Deng X, Fan Y, Sun C, Wang Y, Mehta JL (2014) Hemodynamic Shear Stress Via ROS Modulates PCSK9 Expression in Human Vascular Endothelial and Smooth Muscle Cells and Along the Mouse Aorta. Antioxid Redox Signal . 10.1089/ars.2014.6054 [doi].

45. Dimmeler S, Haendeler J, Rippmann V, Nehls M, Zeiher AM (1996) Shear stress inhibits apoptosis of human endothelial cells. FEBS Lett 399: 71-74. S0014-5793(96)01289-6 [pii].

46. Ku DN, Giddens DP, Zarins CK, Glagov S (1985) Pulsatile flow and atherosclerosis in the human carotid bifurcation. Positive correlation between plaque location and low oscillating shear stress. Arteriosclerosis 5: 293-302.

47. Soulis J, Fytanidis D, Seralidou K, Giannoglou G (2014) Wall shear stress oscillation and its gradient in the normal left coronary artery tree bifurcations. Hippokratia 18: 12-16.

48. Soulis JV, Giannoglou GD, Chatzizisis YS, Farmakis TM, Giannakoulas GA, Parcharidis GE, Louridas GE (2006) Spatial and phasic oscillation of non-Newtonian wall shear stress in human left coronary artery bifurcation: an insight to atherogenesis. Coron Artery Dis 17: 351-358. 00019501-200606000-00005 [pii].

49. Liu Y, Chen BP, Lu M, Zhu Y, Stemerman MB, Chien S, Shyy JY (2002) Shear stress activation of SREBP1 in endothelial cells is mediated by integrins. Arterioscler Thromb Vasc Biol 22: 76-81.

50. Lam CF, Peterson TE, Richardson DM, Croatt AJ, d'Uscio LV, Nath KA, Katusic ZS (2006) Increased blood flow causes coordinated upregulation of arterial eNOS and biosynthesis of tetrahydrobiopterin. Am J Physiol Heart Circ Physiol 290: H786-H793. 00759.2005 [pii];10.1152/ajpheart.00759.2005 [doi].

51. Go YM, Boo YC, Park H, Maland MC, Patel R, Pritchard KA, Jr., Fujio Y, Walsh K, Darley-Usmar V, Jo H (2001) Protein kinase B/Akt activates c-Jun NH(2)-terminal kinase by increasing NO production in response to shear stress. J Appl Physiol (1985) 91: 1574-1581.

52. Hwang J, Ing MH, Salazar A, Lassegue B, Griendling K, Navab M, Sevanian A, Hsiai TK (2003) Pulsatile versus oscillatory shear stress regulates NADPH oxidase subunit expression: implication for native LDL oxidation. Circ Res 93: 1225-1232. 10.1161/01.RES.0000104087.29395.66 [doi];01.RES.0000104087.29395.66 [pii].

53. Geng YJ, Wu Q, Muszynski M, Hansson GK, Libby P (1996) Apoptosis of vascular smooth muscle cells induced by in vitro stimulation with interferon-gamma, tumor necrosis factor-alpha, and interleukin-1 beta. Arterioscler Thromb Vasc Biol 16: 19-27.

54. Harrison M, Smith E, Ross E, Krams R, Segers D, Buckley CD, Nash GB, Rainger GE (2013) The role of platelet-endothelial cell adhesion molecule-1 in atheroma formation varies depending on the site-specific hemodynamic environment. Arterioscler Thromb Vasc Biol 33: 694-701. ATVBAHA.112.300379 [pii];10.1161/ATVBAHA.112.300379 [doi].

55. Conklin BS, Zhong DS, Zhao W, Lin PH, Chen C (2002) Shear stress regulates occludin and VEGF expression in porcine arterial endothelial cells. J Surg Res 102: 13-21. 10.1006/jsre.2001.6295 [doi];S002248040196295X [pii].

56. Li R, Beebe T, Jen N, Yu F, Takabe W, Harrison M, Cao H, Lee J, Yang H, Han P, Wang K, Shimizu H, Chen J, Lien CL, Chi NC, Hsiai TK (2014) Shear stress-activated Wnt-angiopoietin-2 signaling recapitulates vascular repair in zebrafish embryos. Arterioscler Thromb Vasc Biol 34: 2268-2275. ATVBAHA.114.303345 [pii];10.1161/ATVBAHA.114.303345 [doi].

57. Derwall M, Malhotra R, Lai CS, Beppu Y, Aikawa E, Seehra JS, Zapol WM, Bloch KD, Yu PB (2012) Inhibition of bone morphogenetic protein signaling reduces vascular calcification and atherosclerosis. Arterioscler Thromb Vasc Biol 32: 613-622. ATVBAHA.111.242594 [pii];10.1161/ATVBAHA.111.242594 [doi].

58. Sorescu GP, Song H, Tressel SL, Hwang J, Dikalov S, Smith DA, Boyd NL, Platt MO, Lassegue B, Griendling KK, Jo H (2004) Bone morphogenic protein 4 produced in endothelial cells by oscillatory shear stress induces monocyte adhesion by stimulating reactive oxygen species production from a nox1-based NADPH oxidase. Circ Res 95: 773-779. 10.1161/01.RES.0000145728.22878.45 [doi];01.RES.0000145728.22878.45 [pii].

59. Cecchi E, Giglioli C, Valente S, Lazzeri C, Gensini GF, Abbate R, Mannini L (2011) Role of hemodynamic shear stress in cardiovascular disease. Atherosclerosis 214: 249-256. S0021-9150(10)00736-7 [pii];10.1016/j.atherosclerosis.2010.09.008 [doi].

60. Brown HF, Difrancesco D, Noble SJ (1979) How does adrenaline accelerate the heart? Nature 280: 235-236.

61. Difrancesco D (1993) Pacemaker mechanisms in cardiac tissue. Annu Rev Physiol 55: 455-472. 10.1146/annurev.ph.55.030193.002323 [doi].

62. Fox K, Ford I, Steg PG, Tendera M, Ferrari R (2008) Ivabradine for patients with stable coronary artery disease and left-ventricular systolic dysfunction (BEAUTIFUL): a randomised, double-blind, placebo-controlled trial. Lancet 372: 807-816. S0140-6736(08)61170-8 [pii];10.1016/S0140-6736(08)61170-8 [doi].

63. Fox K, Borer JS, Camm AJ, Danchin N, Ferrari R, Lopez Sendon JL, Steg PG, Tardif JC, Tavazzi L, Tendera M (2007) Resting heart rate in cardiovascular disease. J Am Coll Cardiol 50: 823-830. S0735-1097(07)01823-2 [pii];10.1016/j.jacc.2007.04.079 [doi].

64. Scicchitano P, Cortese F, Ricci G, Carbonara S, Moncelli M, Iacoviello M, Cecere A, Gesualdo M, Zito A, Caldarola P, Scrutinio D, Lagioia R, Riccioni G, Ciccone MM (2014) Ivabradine, coronary artery disease, and heart failure: beyond rhythm control. Drug Des Devel Ther 8: 689-700. 10.2147/DDDT.S60591 [doi];dddt-8-689 [pii].

65. Difrancesco D (2010) The role of the funny current in pacemaker activity. Circ Res 106: 434-446. 106/3/434 [pii];10.1161/CIRCRESAHA.109.208041 [doi].

66. Thollon C, Bidouard JP, Cambarrat C, Lesage L, Reure H, Delescluse I, Vian J, Peglion JL, Vilaine JP (1997) Stereospecific in vitro and in vivo effects of the new sinus node inhibitor (+)-S 16257. Eur J Pharmacol 339: 43-51. S0014-2999(97)01364-2 [pii].

67. Bucchi A, Baruscotti M, Nardini M, Barbuti A, Micheloni S, Bolognesi M, DiFrancesco D (2013) Identification of the molecular site of ivabradine binding to HCN4 channels. PLoS One 8: e53132. 10.1371/journal.pone.0053132 [doi];PONE-D-12-28660 [pii].

68. Custodis F, Schirmer SH, Baumhakel M, Heusch G, Bohm M, Laufs U (2010) Vascular pathophysiology in response to increased heart rate. J Am Coll Cardiol 56: 1973-1983.

69. Drouin A, Gendron ME, Thorin E, Gillis MA, Mahlberg-Gaudin F, Tardif JC (2008) Chronic heart rate reduction by ivabradine prevents endothelial dysfunction in dyslipidaemic mice. Br J Pharmacol 154: 749-757.

70. Bolduc V, Drouin A, Gillis MA, Duquette N, Thorin-Trescases N, Frayne-Robillard I, Des RC, Tardif JC, Thorin E (2011) Heart rate-associated mechanical stress impairs carotid but not cerebral artery compliance in dyslipidemic atherosclerotic mice. Am J Physiol Heart Circ Physiol .

71. Custodis F, Baumhakel M, Schlimmer N, List F, Gensch C, Bohm M, Laufs U (2008) Heart rate reduction by ivabradine reduces oxidative stress, improves endothelial function, and prevents atherosclerosis in apolipoprotein E-deficient mice. Circulation 117: 2377-2387.

72. Schirmer SH, Degen A, Baumhakel M, Custodis F, Schuh L, Kohlhaas M, Friedrich E, Bahlmann F, Kappl R, Maack C, Bohm M, Laufs U (2011) Heart-rate reduction by If-channel inhibition with ivabradine restores collateral artery growth in hypercholesterolemic atherosclerosis. Eur Heart J .

73. Baumhakel M, Custodis F, Schlimmer N, Laufs U, Bohm M (2010) Heart rate reduction with ivabradine improves erectile dysfunction in parallel to decrease in atherosclerotic plaque load in ApoE-knockout mice. Atherosclerosis 212: 55-62.

74. Kroller-Schon S, Schulz E, Wenzel P, Kleschyov AL, Hortmann M, Torzewski M, Oelze M, Renne T, Daiber A, Munzel T (2011) Differential effects of heart rate reduction with ivabradine in two models of endothelial dysfunction and oxidative stress. Basic Res Cardiol .

75. Kaplan JR, Manuck SB, Clarkson TB (1987) The influence of heart rate on coronary artery atherosclerosis. J Cardiovasc Pharmacol 10: S100-S103.

76. Perski A, Olsson G, Landou C, de Faire U, Theorell T, Hamsten A (1992) Minimum heart rate and coronary atherosclerosis: independent relations to global severity and rate of progression of angiographic lesions in men with myocardial infarction at a young age. Am Heart J 123: 609-616.

77. Strawn WB, Bondjers G, Kaplan JR, Manuck SB, Schwenke DC, Hansson GK, Shively CA, Clarkson TB (1991) Endothelial dysfunction in response to psychosocial stress in monkeys. Circ Res 68: 1270-1279.

78. Beere PA, Glagov S, Zarins CK (1992) Experimental atherosclerosis at the carotid bifurcation of the cynomolgus monkey. Localization, compensatory enlargement, and the sparing effect of lowered heart rate. Arterioscler Thromb 12: 1245-1253.

79. Beere PA, Glagov S, Zarins CK (1984) Retarding effect of lowered heart rate on coronary atherosclerosis. Science 226: 180-182.

80. Reinhart-King CA, Fujiwara K, Berk BC (2008) Physiologic stress-mediated signaling in the endothelium. Methods Enzymol 443: 25-44. S0076-6879(08)02002-8 [pii];10.1016/S0076-6879(08)02002-8 [doi].

81. Iiyama K, Hajra L, Iiyama M, Li H, DiChiara M, Medoff BD, Cybulsky MI (1999) Patterns of vascular cell adhesion molecule-1 and intercellular adhesion molecule-1 expression in rabbit and mouse atherosclerotic lesions and at sites predisposed to lesion formation. Circ Res 85: 199-207.

82. Wojtala A, Bonora M, Malinska D, Pinton P, Duszynski J, Wieckowski MR (2014) Methods to monitor ROS production by fluorescence microscopy and fluorometry. Methods Enzymol 542: 243-262. B978-0-12-416618-9.00013-3 [pii];10.1016/B978-0-12-416618-9.00013-3 [doi].

83. Bacchi E, Negri C, Targher G, Faccioli N, Lanza M, Zoppini G, Zanolin E, Schena F, Bonora E, Moghetti P (2013) Both resistance training and aerobic training reduce hepatic fat content in type 2 diabetic subjects with nonalcoholic fatty liver disease (the RAED2 Randomized Trial). Hepatology 58: 1287-1295. 10.1002/hep.26393 [doi].

84. Krenek P, Hamaide MC, Morel N, Wibo M (2006) A simple method for rapid separation of endothelial and smooth muscle mRNA reveals Na/K+ -ATPase alpha-subunit distribution in rat arteries. J Vasc Res 43: 502-510. 95963 [pii];10.1159/000095963 [doi].

85. Nakashima Y, Plump AS, Raines EW, Breslow JL, Ross R (1994) ApoE-deficient mice develop lesions of all phases of atherosclerosis throughout the arterial tree. Arterioscler Thromb 14: 133-140.

86. Johnson ME, Howerth EW (2004) Survivin: a bifunctional inhibitor of apoptosis protein. Vet Pathol 41: 599-607. 41/6/599 [pii];10.1354/vp.41-6-599 [doi].

87. Chandele A, Prasad V, Jagtap JC, Shukla R, Shastry PR (2004) Upregulation of survivin in G2/M cells and inhibition of caspase 9 activity enhances resistance in staurosporine-induced apoptosis. Neoplasia 6: 29-40.

88. Bilban M, Buehler LK, Head S, Desoye G, Quaranta V (2002) Defining signal thresholds in DNA microarrays: exemplary application for invasive cancer. BMC Genomics 3: 19.

89. Yuan Z, Miyoshi T, Bao Y, Sheehan JP, Matsumoto AH, Shi W (2009) Microarray analysis of gene expression in mouse aorta reveals role of the calcium signaling pathway in control of atherosclerosis susceptibility. Am J Physiol Heart Circ Physiol 296: H1336-H1343. 01095.2008 [pii];10.1152/ajpheart.01095.2008 [doi].

90. Zhang Y, Li J, Xie Q, Bonanno JA (2006) Molecular expression and functional involvement of the bovine calcium-activated chloride channel 1 (bCLCA1) in apical. Exp Eye Res 83: 1215-1224. S0014-4835(06)00299-5 [pii];10.1016/j.exer.2006.06.011 [doi].

91. Wagner EM, Sanchez J, McClintock JY, Jenkins J, Moldobaeva A (2008) Inflammation and ischemia-induced lung angiogenesis. Am J Physiol Lung Cell Mol Physiol 294: L351-L357. 00369.2007 [pii];10.1152/ajplung.00369.2007 [doi].

92. Yamada S, Wang KY, Tanimoto A, Fan J, Shimajiri S, Kitajima S, Morimoto M, Tsutsui M, Watanabe T, Yasumoto K, Sasaguri Y (2008) Matrix metalloproteinase 12 accelerates the initiation of atherosclerosis and stimulates the progression of fatty streaks to fibrous plaques in transgenic rabbits. Am J Pathol 172: 1419-1429. S0002-9440(10)61900-1 [pii];10.2353/ajpath.2008.070604 [doi].

93. Wagsater D, Johansson D, Fontaine V, Vorkapic E, Backlund A, Razuvaev A, Mayranpaa MI, Hjerpe C, Caidahl K, Hamsten A, Franco-Cereceda A, Wilbertz J, Swedenborg J, Zhou X, Eriksson P (2012) Serine protease inhibitor A3 in atherosclerosis and aneurysm disease. Int J Mol Med 30: 288-294. 10.3892/ijmm.2012.994 [doi].

94. Zhang B, Ma JX (2008) SERPINA3K prevents oxidative stress induced necrotic cell death by inhibiting calcium overload. PLoS One 3: e4077. 10.1371/journal.pone.0004077 [doi].

95. Tabibiazar R, Wagner RA, Ashley EA, King JY, Ferrara R, Spin JM, Sanan DA, Narasimhan B, Tibshirani R, Tsao PS, Efron B, Quertermous T (2005) Signature patterns of gene expression in mouse atherosclerosis and their correlation to human coronary disease. Physiol Genomics 22: 213-226. 00001.2005 [pii];10.1152/physiolgenomics.00001.2005 [doi].

96. Metcalf DJ, Nightingale TD, Zenner HL, Lui-Roberts WW, Cutler DF (2008) Formation and function of Weibel-Palade bodies. J Cell Sci 121: 19-27. 121/1/19 [pii];10.1242/jcs.03494 [doi].

97. Schwanzer-Pfeiffer D, Rossmanith E, Schildberger A, Falkenhagen D (2010) Characterization of SVEP1, KIAA, and SRPX2 in an in vitro cell culture model of endotoxemia. Cell Immunol 263: 65-70. S0008-8749(10)00061-4 [pii];10.1016/j.cellimm.2010.02.017 [doi].

98. Hudry-Clergeon H, Stengel D, Ninio E, Vilgrain I (2005) Platelet-activating factor increases VE-cadherin tyrosine phosphorylation in mouse endothelial cells and its association with the PtdIns3'-kinase. FASEB J 19: 512-520. 19/6/512 [pii];10.1096/fj.04-2202com [doi].

99. Custodis F, Baumhakel M, Schlimmer N, List F, Gensch C, Bohm M, Laufs U (2008) Heart rate reduction by ivabradine reduces oxidative stress, improves endothelial function, and prevents atherosclerosis in apolipoprotein E-deficient mice. Circulation 117: 2377-2387. CIRCULATIONAHA.107.746537 [pii];10.1161/CIRCULATIONAHA.107.746537 [doi].

100. Custodis F, Fries P, Muller A, Stamm C, Grube M, Kroemer HK, Bohm M, Laufs U (2012) Heart rate reduction by ivabradine improves aortic compliance in apolipoprotein E-deficient mice. J Vasc Res 49: 432-440. 000339547 [pii];10.1159/000339547 [doi].

101. Torban E, Eccles MR, Favor J, Goodyer PR (2000) PAX2 suppresses apoptosis in renal collecting duct cells. Am J Pathol 157: 833-842. S0002-9440(10)64597-X [pii];10.1016/S0002-9440(10)64597-X [doi].

102. Buchner DA, Charrier A, Srinivasan E, Wang L, Paulsen MT, Ljungman M, Bridges D, Saltiel AR (2015) Zinc Finger Protein 407 (ZFP407) Regulates Insulin-Stimulated Glucose Uptake and Glucose Transporter 4 (Glut4) mRNA. J Biol Chem . M114.623736 [pii];10.1074/jbc.M114.623736 [doi].

103. Tang SJ, Hoodless PA, Lu Z, Breitman ML, McInnes RR, Wrana JL, Buchwald M (1998) The Tlx-2 homeobox gene is a downstream target of BMP signalling and is required for mouse mesoderm development. Development 125: 1877-1887.

104. Zhang M, Zhou SH, Li XP, Shen XQ, Fang ZF, Liu QM, Qiu SF, Zhao SP (2008) Atorvastatin downregulates BMP-2 expression induced by oxidized low-density lipoprotein in human umbilical vein endothelial cells. Circ J 72: 807-812. JST.JSTAGE/circj/72.807 [pii].

105. Mizutani Y, Kihara A, Igarashi Y (2006) LASS3 (longevity assurance homologue 3) is a mainly testis-specific (dihydro)ceramide synthase with relatively broad substrate specificity. Biochem J 398: 531-538. BJ20060379 [pii];10.1042/BJ20060379 [doi].

106. Haus JM, Kashyap SR, Kasumov T, Zhang R, Kelly KR, Defronzo RA, Kirwan JP (2009) Plasma ceramides are elevated in obese subjects with type 2 diabetes and correlate with the severity of insulin resistance. Diabetes 58: 337-343. db08-1228 [pii];10.2337/db08-1228 [doi].

107. Lumsden NG, Khambata RS, Hobbs AJ (2010) C-type natriuretic peptide (CNP): cardiovascular roles and potential as a therapeutic target. Curr Pharm Des 16: 4080-4088. BSP/CPD/E-Pub/000243-aamir [pii].

108. Suga S, Itoh H, Komatsu Y, Ogawa Y, Hama N, Yoshimasa T, Nakao K (1993) Cytokine-induced C-type natriuretic peptide (CNP) secretion from vascular endothelial cells--evidence for CNP as a novel autocrine/paracrine regulator from endothelial cells. Endocrinology 133: 3038-3041.

109. Kuehnl A, Pelisek J, Pongratz J, Eckstein HH (2012) C-type natriuretic peptide and its receptors in atherosclerotic plaques of the carotid artery of clinically asymptomatic patients. Eur J Vasc Endovasc Surg 43: 649-654. S1078-5884(12)00099-8 [pii];10.1016/j.ejvs.2012.02.010 [doi].

110. Hong TC, Yeh HI, Shih BF, Wang AM, Chen CY, Hou CJ, Tsai CH (2006) Brain natriuretic peptide and C-type natriuretic peptide are differently regulated by age but similarly elevated in coronary artery disease. Acta Cardiol 61: 1-5.

111. Olewicz-Gawlik A, Trzybulska D, Grala P, Hrycaj P (2010) Blood serum levels of amino-terminal pro-C-type natriuretic peptide in patients with rheumatoid arthritis. Adv Med Sci 55: 261-265. R644T18U752U753U [pii];10.2478/v10039-010-0036-1 [doi].

112. Zakeri R, Sangaralingham SJ, Sandberg SM, Heublein DM, Scott CG, Burnett JC, Jr. (2013) Urinary C-type natriuretic peptide: a new heart failure biomarker. JACC Heart Fail 1: 170-177. 10.1016/j.jchf.2012.12.003 [doi].

113. Passino C, Del RS, Severino S, Gabutti A, Prontera C, Clerico A, Giannessi D, Emdin M (2008) C-type natriuretic peptide expression in patients with chronic heart failure: effects of aerobic training. Eur J Cardiovasc Prev Rehabil 15: 168-172. 10.1097/HJR.0b013e3282f10e9b [doi].

114. Chun TH, Itoh H, Ogawa Y, Tamura N, Takaya K, Igaki T, Yamashita J, Doi K, Inoue M, Masatsugu K, Korenaga R, Ando J, Nakao K (1997) Shear stress augments expression of C-type natriuretic peptide and adrenomedullin. Hypertension 29: 1296-1302.

115. Dai G, Kaazempur-Mofrad MR, Natarajan S, Zhang Y, Vaughn S, Blackman BR, Kamm RD, Garcia-Cardena G, Gimbrone MA, Jr. (2004) Distinct endothelial phenotypes evoked by arterial waveforms derived from atherosclerosis-susceptible and -resistant regions of human vasculature. Proc Natl Acad Sci U S A 101: 14871-14876. 0406073101 [pii];10.1073/pnas.0406073101 [doi].

116. Alonso F, Krattinger N, Mazzolai L, Simon A, Waeber G, Meda P, Haefliger JA (2010) An angiotensin II- and NF-kappaB-dependent mechanism increases connexin 43 in murine arteries targeted by renin-dependent hypertension. Cardiovasc Res 87: 166-176. cvq031 [pii];10.1093/cvr/cvq031 [doi].

117. Sandoval R, Malik AB, Minshall RD, Kouklis P, Ellis CA, Tiruppathi C (2001) Ca(2+) signalling and PKCalpha activate increased endothelial permeability by disassembly of VE-cadherin junctions. J Physiol 533: 433-445. PHY_11576 [pii].

118. Wong LS, Oeseburg H, de Boer RA, van Gilst WH, van Veldhuisen DJ, van der Harst P (2009) Telomere biology in cardiovascular disease: the TERC-/- mouse as a model for heart failure and ageing. Cardiovasc Res 81: 244-252. cvn337 [pii];10.1093/cvr/cvn337 [doi].

119. Brewster JL, Martin SL, Toms J, Goss D, Wang K, Zachrone K, Davis A, Carlson G, Hood L, Coffin JD (2000) Deletion of Dad1 in mice induces an apoptosis-associated embryonic death. Genesis 26: 271-278. 10.1002/(SICI)1526-968X(200004)26:4<271::AID-GENE90>3.0.CO;2-E [pii].

120. Charan RA, Johnson BN, Zaganelli S, Nardozzi JD, LaVoie MJ (2014) Inhibition of apoptotic Bax translocation to the mitochondria is a central function of parkin. Cell Death Dis 5: e1313. cddis2014278 [pii];10.1038/cddis.2014.278 [doi].

121. Li D, Mehta JL (2009) Intracellular signaling of LOX-1 in endothelial cell apoptosis. Circ Res 104: 566-568. 104/5/566 [pii];10.1161/CIRCRESAHA.109.194209 [doi].

122. Morawietz H, Duerrschmidt N, Niemann B, Galle J, Sawamura T, Holtz J (2001) Induction of the oxLDL receptor LOX-1 by endothelin-1 in human endothelial cells. Biochem Biophys Res Commun 284: 961-965. 10.1006/bbrc.2001.5044 [doi];S0006-291X(01)95044-2 [pii].

123. Qin L, Zhang M (2010) Maspin regulates endothelial cell adhesion and migration through an integrin signaling pathway. J Biol Chem 285: 32360-32369. M110.131045 [pii];10.1074/jbc.M110.131045 [doi].

124. Li Z, Shi HY, Zhang M (2005) Targeted expression of maspin in tumor vasculatures induces endothelial cell apoptosis. Oncogene 24: 2008-2019. 1208449 [pii];10.1038/sj.onc.1208449 [doi].

125. Garcia-Heredia A, Marsillach J, Rull A, Triguero I, Fort I, Mackness B, Mackness M, Shih DM, Joven J, Camps J (2013) Paraoxonase-1 inhibits oxidized low-density lipoprotein-induced metabolic alterations and apoptosis in endothelial cells: a nondirected metabolomic study. Mediators Inflamm 2013: 156053. 10.1155/2013/156053 [doi].

126. Witte I, Altenhofer S, Wilgenbus P, Amort J, Clement AM, Pautz A, Li H, Forstermann U, Horke S (2011) Beyond reduction of atherosclerosis: PON2 provides apoptosis resistance and stabilizes tumor cells. Cell Death Dis 2: e112. cddis201091 [pii];10.1038/cddis.2010.91 [doi].

127. N.Bourquard (2008) The Role of PON2 and PON3 in Atherosclerosis and Related Traits. In: D.M.Shih CJNNV-GKNDASEOVGNRSYHJZMNAMFSTR, editors. pp. 103-128.

128. Salter RC, Ashlin TG, Kwan AP, Ramji DP (2010) ADAMTS proteases: key roles in atherosclerosis? J Mol Med (Berl) 88: 1203-1211. 10.1007/s00109-010-0654-x [doi].

129. Gao YX, Yu CA, Lu JH, Gao HM, Li G, Kong W, Zheng J (2013) ADAMTS-7 expression increases in the early stage of angiotensin II-induced renal injury in elderly mice. Kidney Blood Press Res 38: 121-131. 000355758 [pii];10.1159/000355758 [doi].

130. Bond AR, Hultgardh-Nilsson A, Knutsson A, Jackson CL, Rauch U (2014) Cartilage oligomeric matrix protein (COMP) in murine brachiocephalic and carotid atherosclerotic lesions. Atherosclerosis 236: 366-372. S0021-9150(14)01305-7 [pii];10.1016/j.atherosclerosis.2014.07.029 [doi].

131. Huang J, Stohl LL, Zhou X, Ding W, Granstein RD (2011) Calcitonin gene-related peptide inhibits chemokine production by human dermal microvascular endothelial cells. Brain Behav Immun 25: 787-799. S0889-1591(11)00057-2 [pii];10.1016/j.bbi.2011.02.007 [doi].

132. Bowen EJ, Schmidt TW, Firm CS, Russo AF, Durham PL (2006) Tumor necrosis factor-alpha stimulation of calcitonin gene-related peptide expression and secretion from rat trigeminal ganglion neurons. J Neurochem 96: 65-77. JNC3524 [pii];10.1111/j.1471-4159.2005.03524.x [doi].

133. Dong YL, Reddy DM, Green KE, Chauhan MS, Wang HQ, Nagamani M, Hankins GD, Yallampalli C (2007) Calcitonin gene-related peptide (CALCA) is a proangiogenic growth factor in the human placental development. Biol Reprod 76: 892-899. biolreprod.106.059089 [pii];10.1095/biolreprod.106.059089 [doi].

134. Hernanz A, De ME, Romera N, Perez-Ayala C, Gijon J, Arnalich F (1993) Calcitonin gene-related peptide II, substance P and vasoactive intestinal peptide in plasma and synovial fluid from patients with inflammatory joint disease. Br J Rheumatol 32: 31-35.

135. Kim WJ, Bae EM, Kang YJ, Bae HU, Hong SH, Lee JY, Park JE, Kwon BS, Suk K, Lee WH (2006) Glucocorticoid-induced tumour necrosis factor receptor family related protein (GITR) mediates inflammatory activation of macrophages that can destabilize

atherosclerotic plaques. Immunology 119: 421-429. IMM2453 [pii];10.1111/j.1365-2567.2006.02453.x [doi].

136. Martin P, Palmer G, Vigne S, Lamacchia C, Rodriguez E, Talabot-Ayer D, Rose-John S, Chalaris A, Gabay C (2013) Mouse neutrophils express the decoy type 2 interleukin-1 receptor (IL-1R2) constitutively and in acute inflammatory conditions. J Leukoc Biol 94: 791-802. jlb.0113035 [pii];10.1189/jlb.0113035 [doi].

137. Colotta F, Dower SK, Sims JE, Mantovani A (1994) The type II 'decoy' receptor: a novel regulatory pathway for interleukin 1. Immunol Today 15: 562-566. 0167-5699(94)90217-8 [pii];10.1016/0167-5699(94)90217-8 [doi].

138. Burleigh ME, Babaev VR, Yancey PG, Major AS, McCaleb JL, Oates JA, Morrow JD, Fazio S, Linton MF (2005) Cyclooxygenase-2 promotes early atherosclerotic lesion formation in ApoE-deficient and C57BL/6 mice. J Mol Cell Cardiol 39: 443-452. S0022-2828(05)00195-1 [pii];10.1016/j.yjmcc.2005.06.011 [doi].

139. Burleigh ME, Babaev VR, Patel MB, Crews BC, Remmel RP, Morrow JD, Oates JA, Marnett LJ, Fazio S, Linton MF (2005) Inhibition of cyclooxygenase with indomethacin phenethylamide reduces atherosclerosis in apoE-null mice. Biochem Pharmacol 70: 334-342. S0006-2952(05)00285-6 [pii];10.1016/j.bcp.2005.04.044 [doi].

140. Passerini AG, Polacek DC, Shi C, Francesco NM, Manduchi E, Grant GR, Pritchard WF, Powell S, Chang GY, Stoeckert CJ, Jr., Davies PF (2004) Coexisting proinflammatory and antioxidative endothelial transcription profiles in a disturbed flow region of the adult porcine aorta. Proc Natl Acad Sci U S A 101: 2482-2487. 101/8/2482 [pii].

141. Marzoll A, Nagy N, Wordehoff L, Dai G, Fries S, Lindner V, Grosser T, Fischer JW (2009) Cyclooxygenase inhibitors repress vascular hyaluronan-synthesis in murine atherosclerosis and neointimal thickening. J Cell Mol Med 13: 3713-3719. JCMM736 [pii];10.1111/j.1582-4934.2009.00736.x [doi].

142. Lin J, Chang W, Dong J, Zhang F, Mohabeer N, Kushwaha KK, Wang L, Su Y, Fang H, Li D (2013) Thymic stromal lymphopoietin over-expressed in human atherosclerosis: potential role in Th17 differentiation. Cell Physiol Biochem 31: 305-318. 000343369 [pii];10.1159/000343369 [doi].

143. Zhao H, Li M, Wang L, Su Y, Fang H, Lin J, Mohabeer N, Li D (2012) Angiotensin II induces TSLP via an AT1 receptor/NF-KappaB pathway, promoting Th17 differentiation. Cell Physiol Biochem 30: 1383-1397. 000343327 [pii];10.1159/000343327 [doi].

144. Lewis RD, Perry MJ, Guschina IA, Jackson CL, Morgan BP, Hughes TR (2011) CD55 deficiency protects against atherosclerosis in ApoE-deficient mice via C3a modulation of lipid metabolism. Am J Pathol 179: 1601-1607. S0002-9440(11)00632-8 [pii];10.1016/j.ajpath.2011.06.015 [doi].

145. Lange C, Starrett DJ, Goetsch J, Gerke V, Rescher U (2007) Transcriptional profiling of human monocytes reveals complex changes in the expression pattern of inflammation-related genes in response to the annexin A1-derived peptide Ac1-25. J Leukoc Biol 82: 1592-1604. jlb.0307158 [pii];10.1189/jlb.0307158 [doi].

146. Peters DG, Zhang XC, Benos PV, Heidrich-O'Hare E, Ferrell RE (2002) Genomic analysis of immediate/early response to shear stress in human coronary artery endothelial cells. Physiol Genomics 12: 25-33. 10.1152/physiolgenomics.00016.2002 [doi];00016.2002 [pii].

147. Cox MA, Jackson J, Stanton M, Rojas-Triana A, Bober L, Laverty M, Yang X, Zhu F, Liu J, Wang S, Monsma F, Vassileva G, Maguire M, Gustafson E, Bayne M, Chou CC, Lundell D, Jenh CH (2009) Short-chain fatty acids act as antiinflammatory mediators by regulating prostaglandin E(2) and cytokines. World J Gastroenterol 15: 5549-5557.

148. Takata Y, Liu J, Yin F, Collins AR, Lyon CJ, Lee CH, Atkins AR, Downes M, Barish GD, Evans RM, Hsueh WA, Tangirala RK (2008) PPARdelta-mediated antiinflammatory mechanisms

inhibit angiotensin II-accelerated atherosclerosis. Proc Natl Acad Sci U S A 105: 4277-4282. 0708647105 [pii];10.1073/pnas.0708647105 [doi].

149. Sukhanov S, Higashi Y, Shai SY, Vaughn C, Mohler J, Li Y, Song YH, Titterington J, Delafontaine P (2007) IGF-1 reduces inflammatory responses, suppresses oxidative stress, and decreases atherosclerosis progression in ApoE-deficient mice. Arterioscler Thromb Vasc Biol 27: 2684-2690. ATVBAHA.107.156257 [pii];10.1161/ATVBAHA.107.156257 [doi].

150. Johnstone DM, Graham RM, Trinder D, Riveros C, Olynyk JK, Scott RJ, Moscato P, Milward EA (2012) Changes in brain transcripts related to Alzheimer's disease in a model of HFE hemochromatosis are not consistent with increased Alzheimer's disease risk. J Alzheimers Dis 30: 791-803. 660L056483470425 [pii];10.3233/JAD-2012-112183 [doi].

151. Rizzo P, Miele L, Ferrari R (2013) The Notch pathway: a crossroad between the life and death of the endothelium. Eur Heart J 34: 2504-2509. ehs141 [pii];10.1093/eurheartj/ehs141 [doi].

152. Quillard T, Coupel S, Coulon F, Fitau J, Chatelais M, Cuturi MC, Chiffoleau E, Charreau B (2008) Impaired Notch4 activity elicits endothelial cell activation and apoptosis: implication for transplant arteriosclerosis. Arterioscler Thromb Vasc Biol 28: 2258-2265. ATVBAHA.108.174995 [pii];10.1161/ATVBAHA.108.174995 [doi].

153. Quillard T, Devalliere J, Coupel S, Charreau B (2010) Inflammation dysregulates Notch signaling in endothelial cells: implication of Notch2 and Notch4 to endothelial dysfunction. Biochem Pharmacol 80: 2032-2041. S0006-2952(10)00521-6 [pii];10.1016/j.bcp.2010.07.010 [doi].

154. MacKenzie F, Duriez P, Wong F, Noseda M, Karsan A (2004) Notch4 inhibits endothelial apoptosis via RBP-Jkappa-dependent and -independent pathways. J Biol Chem 279: 11657-11663. 10.1074/jbc.M312102200 [doi];M312102200 [pii].

155. Walshe TE, Connell P, Cryan L, Ferguson G, Gardiner T, Morrow D, Redmond EM, O'Brien C, Cahill PA (2011) Microvascular retinal endothelial and pericyte cell apoptosis in vitro: role of Hedgehog and Notch signaling. Invest Ophthalmol Vis Sci . iovs.10-7061 [pii];10.1167/iovs.10-7061 [doi].

156. Kitagawa M, Hojo M, Imayoshi I, Goto M, Ando M, Ohtsuka T, Kageyama R, Miyamoto S (2013) Hes1 and Hes5 regulate vascular remodeling and arterial specification of endothelial cells in brain vascular development. Mech Dev . S0925-4773(13)00056-7 [pii];10.1016/j.mod.2013.07.001 [doi].

157. Zhou H, Chen S, Wang W, Wang Z, Wu X, Zhang Z (2012) Nanog inhibits lipopolysaccharide-induced expression of pro-inflammatory cytokines by blocking NF-kappaB transcriptional activity in rat primary microglial cells. Mol Med Rep 5: 842-846. 10.3892/mmr.2011.719 [doi].

158. Lu TM, Luo YJ, Yu JK (2012) BMP and Delta/Notch signaling control the development of amphioxus epidermal sensory neurons: insights into the evolution of the peripheral sensory system. Development 139: 2020-2030. dev.073833 [pii];10.1242/dev.073833 [doi].

159. Zhou B, Wang ZX, Zhao Y, Brautigan DL, Zhang ZY (2002) The specificity of extracellular signal-regulated kinase 2 dephosphorylation by protein phosphatases. J Biol Chem 277: 31818-31825. 10.1074/jbc.M203969200 [doi];M203969200 [pii].

160. Indra MR, Karyono S, Ratnawati R, Malik SG (2013) Quercetin suppresses inflammation by reducing ERK1/2 phosphorylation and NF kappa B activation in Leptin-induced Human Umbilical Vein Endothelial Cells (HUVECs). BMC Res Notes 6: 275. 1756-0500-6-275 [pii];10.1186/1756-0500-6-275 [doi].

161. Takahashi M, Berk BC (1996) Mitogen-activated protein kinase (ERK1/2) activation by shear stress and adhesion in endothelial cells. Essential role for a herbimycin-sensitive kinase. J Clin Invest 98: 2623-2631. 10.1172/JCI119083 [doi].

162. Tiwari S, Zhang Y, Heller J, Abernethy DR, Soldatov NM (2006) Atherosclerosis-related molecular alteration of the human CaV1.2 calcium channel alpha1C subunit. Proc Natl Acad Sci U S A 103: 17024-17029. 0606539103 [pii];10.1073/pnas.0606539103 [doi].

163. Gronich N, Kumar A, Zhang Y, Efimov IR, Soldatov NM (2010) Molecular remodeling of ion channels, exchangers and pumps in atrial and ventricular myocytes in ischemic cardiomyopathy. Channels (Austin) 4: 101-107. 10975 [pii].

164. Diczfalusy U, Olofsson KE, Carlsson AM, Gong M, Golenbock DT, Rooyackers O, Flaring U, Bjorkbacka H (2009) Marked upregulation of cholesterol 25-hydroxylase expression by lipopolysaccharide. J Lipid Res 50: 2258-2264. M900107-JLR200 [pii];10.1194/jlr.M900107-JLR200 [doi].

165. Gold ES, Ramsey SA, Sartain MJ, Selinummi J, Podolsky I, Rodriguez DJ, Moritz RL, Aderem A (2012) ATF3 protects against atherosclerosis by suppressing 25-hydroxycholesterol-induced lipid body formation. J Exp Med 209: 807-817. jem.20111202 [pii];10.1084/jem.20111202 [doi].

166. Monaco C, Paleolog E (2004) Nuclear factor kappaB: a potential therapeutic target in atherosclerosis and thrombosis. Cardiovasc Res 61: 671-682. 10.1016/j.cardiores.2003.11.038 [doi];S0008636303007600 [pii].

167. Orr AW, Sanders JM, Bevard M, Coleman E, Sarembock IJ, Schwartz MA (2005) The subendothelial extracellular matrix modulates NF-kappaB activation by flow: a potential role in atherosclerosis. J Cell Biol 169: 191-202. jcb.200410073 [pii];10.1083/jcb.200410073 [doi].

168. Hajra L, Evans AI, Chen M, Hyduk SJ, Collins T, Cybulsky MI (2000) The NF-kappa B signal transduction pathway in aortic endothelial cells is primed for activation in regions predisposed to atherosclerotic lesion formation. Proc Natl Acad Sci U S A 97: 9052-9057. 97/16/9052 [pii].

169. Hernandez-Presa M, Bustos C, Ortego M, Tunon J, Renedo G, Ruiz-Ortega M, Egido J (1997) Angiotensin-converting enzyme inhibition prevents arterial nuclear factor-kappa B activation, monocyte chemoattractant protein-1 expression, and macrophage infiltration in a rabbit model of early accelerated atherosclerosis. Circulation 95: 1532-1541.

170. Gareus R, Kotsaki E, Xanthoulea S, van dM, I, Gijbels MJ, Kardakaris R, Polykratis A, Kollias G, de Winther MP, Pasparakis M (2008) Endothelial cell-specific NF-kappaB inhibition protects mice from atherosclerosis. Cell Metab 8: 372-383. S1550-4131(08)00283-0 [pii];10.1016/j.cmet.2008.08.016 [doi].

171. Liebner S, Plate KH (2010) Differentiation of the brain vasculature: the answer came blowing by the Wnt. J Angiogenes Res 2: 1. 10.1186/2040-2384-2-1 [doi].

172. Al-Aly Z, Shao JS, Lai CF, Huang E, Cai J, Behrmann A, Cheng SL, Towler DA (2007) Aortic Msx2-Wnt calcification cascade is regulated by TNF-alpha-dependent signals in diabetic Ldlr-/- mice. Arterioscler Thromb Vasc Biol 27: 2589-2596. ATVBAHA.107.153668 [pii];10.1161/ATVBAHA.107.153668 [doi].

173. Ziu E, Mercado CP, Li Y, Singh P, Ahmed BA, Freyaldenhoven S, Lensing S, Ware J, Kilic F (2012) Down-regulation of the serotonin transporter in hyperreactive platelets counteracts the pro-thrombotic effect of serotonin. J Mol Cell Cardiol 52: 1112-1121. S0022-2828(12)00086-7 [pii];10.1016/j.yjmcc.2012.02.004 [doi].

174. Wong SL, Lau CW, Wong WT, Xu A, Au CL, Ng CF, Ng SS, Gollasch M, Yao X, Huang Y (2011) Pivotal role of protein kinase Cdelta in angiotensin II-induced endothelial cyclooxygenase-2 expression: a link to vascular inflammation. Arterioscler Thromb Vasc Biol 31: 1169-1176. ATVBAHA.110.216044 [pii];10.1161/ATVBAHA.110.216044 [doi].

175. Tummala PE, Chen XL, Sundell CL, Laursen JB, Hammes CP, Alexander RW, Harrison DG, Medford RM (1999) Angiotensin II induces vascular cell adhesion molecule-1 expression

in rat vasculature: A potential link between the renin-angiotensin system and atherosclerosis. Circulation 100: 1223-1229.

176. Vestweber D (2008) VE-cadherin: the major endothelial adhesion molecule controlling cellular junctions and blood vessel formation. Arterioscler Thromb Vasc Biol 28: 223-232. ATVBAHA.107.158014 [pii];10.1161/ATVBAHA.107.158014 [doi].

177. Masumura T, Yamamoto K, Shimizu N, Obi S, Ando J (2009) Shear stress increases expression of the arterial endothelial marker ephrinB2 in murine ES cells via the VEGF-Notch signaling pathways. Arterioscler Thromb Vasc Biol 29: 2125-2131. ATVBAHA.109.193185 [pii];10.1161/ATVBAHA.109.193185 [doi].

178. Nigro P, Abe J, Berk BC (2011) Flow shear stress and atherosclerosis: a matter of site specificity. Antioxid Redox Signal 15: 1405-1414. 10.1089/ars.2010.3679 [doi].

179. Chiu JJ, Chien S (2011) Effects of disturbed flow on vascular endothelium: pathophysiological basis and clinical perspectives. Physiol Rev 91: 327-387. 91/1/327 [pii];10.1152/physrev.00047.2009 [doi].

180. Liu B, Cai SX, Zhang L (2008) [Disturbed shear stress affects disposition of caveolin-1 in endothelial cells.]. Zhonghua Xin Xue Guan Bing Za Zhi 36: 927-930.

181. Qian JY, Haruno A, Asada Y, Nishida T, Saito Y, Matsuda T, Ueno H (2002) Local expression of C-type natriuretic peptide suppresses inflammation, eliminates shear stress-induced thrombosis, and prevents neointima formation through enhanced nitric oxide production in rabbit injured carotid arteries. Circ Res 91: 1063-1069.

182. Masumura T, Yamamoto K, Shimizu N, Obi S, Ando J (2009) Shear stress increases expression of the arterial endothelial marker ephrinB2 in murine ES cells via the VEGF-Notch signaling pathways. Arterioscler Thromb Vasc Biol 29: 2125-2131. ATVBAHA.109.193185 [pii];10.1161/ATVBAHA.109.193185 [doi].

183. Chen J, Li D, Schaefer R, Mehta JL (2006) Cross-talk between dyslipidemia and renin-angiotensin system and the role of LOX-1 and MAPK in atherogenesis studies with the combined use of rosuvastatin and candesartan. Atherosclerosis 184: 295-301. S0021-9150(05)00306-0 [pii];10.1016/j.atherosclerosis.2005.04.016 [doi].

184. Zhang Q, Wang C, Liu Z, Liu X, Han C, Cao X, Li N (2012) Notch signal suppresses Toll-like receptor-triggered inflammatory responses in macrophages by inhibiting extracellular signal-regulated kinase 1/2-mediated nuclear factor kappaB activation. J Biol Chem 287: 6208-6217. M111.310375 [pii];10.1074/jbc.M111.310375 [doi].

185. Wang L, Zhang H, Rodriguez S, Cao L, Parish J, Mumaw C, Zollman A, Kamoka MM, Mu J, Chen DZ, Srour EF, Chitteti BR, HogenEsch H, Tu X, Bellido TM, Boswell HS, Manshouri T, Verstovsek S, Yoder MC, Kapur R, Cardoso AA, Carlesso N (2014) Notch-dependent repression of miR-155 in the bone marrow niche regulates hematopoiesis in an NF-kappaB-dependent manner. Cell Stem Cell 15: 51-65. S1934-5909(14)00187-8 [pii];10.1016/j.stem.2014.04.021 [doi].